Numéro d'ordre : 42276

Université de Lille – Science et Technologies
Ecole Doctorale des Sciences Pour l'Ingénieur

Thèse

Pour obtenir le grade de
Docteur de l'Université de Lille1
Spécialité : Génie Electrique

Pour Soutenance publique par
Thomas Sednaoui
Le 14 décembre 2016

Tactile feedback integration on mobile communicating devices: analysis and specification

Membres du Jury :

Pr. Marie Ange Bueno	Ecole Nationale Supérieure d'Ingénieurs Sud Alsace	*Rapporteur*
Pr. Stéphane Régnier	Université Pierre et Marie Curie	*Rapporteur*
Pr. André Mouraux	Université Catholique de Louvain	*Examinateur*
Dr. Cedrick Chappaz	CEO Hap2U	*Examinateur*
Dr. Fabrice Casset	STMicroelectronics, CEA Letti	*Co-encadrant*
Pr. Betty Lemaire-Semail	Université de Lille 1	*Directrice de thèse*

LILLE UNIVERSITY

Résumé

L2EP- Laboratoire d'électrotechnique et d'électronique de puissance de Lille

Docteur en Sciences Pour L'Ingénieur

Intégration du retour tactile sur des objets mobiles communicants : analyses et spécifications

Par Thomas Sednaoui

L'usage des écrans tactiles est devenu omniprésent ces dernières années. Ces appareils prennent une place de plus en plus importante dans notre de vie de tous les jours, on les retrouve dans nos maisons, bureaux et même dans nos poches. L'abondance de ces nouvelles interfaces a soulevé l'intérêt pour les technologies permettant une stimulation tactile, et mis en perspective le manque de ce type d'interfaces dans les nouvelles générations d'appareils mobiles avec écrans tactiles. Aujourd'hui, les appareils possédant ce type d'écran se contentent de fournir un retour sensoriel sous la forme de simples vibrations, qui n'ont pas pour objectif de recréer les sensations du toucher de surfaces. La recherche de nouvelles interfaces tactiles, plus performantes, et assurant une restitution plus proche d'une sensation naturelle est donc en cours. Plusieurs solutions technologiques ont prouvé leur efficacité mais posent des problèmes d'industrialisation. Dans cette thèse, une de ces méthodes adaptées aux écrans tactiles, la lubrification ultrasonique, est présentée. Cette méthode de stimulation s'appuie sur la création d'une onde stationnaire ultrasonore au sein d'un résonateur en verre et est capable de faire varier en temps réel la sensation de frottement entre le doigt de l'utilisateur et la surface du résonateur. Grace à des mesures tribologiques, les paramètres influents tels l'amplitude vibratoire, la vitesse d'exploration du doigt, la fréquence de résonance du stimulateur sont mis en évidence. Cette analyse permet la proposition d'une première série de spécifications techniques pour la conception de dispositifs à retour tactile. L'étude est ensuite complétée par l'analyse des problèmes d'alimentation et de contrôle du système, avec en considération les questions d'intégration au sein de dispositifs portables et les problèmes d'industrialisation du processus de fabrication. Enfin, des études psychophysiques sont menées pour affiner du point de vue perceptuel le cahier des charges de conception d'un tel dispositif.

LILLE UNIVERSITY

Abstract

L2EP- Laboratoire d'électrotechnique et d'électronique de puissance de Lille

Doctor in Engineering Sciences

Tactile feedback integration on mobile communicating devices: analysis and specification

By Thomas Sednaoui

The last few years have seen the emergence of ubiquitous mobile devices and tactile interfaces. These devices take an ever-important place in our daily life, they are present in our home, office, cars and even pockets. The abundance of these novel interfaces raised the interest in touch based human-machine interactions and highlighted the problem of the lack of natural touch feedback in the existing generation of tactile displays. Today's smartphones all possess basic haptic feedback thanks to low frequency vibrations. However, these vibrations are far from the natural touch sensation of a surface. The search for a better tactile feedback, closer to the natural human perception, is ongoing. Multiple solutions are being explored to deliver improved haptic feedback on existing mobile platforms such as smartphones or tablets. In this thesis, we investigate the tactile feedback thanks to ultrasonic lubrication, well adapted to touch screen. This technology uses the creation of a resonating standing wave in a substrate to modulate in real time the friction perceived by user moving his finger on the resonator surface; the principle is effective even on a flat glass surface. By a series of experimental friction measures, the influence of the relevant parameters such as the vibration amplitude, the exploratory speed, the resonance frequency is highlighted. This analysis is used to build advanced tactile interfaces, based on ultrasonic friction modulation. The control and the supply of the tactile interfaces are also investigated, considering the issues of integration and industrialization of the process. Finally, these new interfaces are used to explore advanced control methods, improving further the quality and reliability of the generated sensation. Psychophysical analysis is performed to fulfil the specifications of these devices on a perceptual point of view.

CONTENTS

ACRONYMS

AC	Alternative Current
AlN	Aluminum nitrate
Au	gold
CAD	Computer Assisted Design
CPU	Central Processing Unit
DC	Direct Current
DSP	Digital Signal Processor
EMI	Electromagnetic Impulsions
ERM	Eccentric Rotating Mass
FA I	fast Adapting 1: Meissner cells
FA II	Fast Adapting 2 : Pacini corpuscles
FE	Finite Element
FEM	Finite Element Method
GUI	Graphical User Interface, graphical user interface
HMI	Human Machine Interfaces
JND	Just Noticeable Difference
LCD	Liquid Crystal display
LRA	Linear Resonant Actuator
MCU	Microcontroller Unit
Mo	Molybdenum
PCB	Printed Board Circuit
PWM	Pulse-Width Modulation
PZT	Lead zirconium titanate
RLC	Resistance Inductance Capacitor
RT	Rise Time
SA I	Slow Adapting 1: Merkel cells
SA II	Slow Adapting 2 : Ruffini corpuscles
SAW	Surface Acoustic Wave
SiO_2	silicon oxide
SL	Signal Length
SNR	Signal to Noise Ratio
THD	Total Harmonic Distortion
UL	Ultrasonic Lubrication

INTRODUCTION

Context

Human is a visual and social based creature, and it is thus natural that when the technology became available, the first Human Machine Interfaces (HMI) were focused on the replication of vision and sound. First mobile phones continued this tendency with the implementation of a simple screen and mechanical keyboard, fulfilling all the users' needs. But with the advance of silicon and miniaturization, mobile phones changed name to be called smartphones, reflecting their increasing processing power and applications. Simple mechanical HMIs proved unadapted to the efficient control of such complex devices.

In 2007, a full touch screen device was the game changer. It solved a problem that is, by its nature, grounded in the necessary modularity of complex visual interface. Previous smartphones were limited in their functions, not by technical capabilities and processing power, but by the need for a modular interface that could adapt to the growing need of the users: phone call of course, but also internet browser, text editor, media player, and photo and video camera.

But full touch screen was soon revealed to carry a new inconvenience, felt by users as a step backward in ergonomics. Interacting with a purely visual interface without any inherent tactile sensations felt wrong. And while nowadays most smartphone owners are used to this problem, the search for a solution was not abandoned by industrials and researchers.

Today, multiple technological advancements give hopes that such an HMI will soon be found. With the objective of giving the illusion of a natural touch sensation on touch screen devices, this work focuses on friction modulation: the ability to dynamically change the tribologic conditions between a surface and a user's finger sliding on it. This effect can be reached through several technologies, but the results are similar, they offer the possibility to recreate different roughness or even textures on a perfectly flat glass surface.

PROTOTOUCH Project

This work is part of the European Marie Curie project PROTOTOUCH (www.prototouch.com). This project focuses on the next generation of haptic and tactile interfaces, for the implementation of high definition haptic feedback, i.e. the simulation of the tactile sensation of a texture or a pressed button. The main research goal is to exploit multiscale multiphysics simulation software, supported by neurophysiological measurements, for the virtual prototyping and optimization of tactile displays. With the associated research activities, the project will lead to a radical understanding of the underlying design principles and hence to the development of future generation devices. This objective was achieved by the deployment of an inter-disciplinary network involving experts in tactile displays, computer simulation,

cognitive and neural sciences, psychophysics, information processing, material science, tribology and medical rehabilitation. The inter-sectoral dimension of the consortium links fundamental and applied scientists and engineers in 7 universities.

This thesis is the result of a partnership between two members of the PROTOTOUCH Consortium: the company STMicroelectronics (Crolles, France), and the laboratory L2EP in the University of Lille1 (Lille, France). The main objective of my thesis within the consortium and through this partnership, was to develop a better understanding of tactile stimulation mediated by Ultrasonic Lubrication (UL) thanks to experimental measurements and to implement optimized design for the integration of this technology within touch based mobile phones.

Thesis Structure

This manuscript is organized into four parts:

Chapter 1: This chapter is an introduction to the biological mechanoreceptors involved in the human tactile sense. The anatomical distribution and the electromechanical characteristics of the multiple mechanoreceptors used to perceive touch are described in a first part. In a second part, a review of the different technologies adapted to the fingertip stimulation for mobile device is done. Finally, a more complete look is given to friction modulation mediated by Ultrasonic Lubrication (UL) effect, which is the focus of this thesis.

Chapter 2: In order to gain a better understanding of the UL effect and how it could be better harnessed for the improvement of friction modulation, a series of tribology experiments were conducted. This work, which combines in vivo experiment and measurements with an artificial finger, was used as the groundwork for the refining of the theory behind the Ultrasonic Lubrication effect. Following this better understanding, a set of new design rules for the realization of future UL devices will be presented.

Chapter 3: This chapter capitalizes on the explorative study of the UL effect performed in Chapter 2 and deduces the development process of a series of optimized tactile HMIs. The main problematics which occur while designing a new UL based tactile device are reminded, including integration and industrialization issues. In a second part, the development process of a piezoelectric driver and its control, dedicated to UL devices, is presented and characterized.

Chapter 4: With the help of an advanced UL tactile HMI presented in Chapter 3, a series of psychophysical experiments are conducted to evaluate the limits of the human perception of UL effect. Control systems are then presented to take advantage of these limits to improve the repeatability of the stimulation and to reduce the power consumption of UL devices.

1 LITERATURE REVIEW

Summary

1.1 INTRODUCTION

The last few years have seen the emergence of ubiquitous mobile devices and tactile interfaces. These devices take an ever-important place in our daily life, they are present in our home, office, cars and even pockets. The devices shown in Figure 1-1 are all common appliance of the consumer market in todays developed world.

The abundance of these novel interfaces raised the interest in touch based human-machine interactions and highlighted the problem of the lack of natural touch feedback in the existing generation of tactile displays. This problem was partly responsible for the first slow adoption of the touchscreen technology among consumers. First attempts made in 1985 to add tactile feedback to these first generations of touchscreen showed the ergonomic difficulty of the process [1].

Today's smartphones all possess basic haptic feedback thanks to low frequency vibrations. The search for a better tactile feedback, closer to the natural human perception, is ongoing. Multiple solutions are being explored to deliver improved haptic feedback on existing mobile platforms such as smartphones or tablets.

Figure 1-1: Common Interfaces based on touchscreen technology

The first part of this chapter is dedicated to a better understanding of the biological and anatomical concept of touch for humans. The perception of touch is a complex fusion of the signals sent by multiple specialized cells. The categorization of these structures is necessary to the understanding and classification of the different modalities of tactile exploration.

Based on this understanding of the human touch, a survey of the methods developed to simulate its effects will be presented. The final goal of these methods is to replicate the natural feel of touch on touch screen devices; or at least to create a tactile stimulation which makes sense for finger based perception

Finally, a deeper look will be given to one of these tactile simulation technologies, the Ultrasonic Lubrication (UL) effect. The application of this effect to a surface allows the dynamic reduction of the friction coefficient, which in turn enables the recreation of virtual patterns and textures. The methods used to design and develop a device integrating this technology will be presented.

1.2 HAPTIC: FOOLING THE HUMAN PERCEPTION OF TOUCH

Haptic and tactile perception, in combination with our other senses, is central in our understanding of the world. This central situation makes it difficult to create devices able to simulate the natural sensation of touch. This section focusses on the specialized mechanoreceptors and structures involved in shape, grip and texture perception to provide a basis for the development of specialized tactile illusion devices.

1.2.1 General anatomy of the human hand related nervous system

The somatosensory system, responsible for our understanding of the external world is only one of the five senses typically determined in humans; gustatory, olfactory, visual, auditory and somatosensory. It is the combination of information from all these modalities of perception that shapes the reality around us. Visual interface alone without touch based input feels inadequate and leads to inaccuracies. As soon as we interact with a visual object directly with our hands, a haptic feedback is required to give satisfaction of this reality to the central nervous system. Due to this fact, Haptics should never be analyzed alone, but as a part of the whole process of perception. Care must be taken to ensure the compatibility between what is seen and what is felt.

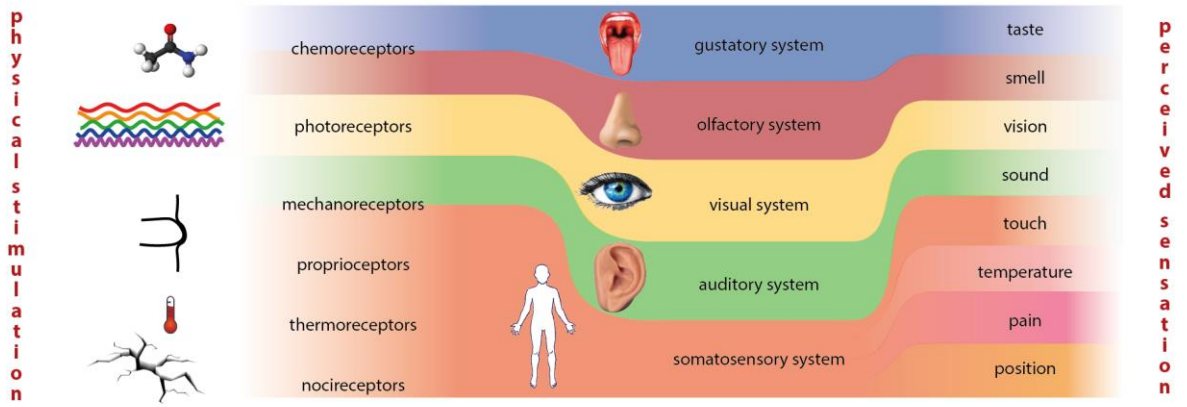

Figure 1-2: General organization of the human perception. The left side represent the different classes of receptors used to detect a stimulus. The center expresses the usual division of perception modalities and the right detailed the encoded perception. Adapted from [2].

A shown in Figure 1-2, the small subset represented by the somatosensory system and the haptic senses can be itself divided into multiples categories:

- *The Tactile sense,* created by the mechanoreceptors, gives us an ability to discriminate between textures touching our skin. This sense is also partly responsible of shape recognition and grip perception.
- *The Proprioception and Kinesthetic sense* allows us to position ourselves in space by giving us acceleration and rotation measure capabilities in all 3 axes. This sense also encompasses the knowledge of members' positions in space.

- *The Thermal sense* gives us information and warning about the absolute and relative temperature of objects. It is also able to differentiate between different thermal transfer rates.
- *The nociception* is responsible for the transfer of pain and all relevant warnings associated with touch exploration (excessive force, compression, shear, heat etc.).

All these senses have been exploited in the past to create illusion of real touch from a simulated contact. This thesis is focused on the tactile sense dedicated to touchscreen devices, the goal is to fool the human perception to create simulated textural environment. But before discussing the various means of haptic feedback and texture reproduction, a better understanding of the mechanoreceptors operating in the skin of the hand is desirable.

1.2.2 Cells and Corpuscles involved in tactile sense

As haptic implementation on smartphones mostly involves the hands and especially fingers, this study will focus on the tactile mechanoreceptors located in the fingers. The skin of the hand is populated by four kinds of mechanical sensing cells with a wide range of densities. The two-dimensional distribution, density and overall size of these mechanotransducers at the fingertips bear a lot of resemblances to the fovea of the retina [3]. Both, of course, present multiple differences as seen in [4]. The skin present on the fingertips and the palm of the hand is called glabrous skin due to its lack of hair follicles, and a different repartition of mechanoreceptors. These mechanoreceptive cells act by converting mechanical stresses and disturbances into action potential that are then transmitted by the nerves to the central nervous system. More information on the pathway of sensory transmission can be found in [5]. This review is focalized on the mechanoreceptors, but the glabrous skin of the hands also possesses other receptors responsible for the transmission of information such as pain and temperature.

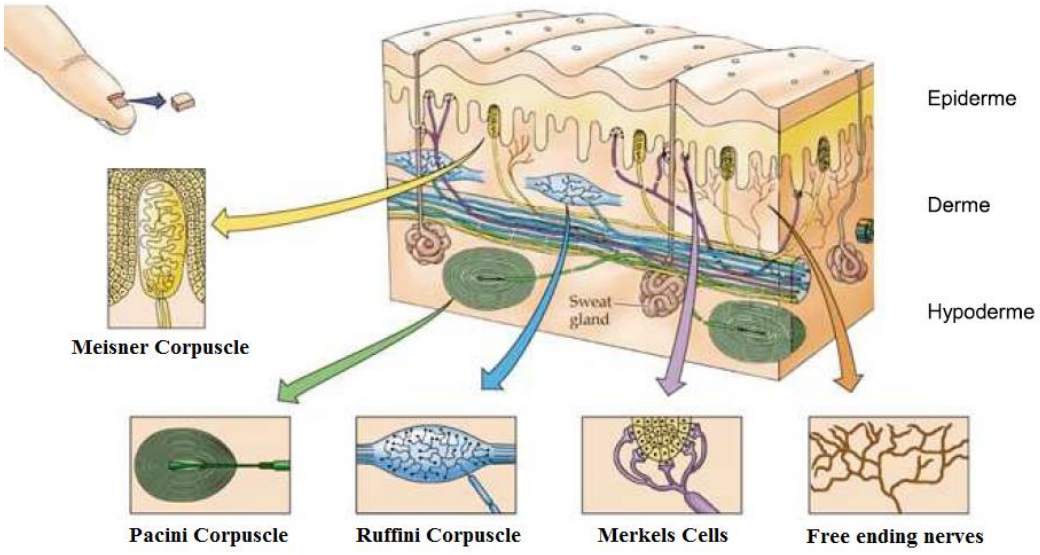

Figure 1-3: Section cut of the human skin displaying the mechanoreceptors, adapted from [6]

The mechanoreceptors present in the glabrous skin were difficult to observe and characterize due to their sub-millimeter size. Two methods were mainly used to understand their electrical and mechanical response: anatomical observation and electrophysiology. The first method helps reveal the presence of four categories of mechanotransducers connected to the myelinated nerve endings reaching the hands. This nerve ending then interfaces with the central nervous system. These receptors present different densities in the glabrous skin and anchor at different depth and positions in the primate hand. These location differences are thought to offer a larger range of static and dynamic mechanical perceptions.

Electrophysiology is a set of methods used to directly record the electrical signals sent by the mechanoreceptors during a mechanical stimulation of the hand's skin. To reach this result, an electrode is inserted in the arm of the participant and clamped directly in the ulnar or median nerve bundle. Microneurography (shown in Figure 1-4) uses this method to measure directly the signal transmitted by a single nervous afferent, allowing their precise classification.

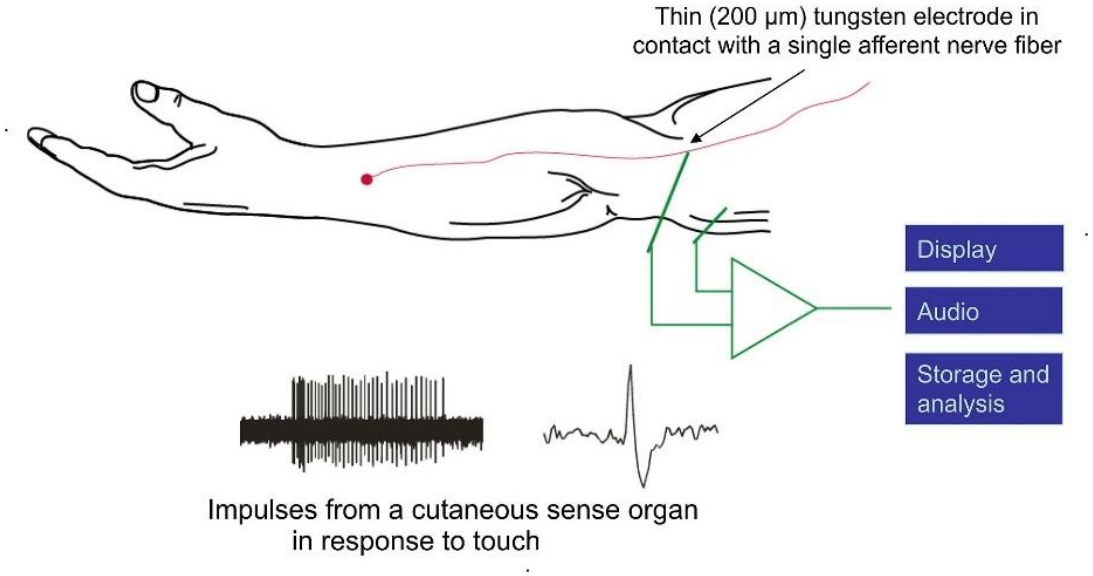

Figure 1-4: The microneurographic technique. An electrode is implanted into the nervous nerve bundle to find a single afferent [7].

The electrical signals corresponding to the afferents of the four receptors can then be categorized with two main parameters. First, the precision and size of their receptive zones; classified as type I for small and sharply defined receptive field and type II for larger and blurrier perception zone. The second main characteristic of the mechanoreceptors is the evolution of their response (called adaptation) during a mechanical stimulation; slowly adapting receptors (called SA) present a sustained response if the mechanical stress is maintained. On the contrary, fast adapting cells (FA) respond by a short burst of electrical signal at the start of the stimulation that declines rapidly. The anatomical and nervous knowledge of the four mechanoreceptors detailed here, mainly comes from the result of Johansson and Johnson studies on monkeys and humans [8].

- *The Merkel cells:* Slow Adapting (SA I).

Merkel cells are the most commonly found receptors in the human hand. They can be found in large number (up to 100 per cm² [8]) at the tip of each undulation of the dermis (for example patterns of the fingerprints). Positioned at the interface with the hypodermis, these cells also called “Merkel disks”, are connected together locally (maximum 200 µm) to form a Neurite complex connection of up to 90 of them. This Neurite complex is then fused into a single SA I nerve afferent.

Figure 1-5: Single Merkel cell afferent firing in function of time. Two indentation depths (0.59 and 0.69 mm) over the receptive field of the mechanoreceptor. A clear correlation between the indentation and the firing rate is visible. The long adaption time can be seen in the almost continuous firing of the afferent as long as the probe is indented in the skin. The bottom line represents the profile of indentation [9].

As measured in primates, these afferents’ discharge occurs at a rate that is linearly correlated to the indentation depth of a square probe (Figure 1-5) [10]. SA I are limited, by their continuous activation, to the perception of low frequency signals, and thus are used to discriminate coarse texture. Their sharp detection field and almost continuous activation help with the precise detection of relatively large patterns and forms.

- *Ruffini corpuscles :* Slow Adapting (SA II).

Ruffini receptors are a contentious topic due to their inexistence in monkey and their difficult study in human. Adding to the controversy is the fact that these mechanoreceptors have the sparsest density with only a few ever detected by biopsy in the hand, but nevertheless represent up to 15 % of the nerve’s afferents found by microneurography [11]. Nevertheless, an analysis of the found afferents reveals a clear association with lateral stretch of the skin which could help detect the start of slip.

Their presence between the skin and the nail and their detection of large tangential force [12] at the fingertip could be explained by a role in the proprioception of the hand and fingers. They are located deeper in the dermis than Merkel and Meissner corpuscles as can be seen in Figure 1-3.

- *Meissner corpuscles:* Fast Adapting (FA I).

Similarly to the Merkel mechanoreceptors, the Meissner corpuscles can be found at the interface between the dermis and hypodermis. Located inside the skin undulations, they are directly impacted by any stretch of the finger skin due to a natural lever-like amplification

effect [13]. Composed of multiple Schwann cells stacked together, they are extremely close to the surface of the skin.

Figure 1-6: Single Meissner afferent firing in function of time under different indentation speeds. Firing mainly occurs during the transient part of the movement of the probe and it adapts fast. The bottom line represents the profile of indentation [9].

This amplification effect and closeness to the surface, allow these cells to have an extremely low detection threshold of short mechanical stretches of the skin as seen in Figure 1-6. It has been reported that generation of nerve signals in the afferents can be produced by a single 2 µm dot sliding under the finger [14]. With a high spatial density and a fast adaptation, the FA I mechanotransducers are thought to be the main mean of slip detection of a grasped object [15]. They respond to relatively low frequency which does not give them a big role in fine texture discrimination.

- *Pacini corpuscles :* Fast Adapting (FA II).

Finally, the Pacini corpuscles, found deep into the dermis of the hand, are the easiest to study anatomically. Indeed, these cells have the biggest dimensions of all mechanoreceptors (between 1 and 4 mm) and can be kept alive in a petri dish for precise electromechanical studies. FA II presents an ovoid shape and is connected to a single myelinated afferent [16]. About 350 of these corpuscles can be found in the index finger and 800 in the palm of the hand [17]. These corpuscles are strongly responsive to high frequencies of vibration as shown by their phase locking on the period in Figure 1-7. They are the most sensitive of all types with a sensitivity of 40 nm and 3 nm when stimulated directly *in vitro* [16]. They also offer the largest bandwidth of detection with their range of 40 Hz to 1 kHz.

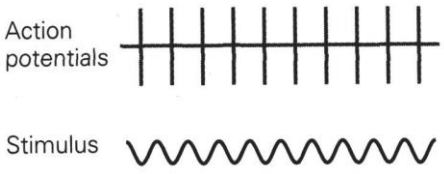

Figure 1-7: Single Pacinian afferent firing in a phase locked manner with the 110 Hz frequency of stimulation. The bottom line represents the profile of indentation [9].

This broad bandwidth and extreme sensitivity of fast periodical stresses contribute to make them the main receptors used for fine texture discrimination and hand-held tool usage. In contrast, their sensitivity to purely spatial deformation is almost null.

1.2.3 Discrimination of frequencies

As described in the previous section, the four human mechanoreceptors express different sensibilities to the multiple kinds of stimulus that we encounter every day. This extends to the discrimination of frequencies, which is fundamental to our perception of texture and hand-held tool usage. A comprehensive measurement of the frequency response of each of the four mechanoreceptors was done by Johansson et al. in 1982 [18]. After a full adaptation of the finger to the indentation created by the stimulating probes, measures of frequency discrimination to a sinusoidal stimulation were done.

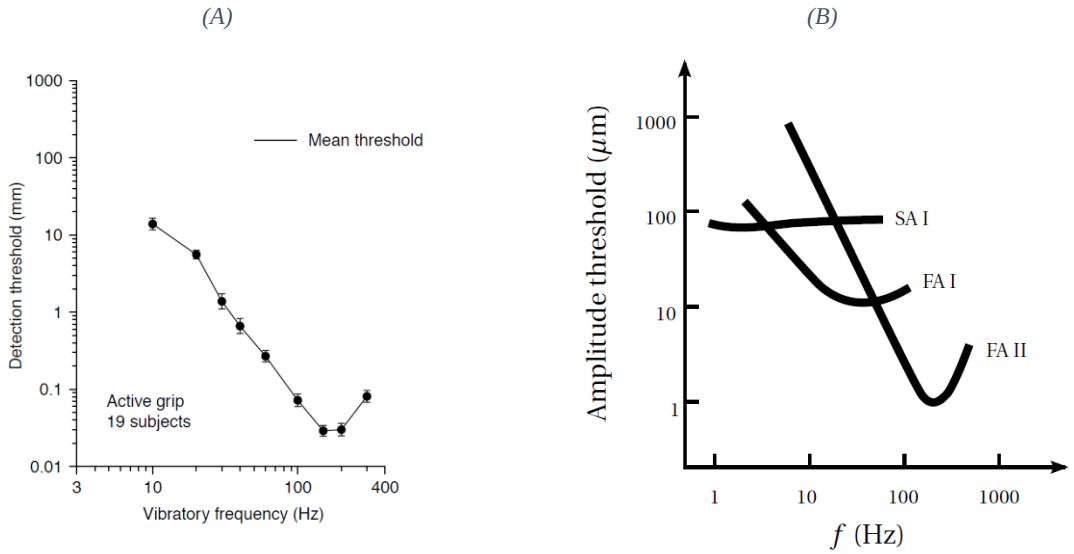

Figure 1-8: Detection range of the mechanoreceptors in the human hand. (A) Shows the psychophysical threshold of detection reported by participants when subjected to the vibration of a 32 mm rod held in the hand. Adapted from [19] (B) Frequency range of Slowly Adapting I and Fast Adapting I, II mechanoreceptors [20].

As succinctly described in the previous paragraph, both SA receptors present a slow adaptation time with a bandwidth discrimination between 2 and 32 Hz. FA receptors present a more contrasted discrimination range. The Meissner Corpuscles (FA I) respond highly to stimulation from 8 to 64 Hz, while the Pacinian cells (FA II) have a maximum sensitivity between 64 and 400 Hz (but can detect vibration up to 1 kHz). Moreover, the signals measured by the FA II receptors are significantly more sensitive than the Meissner FA I, with a 20 to 30 dB difference. As summarized in [20] the maximum range of each mechanoreceptor can be seen in Figure 1-8 (B). It is interesting to note the similar behavior between the psychophysical detection curve in Figure 1-8 (A) which involves all the mechanoreceptors, and the mechanoreceptors' response in (B). This is especially true for the FA II which are receptive on almost all the frequency range.

1.2.4 Creating Haptic Illusions

The high concentration of multiple kinds of receptors, presented in the previous section, helps to infer the correct characteristic of the object being explored, even in the absence of complete data. In some cases, an incomplete input of sensory stream can cause tactile illusion with similar mechanisms as well-known optical illusions. All haptic feedback systems use this

principle to generate “virtual” mechanical sensation for the user, that is not physically present around him.

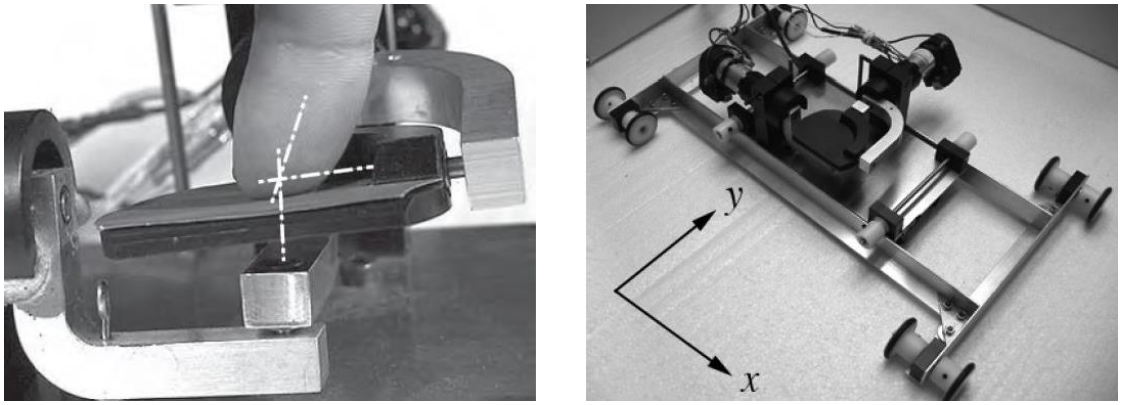

Figure 1-9: Device creating a virtual curvature sensation for the user [21]

An example of such an illusion is the feeling of curvature that can be simulated using specific apparatus like in [22] [23]. An implementation of such a device is illustrated by Figure 1-9. The feeling of curvature is obtained by orienting the finger’s contact plate in function of the lateral position of the device.

As previously mentioned, these illusions have been exploited for haptic feedback in multiple studies. Figure 1-10 describes the relation between the interaction mode being exploited and the Technology used to achieve the goal. Although the newest references are missing, this graph gives a good idea of the pallets of technologies available.

A multitude of technologies and associated applications which were tested to provide new and useful haptics cues to users. Most of these technologies proved to be quite effective in their specific application cases, but failed to be sold industrially due to manufacturing difficulties, or size of the market concerned (this is the case of the device presented in Figure 1-9). Nevertheless, two interaction modes found a large success with the public: normal indentation (braille technologies) and vibrations (standard mobile device and game controller feedback).

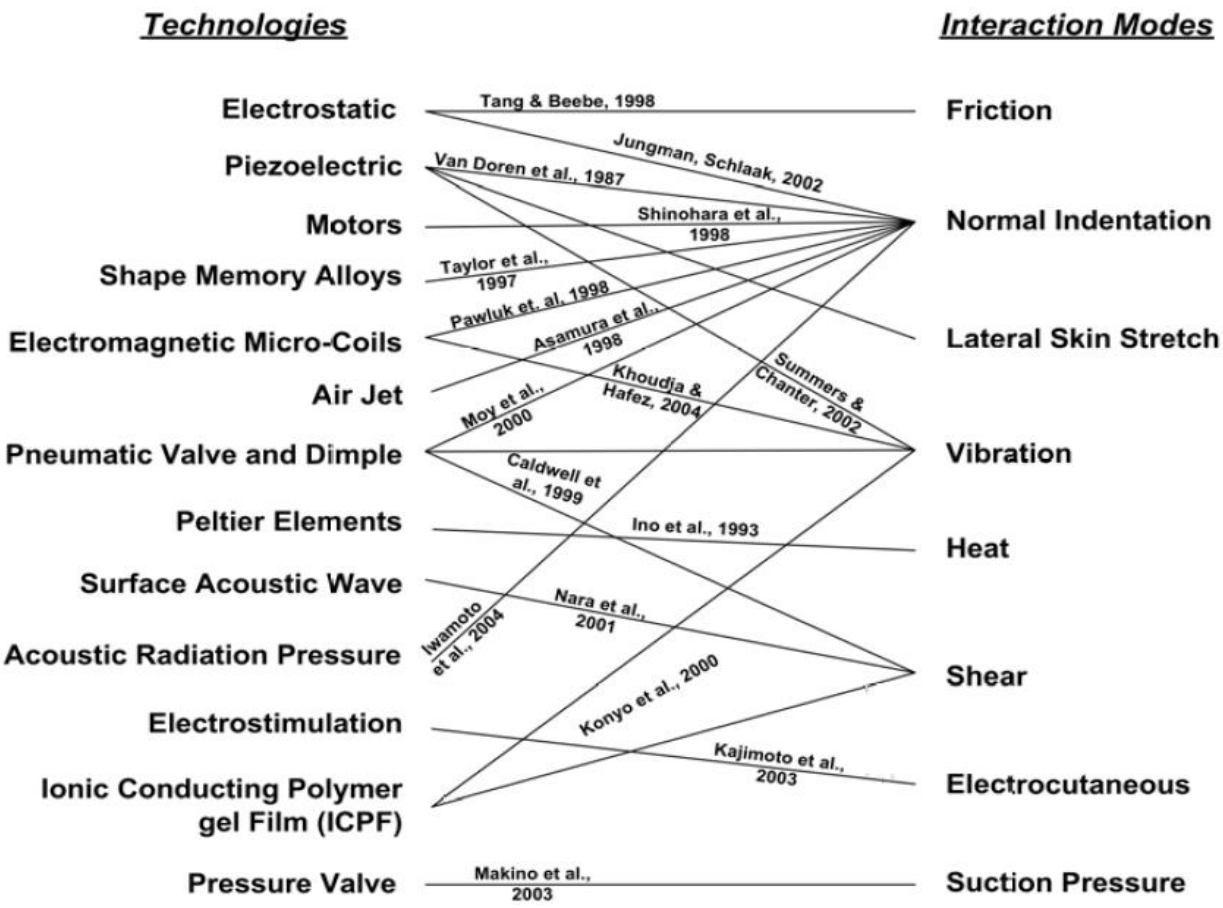

Figure 1-10: Representation of haptic devices' technologies and their interaction modes. Adapted from [24].

1.3 TACTILE STIMULATION ADAPTED TO MOBILE DEVICES

Most of the interaction modes presented in Figure 1-10 are uneasy to integrate with mobile applications due to the form factors of the technologies used. Such devices generally involve one or multiple bulky actuators and mechanical transmission. To alleviate this problem, other solutions have been developed with portable device and touch-screen in mind.

This thesis focuses on the way to transmit tactile information to the user, and more specifically, texture illusion based tactile information. Ultimately, the goal is to integrate this type of tactile feedback into mobile devices to offer a more natural stimulation. Texture based stimulation is relying more on the FA II mechanoreceptors to imitate a real touch interaction (compared to simple low frequency vibrations which affect only the SA I and FA I).

This section reviews the haptic systems applicable to the large touch screen now ubiquitous in all mobile devices. Today, only vibrating load stimulation has been implemented into consumer devices. However, texture reproduction presents a lot of potential and attracts the attention of industrials and consumers; if its industrialization issues find a solution, it will make its entry into the consumer market.

1.3.1 Growth of the haptic industry

Haptic promises an increase in the comfort, ergonomics and precision in the use of touch based interfaces. With a growth already confirmed since multiple years, haptics applied to the new “Internet of Thing” connected devices promises to continue its expansion for the years to come. A forecast created by LuxResearch predicted an important inflexion point between 2014 and 2015 for the market of haptic touch screen [25]. But the market of haptic itself is larger than that, especially with the addition of upcoming virtual reality systems, its ecosystem of game controller, and professional design tools.

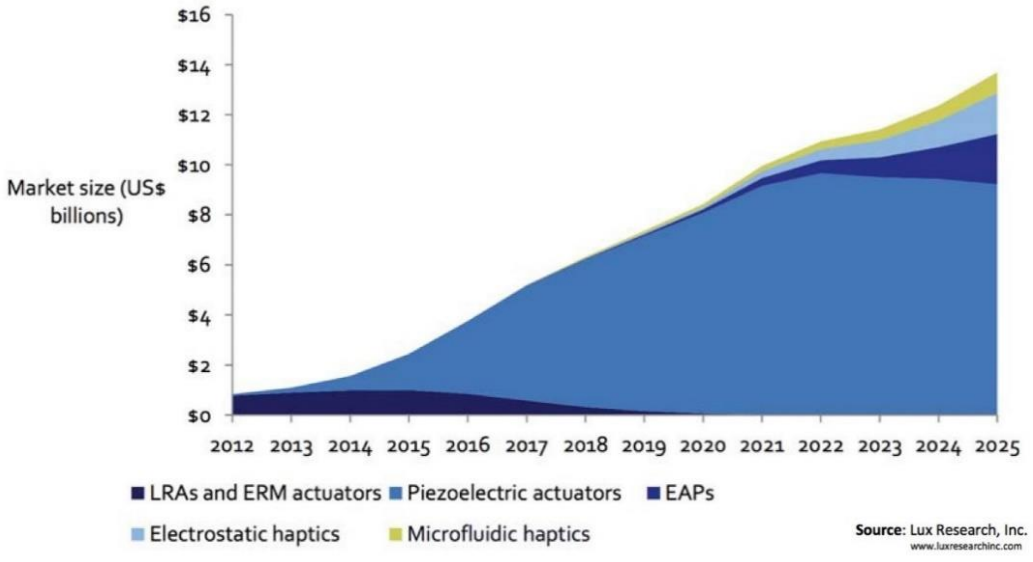

Figure 1-11: Market Forecast of the touch panel integrating haptic feedback technologies [25]

A shift in the technology used to create vibrations on mobile phones and tablets is already underway as can be seen in Figure 1-11 with the growth of piezoelectric actuators' use. As for Friction based tactile interfaces, they are expected to enter the mainstream consumer market in less than 10 years with the introduction of electrostatic technology.

1.3.2 Vibrating Load

The most common tactile stimuli used in mobile device today are based on the generation of low frequency vibration in the device held by the user. Multiple technologies are used to generate this effect in smartphones as can be seen in Figure 1-12.

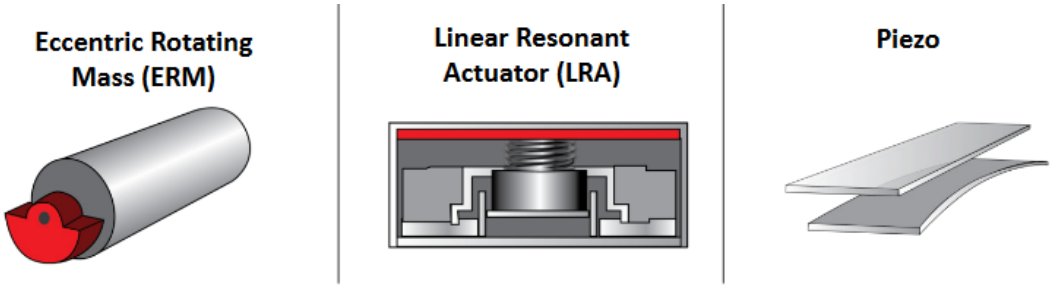

Figure 1-12: Three types of vibrotactile actuators used in mobile devices [26]

The three mechanical solutions shown above return a strong, low frequency vibration to the hand of the user. Multiple companies such as Texas Instruments Inc™ (USA), AAC technologies Holdings Inc. (China), Densitron Technologies Pic (UK) and Immersion Corp (USA) share most of the world market.

The first solution, known by the name of Eccentric Rotating Mass (ERM) is the most well-known solution for haptic feedback in phone, tablets and gamepad controllers. It is implemented in most devices nowadays [27]. This technology uses a small electric motor connected to an asymmetric load to generate vibration in the handheld device. First used as a mean of force feedback in gaming application, it is nowadays implemented in complement with graphical user interface (GUI) in most touchscreens. ERM are the cheapest solution to integrate but present a relatively large form factor and the highest power consumption of the three technologies, with up to 5 % of the total smartphone consumption [26].

(a) *(b)*

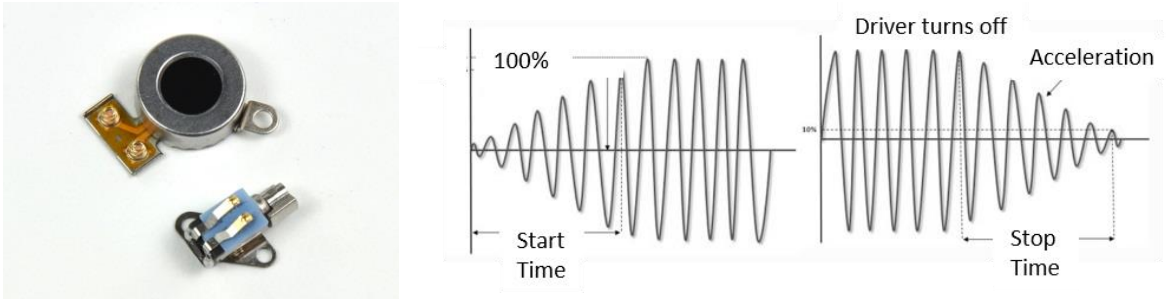

Figure 1-13: (a) ERM and LRA actuators respectively inside the iPhone4© and iPhone5© of Apple™ (b) Acceleration and deceleration pattern of ERM motors

The Linear Resonant Actuator (shown in Figure 1-13 (a)) is able to generate a similar amplitude of vibration than the ERM but presents the advantages of a smaller form factor and power consumption (only 2.5 % of the total energetic consumption for a normal smartphone day use [26]). LRA resonant mode of operation limits its frequency bandwidth to only a few hertz, which reduces the sensory modalities able to be excited by it. Moreover, its optimal resonant frequency tends to drift due to temperature and needs to be actively tracked by the smartphone for reliable tactile feedback.

Piezo actuators are relatively new and start to be integrated into the last generations of devices. They present an extremely low form factor which makes them interesting for high tech smartphones. Their power consumption, while smaller than the other to generate a simple “click”, is similar to the ERM for longer “buzz” type of stimulation.

1.3.3 Texture based tactile feedback

While the ease of integration of vibrating load made it quickly ubiquitous, this solution offers at best a limited feedback in the tactile sense; as a matter of fact, most of the feedback is perceived as a vibration of the whole hand and thus, uses the kinesthetic more than the tactile sense. On the other hand, users may be interested by a better tactile feedback, only perceived by the finger, and closely related to texture simulation. This subsection presents three technologies that offers the possibility to recreate the illusion of real textures. These solutions aim to modify the friction coefficient between the finger and the plate.

1.3.3.1 Surface Acoustic Wave

One of the technological approaches is to apply Surface Acoustic Wave (SAW) to the medium. This approach was first described by [28]. Using piezoelectric material glued on the surface of the display, a SAW in the Megahertz range is generated on it. This makes it possible to temporally reduce the friction between a slider part, composed of a plate with small steel balls, and the medium where SAW is propagated. In later design, it was shown that the steel balls were not necessary if using a rigid slider (metal plate). Transparent device with an integrated LCD was also presented [29]. SAW are characterized by a wave frequency above 1 MHz and a vibration amplitude around 1 nm.

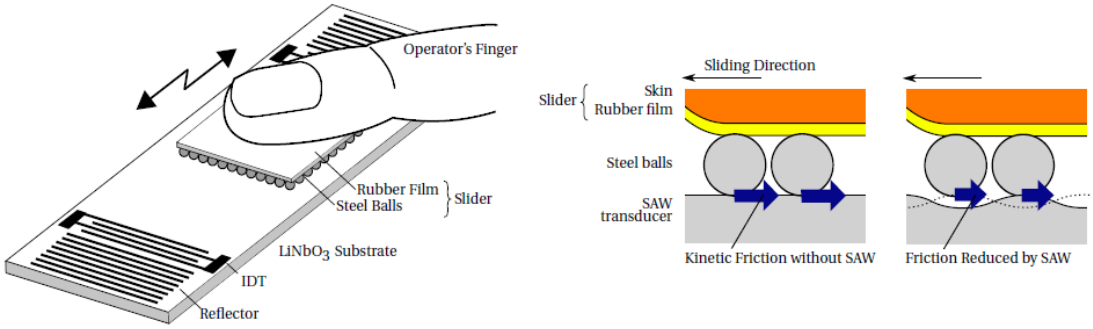

Figure 1-14: First implementation of SAW based haptic device with ball bearing under the slider [28].

This interface might be interesting due to its extremely simple potential integration into existing touch screen devices. Indeed, as the wave propagate on the surface of the substrate, it might be possible to fully glue the resonating glass on the screen underneath, improving the integrability and reliability. Besides, glasses incorporating the SAW principle as a mean to measure the position of the finger are already sold worldwide for their small form factor of detection and extreme robustness (use in ATM and diverse ticket vending machines). Combining both technologies would present a large reduction in cost and complexity.

But the necessity of a sliding interface is extremely constraining for an application into a mobile platform, consumers would perceive this interface as a step backward in term of integration and ease of use.

1.3.3.2 Increasing the Friction: The Electrovibration stimulation

Another way to generate tactile information for the user was found first by Mallinckrodt in 1954 [30] whom reported: *"... that dragging a dry finger over a conductive surface covered with a thin insulating layer and excited with a 110 V signal, created a characteristic rubbery feeling"*

Applying a voltage between a surface and the finger with a small isolator in between creates an attractive force (shown in Figure 1-15). While this force is not perceivable by the user directly, its consequence on the friction between the finger and the surface is relevant on the haptic point of view, especially when the friction is modulated as the finger is sliding above the surface in an exploratory movement [31]. This solution also allows for multi-touch solution [32]. The main drawback is the need for a high voltage (in the order of the kV) with a thin insulation layer prone to abrasion by repeated use [30]. Multiple laboratories and companies are nonetheless involved in improving and commercializing this technology. Recently, a new model has been proposed to explain the frequency dependence of the electrostatic force [33] and the technology has been merged with another one to improve haptic feedback [34].

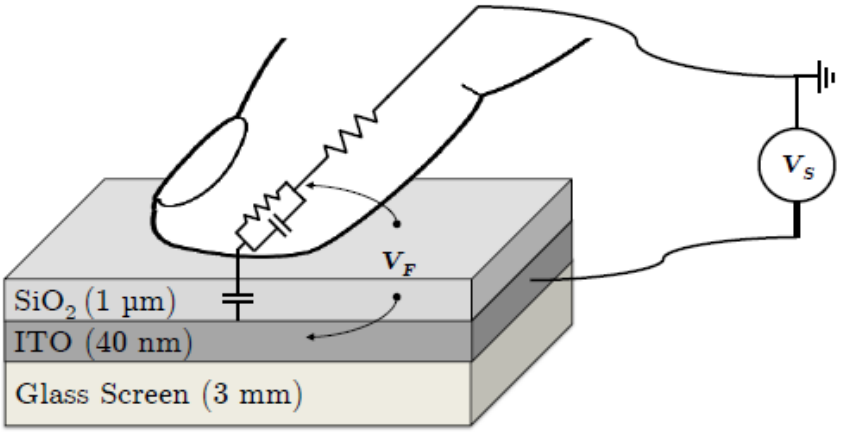

Figure 1-15: Principle of an electrovibration haptic device integrated into a transparent screen. ITO is a thin-film conductive and transparent material used to propagate the charge across the whole screen of the device. SiO2 is also a thin-film but acts as an insulator and can be deposited in an extremely small stack, improving the friction increase effect [31].

However, even with this constraint, startups have been created in recent years with the ambitious goal of pushing this technology to the mass consumer as part of our standard smartphones: Tanvas™ and Senseg™ (recently bought by the Chinese phone maker O-Film), are currently selling demonstrators and developments kits as seen in Figure 1-16.

(A) *(B)*

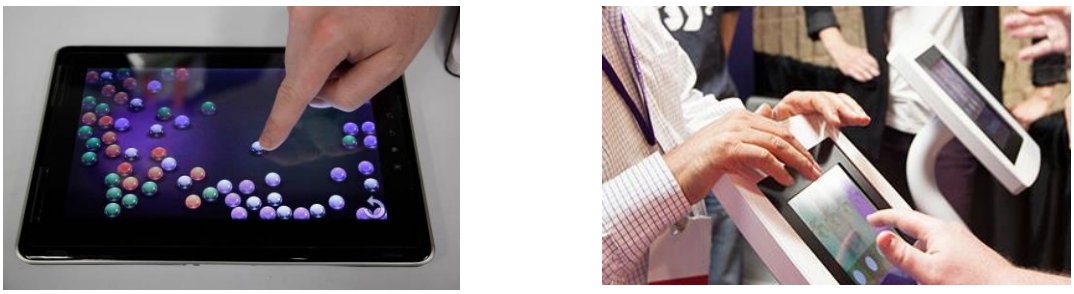

Figure 1-16: Development Kit and showcases by startups involved in electrostatic stimulation (A) Shows the dev-kit tablet developed by Senseg™, company recently bought by the Chinese phone maker O-Film (B) Showcase application by Tanvas™ in WorldHaptics 2016

It must be noted that despite the progress made by these new companies, the electrostatic stimulation still faces large challenges. The large cost of the thin-film deposition (both ITO and SIO2 shown in Figure 1-15) and the fear of the high voltage close to the skin makes it difficult to sell to the mass market.

1.3.3.3 Decreasing the Friction: The Ultrasonic Lubrication stimulation

Another way to control the friction between the finger and a surface relies on Ultrasonic Lubrication (UL). This effect, applied to the human hand, was first described by T. Watanabe and S. Fuikui in 1995 [35]: when a planar surface is put under ultrasonic vibration, a change in the dynamic friction coefficient between the finger and the surface can be observed. The dynamic friction coefficient is then shown to be reduced more and more for an increase of the amplitude of vibration.

The first theory proposed to explain the phenomenon is the squeeze film effect, as first described by O. Reynolds (1842-1912) [36]. Similarly to friction free air-table, a local overpressure is created between the surface of two objects, which then reduces the measured dynamic friction coefficient between these objects [37]. While a porous material and a compressor cannot be implemented in a portable device, squeeze film effect showed that it can compress the air locally under the finger by applying an ultrasonic vibration to the device. As seen in Figure 1-17, a rough surface is perceived by the participants as smooth when an ultrasonic vibration is applied to the surface. These first studies use a frequency of vibration just above hearing range (around 20 kHz) but not too large, to limit the complexity of actuation and control.

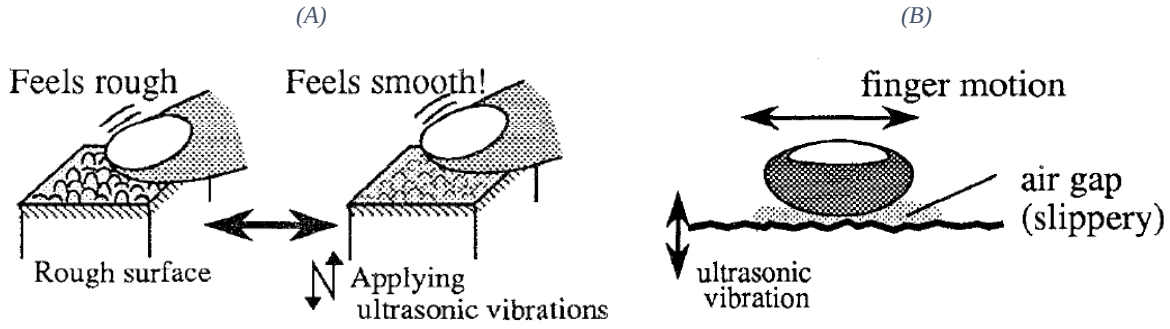

Figure 1-17: T. Watanabe & S. Fuikui description of ultrasonic vibration applied to haptic feedback

The methodology was then explored again by M. Biet [38] in 2007, to put a full copper-beryllium surface under vibration by taking advantage of a resonant mode of vibration. Actuated by a matrix of Lead Zirconium Titanate piezoelectric ceramics, as seen in Figure 1-18, the technology was capable to reduce strongly the friction coefficient across a large area.

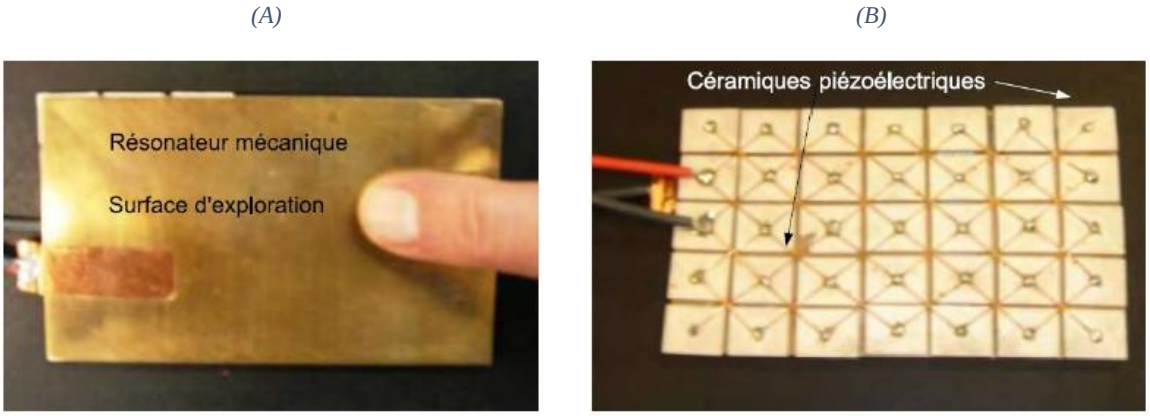

Figure 1-18: Copper-beryllium ultrasonic haptic device. (A) Surface explored by the user, friction is reduced when the plate is under vibration. (B) Matrix of PZT actuators used to put the plate under vibration

From these first studies, multiple iterations and optimizations have been proposed through the years. These studies will be described in details in the following section.

1.4 TACTILE STIMULATION MEDIATED BY ULTRASONIC LUBRICATION EFFECT

Ultrasonic Lubrication presents multiple advantages compared to other tactile stimulation techniques. First, it provides a strong tactile stimulation felt directly by the fingertip without any additional slider, as for SAW. Second, there is no issue with large voltage close to the skin since the piezoelectric actuators are placed under the surface to explore and can be supplied by low voltage. This section first presents the evolution in the design of UL stimulation since the discovery of the phenomenon in 1995. A second part then focuses on methods developed to help with the design and development of such a device.

1.4.1 Development of the UL based tactile stimulation

The following subsection describes in details the principle of UL stimulation and the optimizations done since its inception.

1.4.1.1 First observation of the UL effect on Human fingers

As first defined by T. Watanabe in [35], UL generates a tactile sensation by temporarily changing the perception of the state of the surface, from rough to totally "smooth". In his experiment, a steel beam is led in vibration at its extremities by two Langevin actuators. At a frequency of 77kHz, a resonant flexion of the beam up to 2µm is observed. A participant was then asked to displace his finger across the beam. Participants systematically noticed a difference in the perceived roughness of the beam between the vibrating and non-vibrating states. The limits of this effect were then quantified by presenting beam of different inherent surface roughness. A seen in Figure 1-19, they found that for a higher roughness of the beam a larger amplitude of vibration was necessary to reach a "smooth" perception of the surface by the participants.

(A) *(B)*

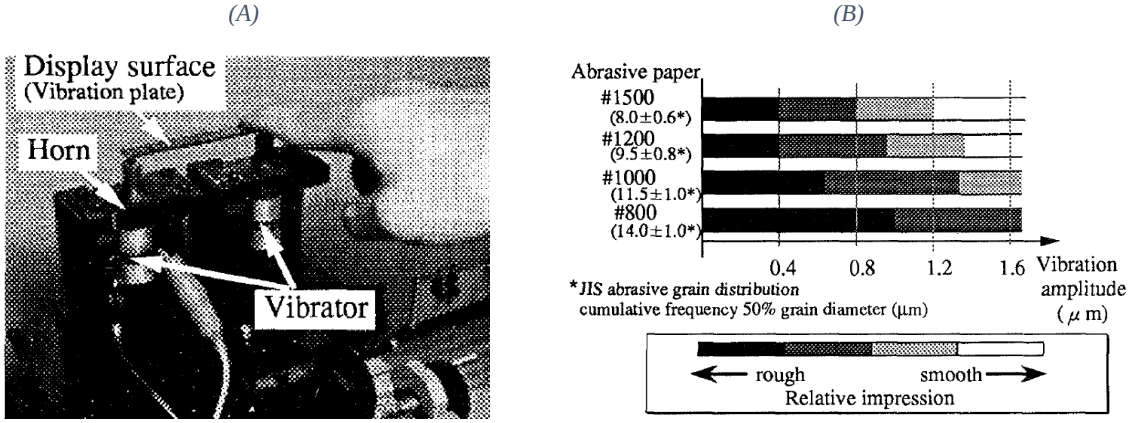

Figure 1-19: Watanabe Experiment in [35]. (A) Experimental setup with its two Langevin actuators. (B) Perception of the roughness of surface in function of the amplitude of vibration of the beams. Four beams of different inherent roughness are presented.

Subsequent measures with different modes of resonance of the beam showed that the change of roughness perception does not occur under a frequency of at least 10kHz.

In this first paper Watanabe proposed the mechanism of "squeeze film" to explain the reduction of the dynamic friction coefficient observed between the beam and the participants' fingers. The squeeze film effect is well known in industry to provide a "dry" lubricating process; one of the most commonly found application is its use in hard-drives to provide a self-bearing between the reading head and the disks' surface [39]. In this application, the air film is created by the fast tangent speed of the reading head compared to the disk's surface. Squeeze film model will be presented in more details in Chapter 2.

1.4.1.2 Evolution of Ultrasonic Lubrication based displays

Since this first experimental proof of the UL effect by Watanabe, multiple prototypes and demonstrators have been built. In most cases, a square surface is put under vibration at an inaudible frequency (above 20kHz) with the help of a resonant mode. In order to present an homogeneous effect across the surface, a standing wave mode of vibration is generally preselected by simulation before building the device (see Figure 1-20 A). The vertical displacement achievable by this method is highly dependent on the precision of the excitation frequency as seen in Figure 1-20 (B).

(A) *(B)*

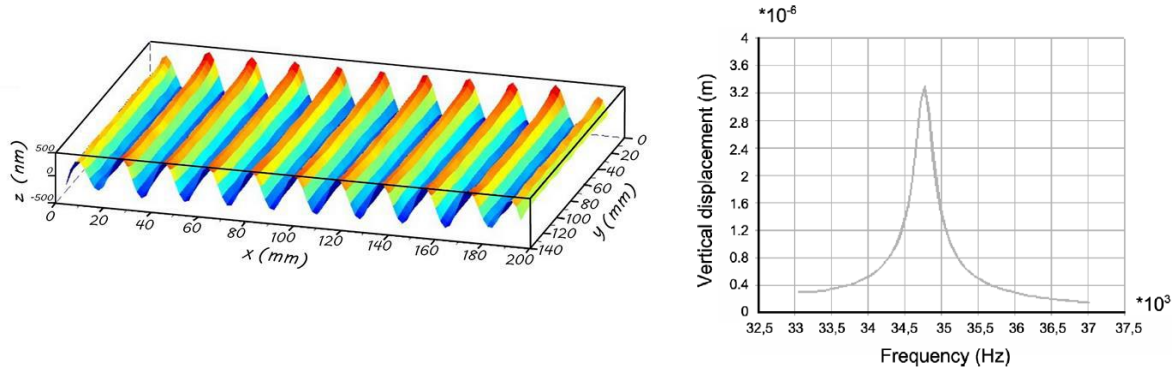

Figure 1-20: Simulation of the dynamics of the resonating plate before its creation. (A) Longitudinal lamb wave, propagating in the direction of the long axis of the rectangular plate. (B) Results of an harmonic analysis: absolute vertical displacement of a surface point in function of the frequency (ANSYS software®), adapted from [40]

Using these methods, the first tactile feedback devices were proposed by Windfield et al. in 2007 [41]. This new tactile interface called the Tpad was composed of a circular piezoelectric actuator glued to a 25mm diameter glass that can be touched and explored by the user. The vibration can be modulated in function of the position of the finger which enables the creation of virtual texture and tactile patterns. Following work increased the size of the device and added LCD underneath [42] [43] [44].

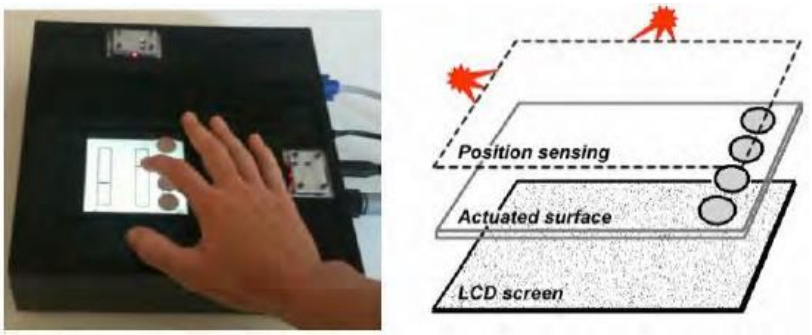

Figure 1-21: Tpad created by Windfield et al. at Northwestern University [41]

Another important study was performed in the L2EP in University Lille1 by M. Biet under the supervision of B. Semail; a copper-beryllium plate with piezoceramic elements, attached under it in a matrix pattern, can generate strong tactile sensation to the user [38] [40].

Subsequent developments performed in the L2EP made possible the integration work of the technology in a mobile package and in multiple form factors [45] [46] [47]. Follow up work was presented implementing a transparent device with a LCD underneath [46], shown in Figure 1-22. These works lead to the design of the Stimtac®, an integrated haptic device [48] [49].

(A) *(B)*

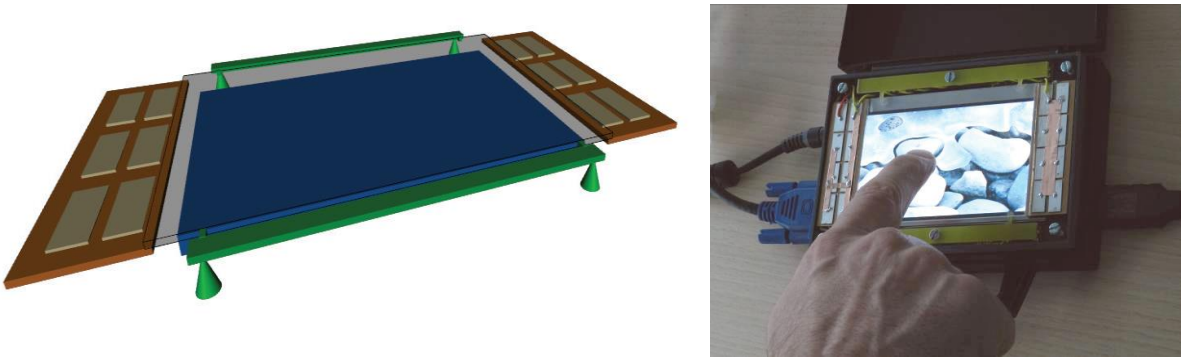

Figure 1-22: Transparent UL tactile stimulator based on the Stimtac® [46]. (A) Schematics of the resonant tactile stimulator with the LCD underneath in Blue. Forces sensors (Green Cones) are used to measure the position of the fingertip (B) The final assembly of the tactile stimulator in operations.

The finger position in these devices is inferred by reading 4 strain gauges on the sides of the screen. A single or a double row of piezo-actuators on the side of the transparent interface is used for actuation. Finally, in recent designs, some of the piezo-ceramics are used as sensor (the bending constraint generates an electric field that can be measured). To increase the repeatability of the haptic signal transmitted, the amplitude and phase data can then be used to close amplitude and frequency control loops with a microcontroller (MCU) [50].

To be complete on UL devices, it may be noted that other institutes have worked on the analytic modeling and Finite Element Modeling of lamb wave propagation in resonator to induce friction control [51] [52] [53] [54] [55].

1.4.1.3 Optimizations and coupling of Ultrasonic Lubrication with other mode of stimulation

The concept of Ultrasonic Lubrication has been used in combination with other technologies to create enhanced haptic feedback effect. The first coupling was presented by Erik C. Chubb in 2009 with the ShiverPad: a device capable of controlling the shear force on a bare finger. Using an UL TPad developed by the same laboratory, coupled with a lateral linear actuator, the authors could generate a force at the tip of a static bare finger in contact with the UL surface. As seen in Figure 1-23, the UL effect is only activated when the surface is moved in one direction, resulting in a net force on even an immobile finger. This effect was then optimized in subsequent study to reduce the perceivable artifacts [56].

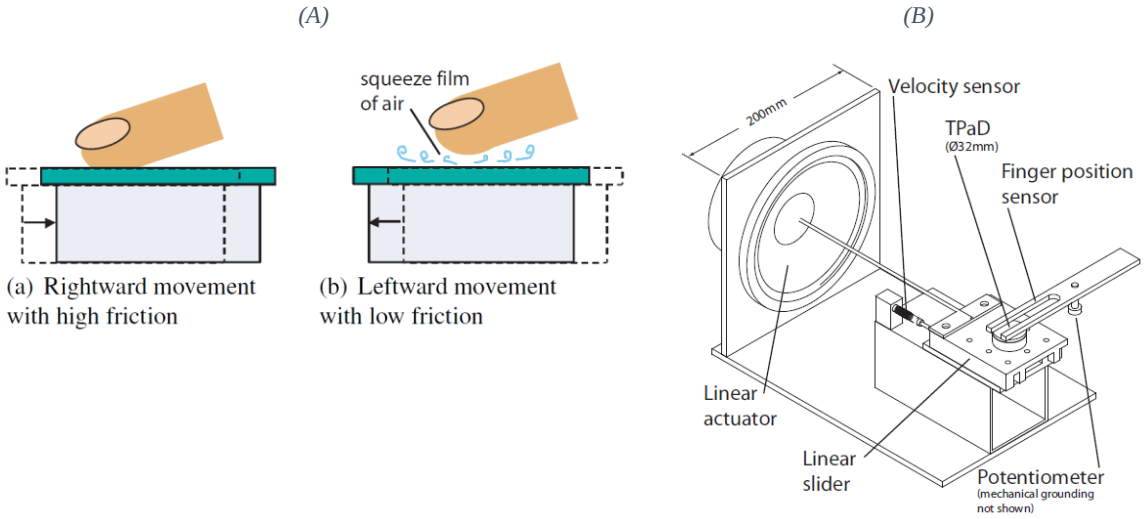

Figure 1-23: The ShiverPad proposes a solution to generate forces at the tip of a static finger [57]. (A) Friction reduction effect of UL is applied synchronously with the lateral vibration to generate a force (B) Use of a TPad connected to a lateral linear actuator.

A second notable coupling has been proposed by F. Giraud in [34]. In this study the friction reduction effect of UL is combined with the friction increase effect generated by electrostatic stimulation presented in section 1.3.3.2. Being this concept is the hope that, by combining these technologies, it might be possible to generate an enhanced friction modulation effect (with even more perceivable differences between the states of high and low friction). Later validated by D. Mayer in [58], an in-depth comparison of both effects showed that despite its slowest modulation dynamics, UL modulation provide a larger range of stimulation compared to electrostatic displays, going from a coefficient of friction as high as 1 to frictionless contact. The coupling of both effects on the same devices would potentially be able to offer the best of both world, strong and high frequency friction modulation.

1.4.2 Design and Optimization of an Ultrasonic Lubrication plate

The UL devices presented in this chapter and in the rest of this thesis were designed using similar methods. This section explores these methods to provide an understanding of the creation process involved in their development.

The fundamental goal of the procedure is to create a flat rectangular plane of the required dimensions that presents a resonant vibration across its surface. When building experimental devices, our choice goes to standing wave mode of vibration. Specifically, a Lamb waves presenting a homogeneous maximum amplitude of vibration across the whole surface is selected. Lamb waves, are elastic waves whose particle motion lies in the plane that contains the direction of wave propagation and the plate normal (the direction perpendicular to the plate).

1.4.2.1 Iterative Simulation Method

The first step of the design is to model the geometry of the plate and the piezoelectric actuators with a Computer Assisted Design (CAD) tool (Especially for complex geometries). The final geometry can then be transferred to finite element software (Salome Meca®, Comsol®, ANSYS® or Coventor®). When the geometry has been designed, and meshed with the correct material properties (Figure 1-24 (a)), it is then possible to calculate the Eigen frequencies for the range of frequencies of interest (typically between 25 kHz to generate the lubrication effect and to be above audio, and 100 kHz for ease of control). The size of the meshing has a large effect on the accuracy of the FEM simulation, proper care should be taken to make sure a meshing small enough is selected as in Figure 1-24 (b).

(a) *(b)*

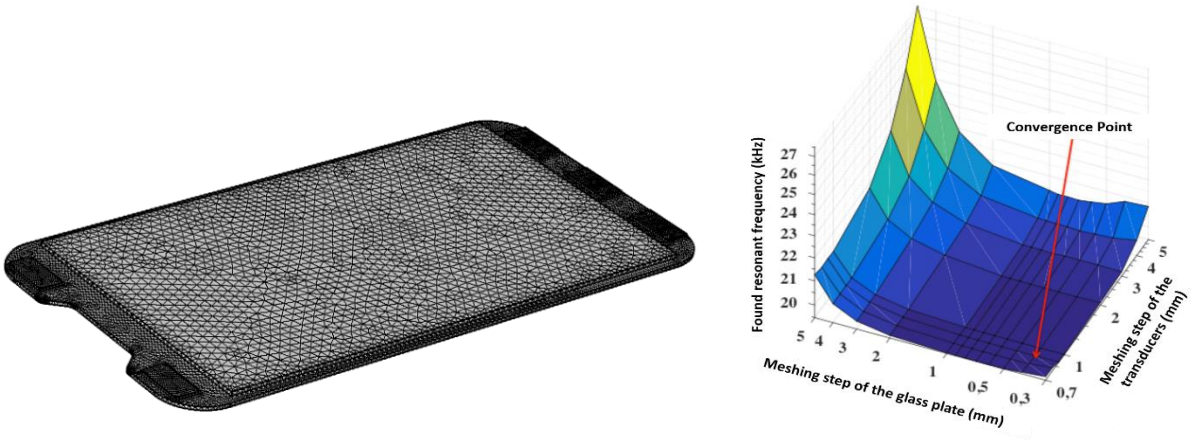

Figure 1-24: (a) Meshing of a complex glass plate supporting piezoelectric ceramic actuators and a second layer of glass touchscreen on the top (b) Convergence of the meshing to determine the resonant mode of vibration [59].

Once simulated, the vibration deformation pattern for each resonant frequency can be displayed and the proper Lamb wave can be selected. One important factor in this choice is the distance between the nodal lines. Devices with large spacing between nodal lines present a noticeable decrease of the friction reduction when the finger is above the nodal lines. A distance inferior to the width of a fingertip is chosen to avoid these effects (usually inferior to 8 mm [38]). Once a specific resonant mode is selected, two factors need to be optimized before the geometry is chosen:

- The presence of parasitic modes of vibration too close to the frequency of the selected Lamb wave needs to be checked. These parasitic modes might get excited during the experiment due to a local variation of damping caused by the user's finger. These parasitic modes can reduce the electro-mechanical coupling and thus the maximum amplitude of vibration which then affects negatively the friction coefficient reduction. Typically, these modes of vibration present crisscrossing nodal lines across the whole surface and non-homogeneous amplitude of vibration.
- The second point to take into consideration is the homogeneity of the standing wave amplitude of vibration across the surface. A non-homogeneous wave will automatically create zones of higher and lower friction reduction for a given excitation.

As described by F. Casset in [60], an iterative optimization using harmonic simulations is used to find the best position for the actuators. A voltage gradient is applied across the virtual electrode and a mechanical damping parameter is used to find the maximum displacement of the substrate. This damping can be estimated using measures on a device with similar properties as in [61]. If an arbitrary damping parameter is chosen, only relative information can be extracted from simulation.

Once calculated, the geometry and position of the piezoelectric actuators is changed slightly in an iterative approach. A new simulation of the frequency region around the selected mode of vibration is then recalculated to evaluate the effect of the changed actuators' location (Figure 1-25). This last procedure is repeated until the resonant mode presents a maximum displacement of the substrate, while keeping a good homogeneity and distance with the parasitic modes.

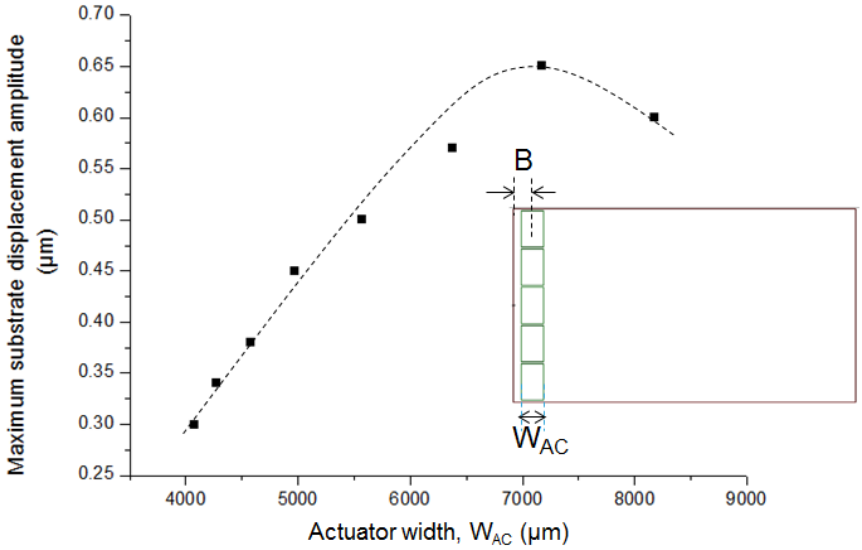

Figure 1-25: Optimum actuator width for a 110 × 65 mm² glass plate determined using harmonic simulations. [61] [60]

1.4.2.2 Analytic analysis

While this iterative simulation approach gives good results, an analytical solution would improve the time and precision of the design and optimization of such a system. This analytical approach was first described by M. Biet in [38]. To determine the wavelength necessary for the resonant actuation of the haptic plate, she developed models of the vibration to reduce the complexity of the calculus.

The simplified system is defined as a stack of piezoelectric material and the vibrating substrate. By reducing the study to a single half wavelength, it is possible to consider the plate supported at its extremities (as seen in Figure 1-26 (a)). The resolution of the system is based on the study of the static and dynamic deformation of the stack when considering uniquely the flexion mode of movement. The half wavelength beam displacement is then found by:

$$w_{dyn} = Q_m \frac{-3d_{31}V_z}{16h_p^2}\left(\frac{\lambda_{onde}}{2}\right)^2\left(\frac{1-2f_0}{1-3f_0+3f_0^2}\right) \quad (1)$$

Where w_{dyn} is the maximum displacement of the plate. Q_m is the quality factor of the piezoelectric ceramic, with d_{31} its piezoelectric coefficient and h_p its thickness. f_0 is the ratio between the piezo-ceramic and the substrate. Finally, V_z represents the voltage supply necessary to obtain a displacement of w_{dyn}.

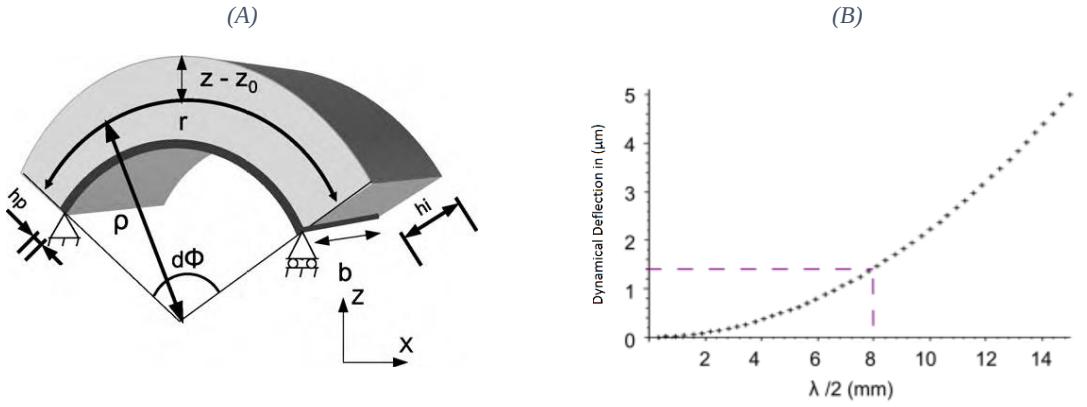

Figure 1-26: (a) Simplified part of the half wavelength beam. Its bending is the effect of the piezoelectric material at the bottom. (b) Calcul of the curvature in function of the half wavelength for a voltage supply of 15 V AC. [38]

In the model, Biet uses a Copper-Beryllium plate with a 2 mm thickness on which are glued 1 mm piezoelectric ceramics. For an excitation of 15 V AC, it was then possible to calculate the evolution of w_{dyn} in function of the wavelength as presented in Figure 1-26 (b). Increasing the distance between the nodes improve quickly the achievable amplitude for a given voltage. However, this distance cannot be increased too much, otherwise the user will start to feel the presence of the nodal lines. As said before, an 8 mm half wavelength is usually chosen to reduce this effect.

Analytical models to help with the piezo-ceramics placement optimization have been extensively studied by C. Nadal in 1 dimension [62]. Similarly, F. Bernard studied the placement of thin-film piezo-ceramics on a transparent surface in 2 dimensions using an energetic approach Figure 1-27.

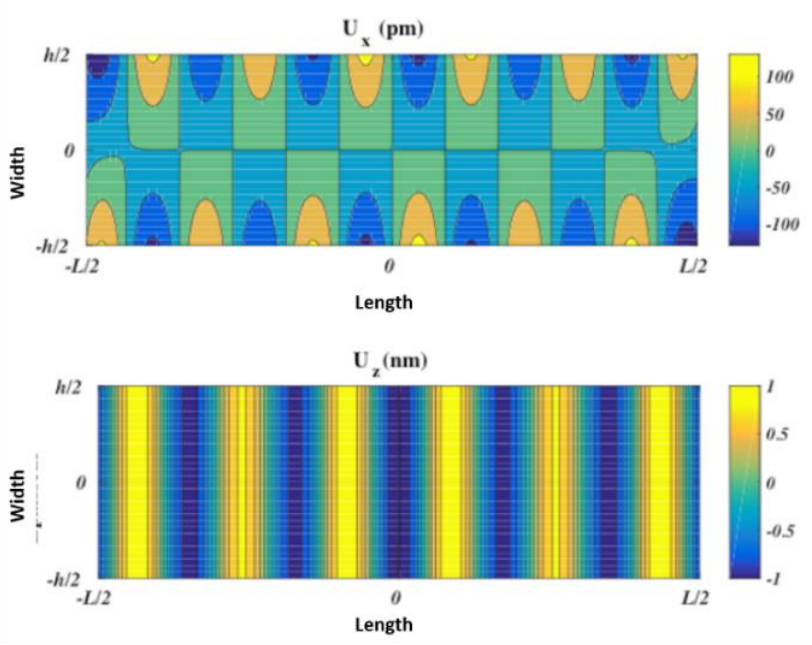

Figure 1-27: Analytic calculation of the Lateral and Normal displacement of a simulated glass of 0.5mm for a resonant mode at 19652Hz. [59]

1.5 CONCLUSION

Up to recently, research in finger and hand biomechanics was motivated by medical reasons. But with the rapid diffusion in the consumer market of devices including basic haptic rendering, these problematics came back to the frontline of research and extended their range of applications. As a matter of fact, understanding the mechanical perception of environment by human is critical for a correct development of good haptic illusion effects. The market of haptic is still expanding quickly with the multiplication of touch based devices and the explosive growth of virtual reality systems. It is estimated that it will double in the coming years to reach 30 billion dollars.

Even with this large expansion, no device currently sold can recreate our most natural tactile interaction, that is the perception of textures and roughness. Ultrasonic Lubrication presents a unique opportunity to solve this absence by the modulation of its friction reduction effect. As shown in this chapter, multiple companies have tried to push for the adoption of tactile and texture rendering on mobile platforms. The fact that none have been successful until now, despite the strong interest from the consumers, is due to the show-stopping constraints of all the possible technologies. All the possible constraints: Fear and durability in the case of Electrostatic, bad ergonomics for SAW and integration constraints for ultrasonic lubrication.

Even with its issues, UL stimulation exceptionally strong feedback, and comparatively simple constraints (Engineering problems), has the best hopes to present a new standard of tactile stimulation. As part of the European PROTOTOUCH Project, the objective of this thesis was to iterate on the design and development of UL devices to provide a better understanding of the conditions necessary to create an industrially exploitable effect. To this end, the next chapter will measure precisely the effects of UL modulation on the dynamic friction coefficient to validate the previously proposed models. Using this better understanding of the phenomenon, improved UL tactile stimulator design will be proposed in chapter 3. Finally, the last chapter will use these improved devices to study control scheme, aiming to reduce the relatively high power consumption of UL devices.

2 PHYSICAL CHARACTERIZATION OF THE INTERFACE BETWEEN HUMAN FINGERS AND AN ULTRASONIC VIBRATING SURFACE

Summary

2.1 OBJECTIVES: CREATING A SET OF DESIGN GUIDELINES FOR THE DESIGNERS OF UL DISPLAYS

This chapter explores the choices and tools currently available to the designers of ultrasonic lubrication (UL) displays and their limitations. The creation of a tactile display based on ultrasonic vibration is constrained by a few hard limits that were identified since the first proposed prototypes [46] [38] [48]. These original limits and constraints can be divided into three categories:

- Minimum amplitude of vibration of the resonant mode. This parameter has a direct influence on the reduction of coefficient of friction and is the simplest to drive in real time to modulate the friction perceived by the user. Nevertheless, while psychophysical studies have been conducted to assess the influence of this parameter [38] [63], few exhaustive physical characterizations of the friction coefficient in function of the amplitude of vibration has been conducted [64] [65].
- Frequency of the resonant mode. As will be shown in paragraph 2.5.2 the carrier frequency was first thought to be limited by the need to generate a squeeze number high enough to create the UL phenomenon. This limit of ~25 kHz is also close to the human ear perception limit of ~21KHz. No other constraint exists in the literature to help the designer choose the resonant frequency of its tactile display.
- Homogeneity of friction coefficient reduction across the screen. The first experiments involving ultrasonic lubrication by [35] were not concerned about the shape of the resonant mode since Langevin actuators were used. In subsequent studies, the influence of the nodal lines' position on friction coefficient was highlighted [66]. Current devices tend to use mainly static Lamb waves to simplify the design and insure a constant mean amplitude of vibration across the device.

These original constraints provide rough boundaries for the choices of frequency and amplitudes of the resonant devices. However, they are insufficient to optimize the quality and strength of the tactile feedback given to the users. Moreover, the analytic solution of the "squeeze film" effect presented in paragraph 2.5.2 as shown by [40] and [35] was never validated by proper tribology measures and thus cannot permit a purely analytical exploration of the effect of each parameter.

Another parameter that can have a large influence on user's perceptions is the time necessary for the plate to attain the requested amplitude command. This rise time is mainly dependent on the electromechanical coupling between the piezo ceramics and the resonator, therefore an increase of the rise time results in a diminution of the available bandwidth of friction coefficient modulation.

This chapter will first present the methodologies used to characterize the effects of these parameters on friction coefficient variations and their perceptions by the users. In a second part, the influence of multiple parameters such as the amplitude of vibration, the velocity of exploration and the normal force applied will be assessed using tribology measures. The next

section evaluates the impact of the resonant frequency on friction coefficient reduction. Finally, the data acquired in the previous sections are compared to two models of ultrasonic friction reduction in order to select the best fit of the dataset. The last section draws conclusions from the set of experiments and the selected analytic model to propose new design rules and requirements for the next generation of tactile devices.

2.2 DESCRIPTION OF THE METHODOLOGIES

This first part presents the methods and the experimental devices used in the rest of the chapter to conduct experimental characterization. The first section describes the method typically used to design the ultrasonic tactile interfaces. A second part compares the benefits and drawbacks of the different tribometer approaches; active and passive touch conditions. The typical data extraction process and statistics used to calculate the friction coefficient data are then explained. The final section describes the methods of control used to stabilize the amplitude of vibration during the experiments.

2.2.1 Design and control of the UL devices specialized for tribological measures

This chapter presents two experimental setups dedicated to the measure of friction coefficient variation created by UL displays. The analysis, design and assembly processes related to the creation of such an UL device are similar to the ones used in the creation of a complete tactile interface that is described in Chapter 1. Here we will highlight the constraints associated with UL device fabrication and control.

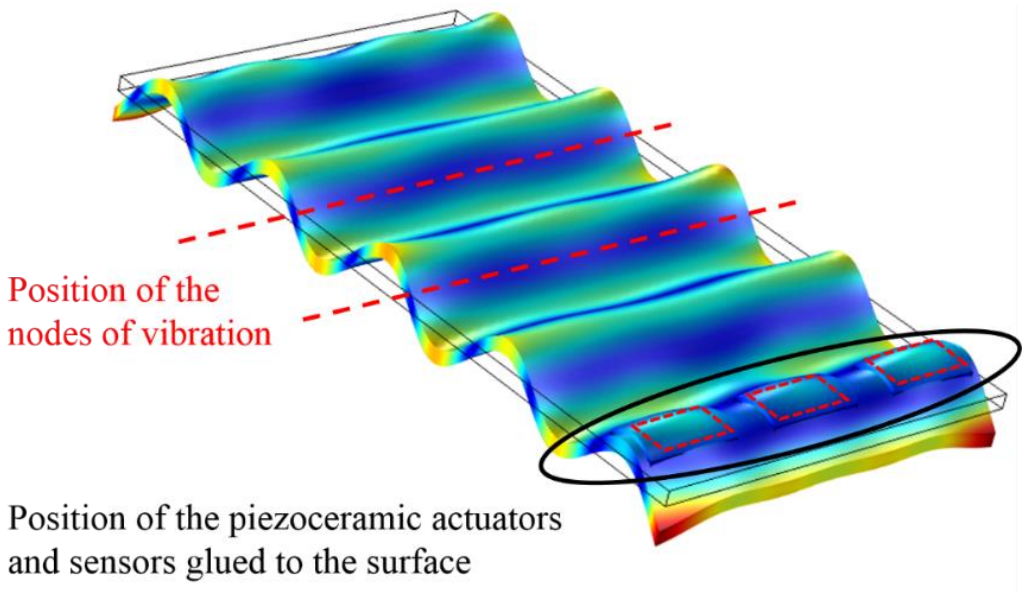

Figure 2-1: Simulation of Lamb wave propagating across an UL device (27 kHz mode on aluminum substrate). Red dotted lines give two examples of nodal line positions. The black ellipse on the ventral line of deformation gives the position of piezoceramic actuators and sensor in this simulation. Any of the three ceramics in this example can be chosen as a sensor with limited impact on performances

The fundamental goal of the procedure is to create a flat rectangular plane of the required dimensions that presents a resonant vibration across its surface. When building experimental devices, our choice goes to standing wave mode of vibration, specifically Lamb waves that present a homogeneous maximum amplitude of vibration across the whole surface. As it can be seen in Figure 2-1, and already mentioned in chapter 1, Lamb waves are elastic waves whose particle motion lies in the plane that contains the direction of wave propagation and the plate normal (the direction perpendicular to the plate). For the resonator in which these waves propagate, the design approach can be either analytic or simulation based. Using one

of these methods, the optimal placement of the piezo-ceramics actuators is found to promote the highest and most homogeneous amplitude of vibration across the device. Piezo-ceramics used as actuators produce a deformation when an electric field is applied across its their electrodes. Alternatively, the same type of piezo-ceramics can be used as sensors if the electric charge between their electrodes is measured while it is constrained (Figure 2-1).

Once a system possesses both actuators and sensors, it is possible to implement a real-time control system of the amplitude of vibration. Indeed, the control of the friction reduction in an ultrasonic device is achieved by modulating the amplitude of the vibration developed. As it will be seen along this chapter, this control system is made necessary by the need for precision in the amplitude of vibration applied to the system. Usually, this control is done by changing the amplitude of the sinusoidal voltage applied to the piezo-ceramics. This simple approach has the drawback of not controlling the variable damping effect imposed by the finger when it moves across the vibrating surface. This variable damping is mostly dependent on the force applied by the finger and its position relative to the nodes of vibration (a finger on a node will have less damping effect than a finger placed between 2 nodes). While the variable damping is not necessarily an issue in haptic devices, it does have a large impact when making precise friction coefficient measures. This issue can be solved by measuring in real time the amplitude of vibration across the surface using the sensor piezo-ceramics and adjusting the voltage command to the actuators to compensate any variable damping.

All the experimental devices created for the specialized measures in this chapter respect the general structure presented in Figure 2-1. They all present a lamb wave shaped resonant mode actuated by Lead zirconium titanate (PZT) piezoelectric actuators and include one PZT piezoelectric ceramic to measure and control the amplitude of deformation in real time.

2.2.2 Tribometric approach to measure the dynamic friction coefficient

In order to evaluate the effect of ultrasonic lubrication on the friction perceived by the user, a physical measurement method is used. This method relies on the precise measure of the reaction forces applied by the surface on the finger (or artificial finger) on a resonant plate, while a sliding movement is applied. The dynamic friction coefficient is a unit-less value expressed as the ratio between the normal and lateral forces. The following paragraphs detail the mechanical and software tools pertaining to tribology that are used in this chapter experiments.

2.2.2.1 Tools used in friction coefficient measures

Multiple approaches are used to measure the dynamic friction coefficient between a live tissue and a plane substrate. They can be separated into two broad categories:

- “Active touch” where the substrate is maintained static and the live tissue (the fingertip in our case) is put into contact directly by the user who explores the surface autonomously.

- "Passive touch" where the live tissue is maintained static by an apparatus and the plane surface is put into a sliding contact against it.

Measuring a coefficient of friction between a finger and a surface in "active touch" presents some advantages. The design of an "active touch" tribometer only consists in a system capable of measuring normal and lateral forces applied to the static surface in real time. This configuration also represents a more natural interaction for a user considering the human tendency to adapt its exploration speed and force per the properties of the material being explored [67]. However, this method may present disadvantages if the different parameters of the experiment need to be tightly controlled. It is especially true if the speed of exploration or the normal force must stay within stable boundaries during the measures.

"Passive touch" can solve this issue by constraining the hand of the participant in space and controlling precisely the speed of exploration and the normal force applied. A passive touch system can either move the hand or the surface of exploration to achieve this goal. In most cases, it is chosen to fix the hand to simplify the mechanics of the system and for the comfort of the participants. The two tribometers used in this chapter present a "Passive touch" configuration to reduce the variability of the different parameters to the minimum.

2.2.2.2 Data extraction and Statistics from a "Passive touch" tribometer

Following the acquisition of data from "passive touch", the relevant information is extracted from the raw data using MATLAB scripts. In our experiments, the raw data from a tribometer are always composed of the same values:

- **Lateral Force:** this force is the most important in any tribometer since for a given experiment, the other parameters tend to stay the same during one experimental run in these conditions. The lateral force can be measured thanks to different sensors such as piezo-electric or Hall sensors which measure a deformation. In both tribometers used in this chapter, the force is acquired through a strain-gauge sensor placed on the arm of the system to estimate the torsion applied to it and thus, the force.
- **Normal Force:** it is not always necessary to include a normal force measurement system in a "passive touch" tribometer since the force applied for a given experiment is usually setup at the start of the experiment and doesn't change throughout. Typically, the normal force is applied by placing weights on top part of the measurement system, taking advantage of the gravity to generate a constant normal force.
- **Probe Position:** this parameter is useful to help the post-treatment of the data after acquisition. Using directly this parameter, it is possible to select precise window of measures on the surface to avoid parasitic effects.
- **Amplitude of the Vibration:** this is specific to ultrasonic friction reduction. High precision and data-rate of amplitude measure are necessary in our experiments to evaluate precisely its effect on ultrasonic friction reduction.

For the different "passive touch" tribometers used in this chapter, the approach to extract the relevant friction coefficient data stays relatively similar. In most cases, the normal force and velocity of exploration are imposed and then the tribometer is set to run with an automatic increase of the vibration amplitude.

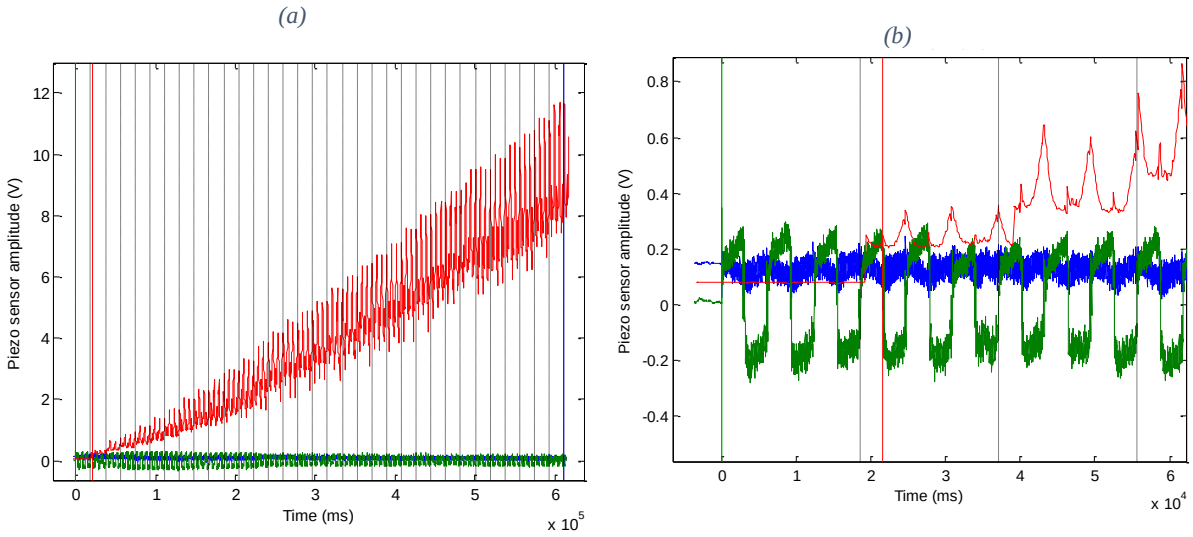

Figure 2-2: Example of tribologic measures on a passive touch tribometer. Red line represents the amplitude of vibration expressed in Volts as measured by the sensor piezoceramic, Blue line is the normal force and Green line the Lateral force. Dashed vertical lines separate each cycles of 3 runs at the same amplitude of vibration. (a) Represent the full measure of the 3 parameters for an increasing amplitude of vibration. Figure (b) Shows a zoom at the start of the same dataset. The measure starts by 3 cycles with no vibration to measure the original friction coefficient.

The first step is to define the raw data into separate "runs" of the tribometer where each "run" represents one back and forth of the machine's arm (the finger is static in "Passive touch"). This discrimination could be easily achieved if the position data are included. However, in Figure 2-2 which is an early experimental data without position measurement, the "runs" are detected automatically by applying a threshold on the derivative of the lateral force. In Figure 2-2 (a), the increase of the amplitude of vibration during the whole experiment can be seen in red. The green line represents the lateral forces that get reversed at each half cycles of the machine's arm. The absolute value of the lateral force is decreasing slowly with the increase of the vibration amplitude (can be seen by comparing the thickness of the green line between the start and the end of the measure).

Once each cycle of runs (3 successive runs at a given amplitude) is clearly delimited, the Matlab script proceeds to a windowing on all the runs to remove the transition periods between one direction and the other. This windowing can also be used to avoid certain zones of the vibrating surface that might have different properties (in the next section this is used to avoid non-homogeneous amplitude of vibration across the surface). An example of this windowing can be seen in Figure 2-3 (a). The windowed data are subsequently used to calculate the mean and standard deviation ($\sigma_{F_l}, \sigma_{F_n}$) of each parameter for the run as seen in Figure 2-3 (b).

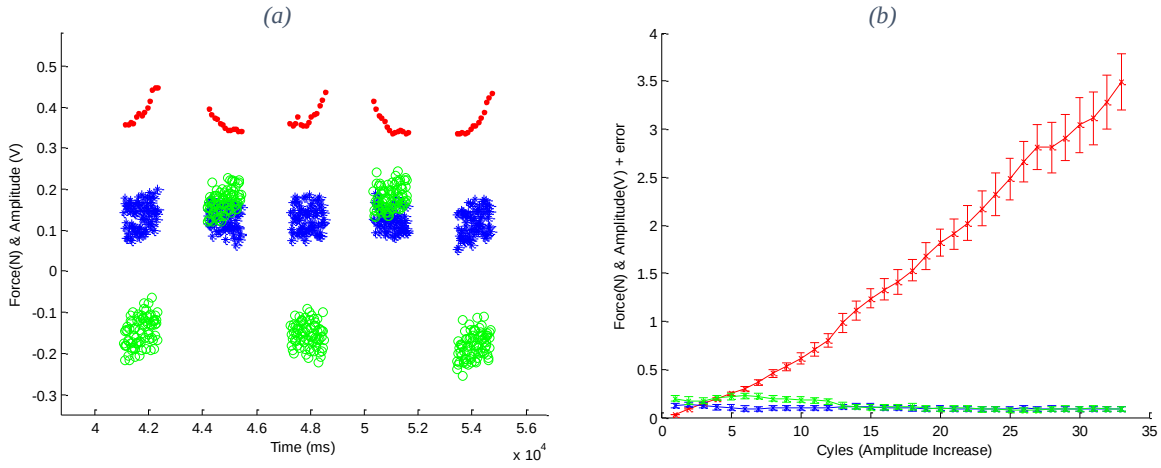

Figure 2-3: Figure (a) represents the second step of the data extraction, green points represent the lateral force, blue points are the normal force and red points represent the amplitude of vibration in µm. Window extracted from the raw data to avoid borders. Figure (b) represents the mean (cross) and the standard deviation (vertical bars) of each parameter calculated on windowed data.

The last step is to calculate the dynamic friction coefficient µ for each amplitude of vibration.

$$\mu = \frac{F_l}{F_n} \qquad (2)$$

Finally, the error propagation of the standard deviation of the dynamic friction coefficient, μ, is calculated using the standard deviation ($\sigma_{F_l}, \sigma_{F_n}$) of the normal and lateral forces (F_l, F_n) as follows:

$$\sigma_\mu = |\mu| \sqrt{\left(\frac{\sigma_{F_l}}{F_l}\right)^2 + \left(\frac{\sigma_{F_n}}{F_n}\right)^2 - \frac{2COV_{F_l F_n}}{F_l F_n}} \qquad (3)$$

An example of the friction coefficient results and the standard deviation obtained from this method can be seen in Figure 2-4.

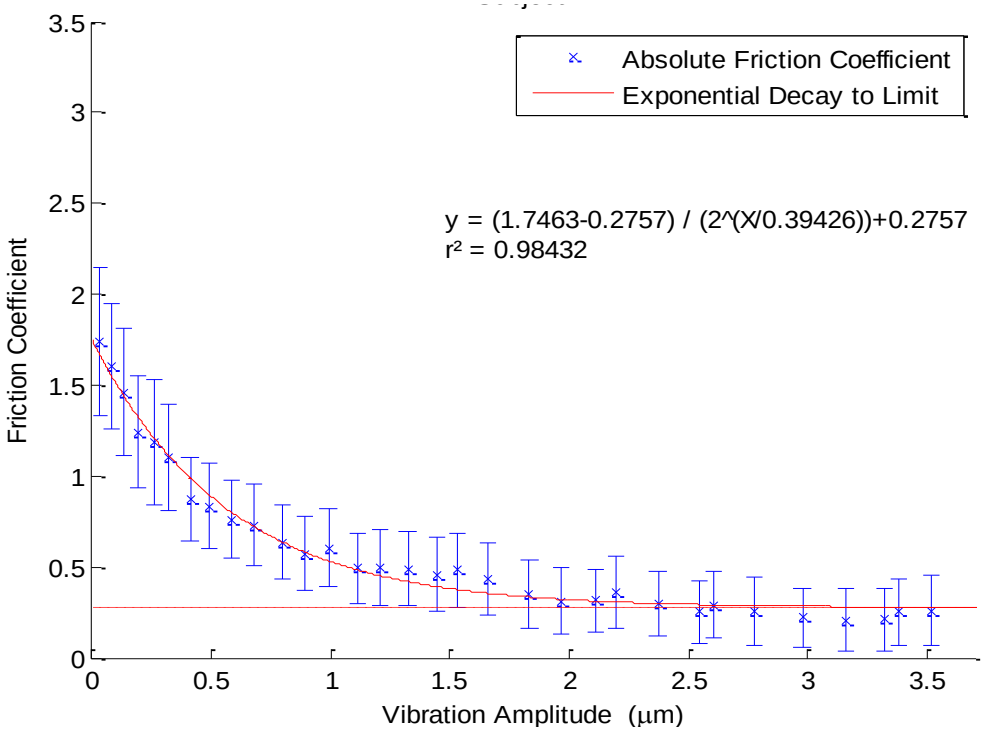

Figure 2-4: Friction coefficient as a function of vibrational amplitude for a normal force of 0.093 N on aluminum. The data points represent the mean coefficient of friction calculated for three cycles at the same amplitude of vibration. Vertical bars correspond to the propagated standard deviation over stimuli. The red curve shows an exponential decay fit. The dashed line is the limit of the decay fit.

2.3 ASYMPTOTIC LIMIT OF ACHIEVABLE REDUCTION OF THE FRICTION COEFFICIENT

2.3.1 Objectives of the Experiment

Commercial applications of Ultrasonic Lubrication between a finger and a surface are still in their infancy since the discovery of the effect in 1998 [35]. As described in chapter 1, the commercial applications have been limited to development kits. In order to improve ultrasonic devices, a better understanding of the influence of UL and its relevant parameters needs to be achieved. The amplitude of vibration is one these parameters; it is necessary to define a minimal amplitude of vibration during the design phase to insure a strong haptic feedback to the user. An amplitude of 1µm peak to peak was sometimes deemed sufficient to give a strong feedback to the users [59]. However, this minimal amplitude value may be questioned when prototypes achieving it failed to provide sufficient haptic feedbacks. Other psychophysical experiment showed a necessity for an amplitude above 2 µm peak to peak [38]. It may be noted that an extensive study has been performed in [68] [64] to determine the perception threshold in given normal force and speed conditions, and the result for young and older subjects is between 0,65 and 0,8 µm peak to peak.

While an analytic solution based on Reynold's fluid equation has been developed to explain the friction coefficient reduction [35] [40] [69], no experimental measures were done to assess the validity of this model on a large range of amplitude of vibrations. As it will be shown in paragraph 2.5.2, the "squeeze film" model of UL postulates that the friction coefficient should decrease faster for an increasing amplitude of vibration. One of the consequences is that the friction coefficient should be null above a specific amplitude of vibration which is dependent on the normal force and on the roughness of the surface.

We built an experimental setup to test this analytic model and get a better understanding of which parameters are critical to the design and operation of such a device. The experiment described in this chapter is the result of a cooperation with Brygida Dzidek and Eric Vezzoli conducted at the University of Birmingham.

2.3.2 Experimental Setup

This section introduces the two specialized pieces of equipment required for the study. Firstly, a passive touch tribometer and then the ultrasonic friction reduction devices that were specifically developed.

2.3.2.1 Passive Touch Tribometer

To control as many parameters as possible in the analysis of UL, a tribometer was designed at University of Brimingham that was capable of accurately measuring the friction while controlling the speed of exploration and the normal force. For that aim, a passive touch tribometer was adapted to measure the friction of the finger pad (Longshore System Engineering, Cornwall, UK). It comprises an arm support to secure the participant's hand in the correct position as shown in Figure 2-5. A holder is provided to position the finger at the

required angle regarding the measured surface. The moving part is composed of a 2-axis strain gauge sensor attached to the head of a beam supported by a bearing. It can rotate freely and a counterweight can be affixed to balance the mass of the sampled surface. The normal force applied by the studied surface (tactile plate) to the finger pad can be selected by adding a mass on the top of the beam. This method was used to investigate different normal forces, to determinate its effect on UL.

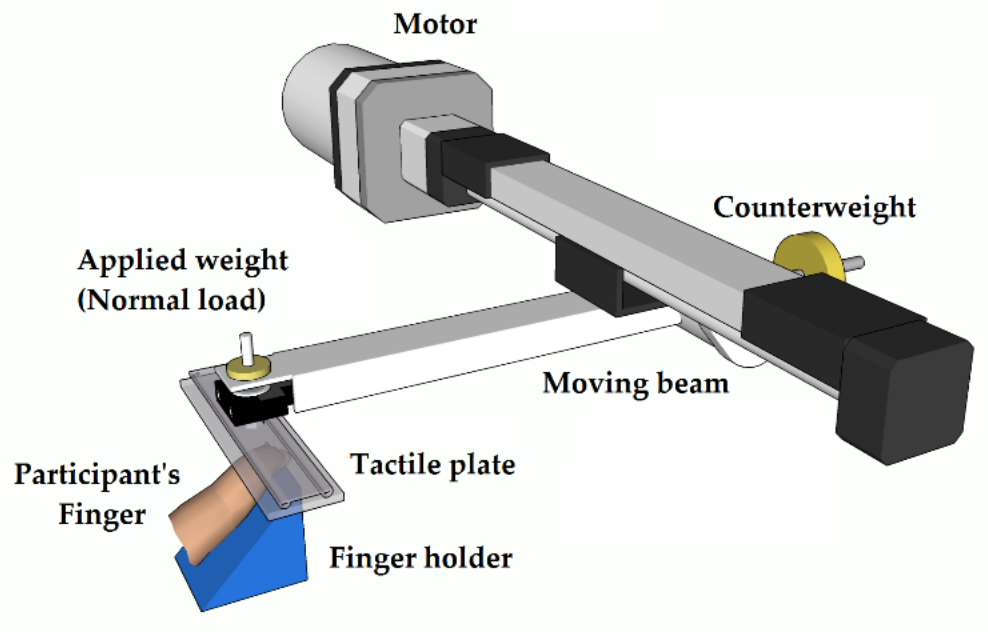

Figure 2-5: Schematic of the tribometer and finger.

The tangential and normal forces were measured using two strain gauge ADC interfaces with 16-bit precision and a sampling frequency of 100 kHz implemented on a National Instrument™ ADC system. The force measurements, amplitude data and position of the arm were then stored on a Windows computer using Labview® and re-sampled using Matlab. Windowing was done to only extract the forces while the finger pad was located in the center of the moving plate; data from the borders of the plates were removed to reduce the noise in dynamic friction imposed by the triangular displacement profile of the tribometer beam.

2.3.2.2 Tactile Plate

This section describes the UL stimulators created for the study. A specific haptic stimulator was developed in order to obtain the most stable friction reduction. As described in Chapter 1, UL is mostly used on large devices with a Lamb wave propagating on the plate length. The wavelength of the resonant mode is usually chosen to be under 10 mm to prevent the participants from feeling the reduction of amplitude around nodal lines. For this study, ultrasonic stimulators were designed and fabricated with a mode of vibration seldom used in such devices; this involved having the standing wave (Lamb wave) propagating along the short axis of a rectangular plate. As shown in Figure 2-6, the exploration is done on the long axis by the tribometer thus ensuring no crossing of nodal lines to induce a stable amplitude across all

the exploration range. The electromechanical characteristics of the two created stimulator are summarized in Table 1.

Using SALOME-Meca finite element software, the device was simulated such that the first dimension of the short axis was matched with the first resonant mode on this axis. This specific configuration eliminates the possible perturbation on the perceived friction. The device incorporates one piezo-ceramic used as a sensor to measure the amplitude of vibration in real time. The relationship between the piezoceramic transducers and the amplitude of vibration for the mode selected was calibrated by using an interferometer vibrometer (OV-5000, Polytech, Germany).

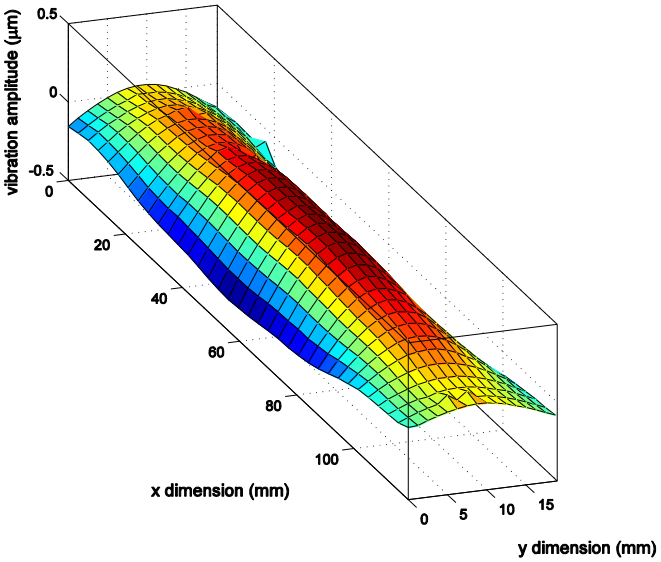

Figure 2-6: Measured amplitude of vibration of one of the steel plate equipped with ultrasonic actuator (phase locked).

Two devices with the same general dimensions were made of aluminum and steel respectively to further investigate the effects of surface properties on the frictional reduction effect. The steel device was built to improve the performances following our preliminary measurements [70]. The greater Young's modulus of the steel device allows us to increase the y dimension to present a better homogeneity of vibration amplitude above the finger pad. The mean roughness of the aluminum and steel plates was characterized using a MicroXAM 100HR Surface Profiler.

Table 1: Parameters of the tactile devices

	Steel	**Aluminum**
Young Modulus [GPa]	203	69
Resonant frequency [kHz]	24.7	25.1
Surface Roughness [µm]	0.36(±0.03)	0.32 (±0.06)
Undamped voltage to amplitude ratio [µm/V]	0.0448	0.0415

2.3.2.3 Amplitude Control

A first implementation of the measurement system was tested without any kind of vibration amplitude control. In this first uncontrolled experiment, the protocol to setup the amplitude of vibration was the following: at the beginning of the experiment, the participant finger was placed under the resonant plate (the normal force creates a damping effect), then the voltage of excitation applied was increased until the sensor voltage corresponding to the correct amplitude was reached. The tribometer was then allowed to move back and forth as described in section 2.2 to measure the frictional forces. However, the lack of active control on the vibrational amplitude led to a large variation of the amplitude depending on the finger position relative to the x axis of the tactile plate. This phenomenon was particularly visible at high speeds, preventing usable friction measurements at variable velocity [70].

A second setup was then developed to solve the above issue by incorporating a real-time control loop in order to stabilize the amplitude of vibration independently of the normal force or the position of the tribometer arm. To measure the amplitude, the voltage given by the piezo-ceramic sensor is under-sampled (compared to the resonance frequency) and the maximum amplitude is measured during 10ms. The error between the requested vibration amplitude and the measured plate amplitude is calculated with LabVIEW in real time and fed into a PI controller at a frequency of 80 Hz which then act on the voltage amplitude. This type of control will be detailed in Chapter 3. Once tuned with a Ziegler-Nichols method, this simple control system gives a good stability of the amplitude with less than 5 % overshoot for a time response of 0.5 s as seen in Figure 2-7. The speed of exploration was limited to 100 mm/s to remain within the stability region of the control system. It is to be noted that the high response time of the control system is not a problem for us since the damping perturbation created by the movement of the tribometer is also extremely slow (minimum 1 second)

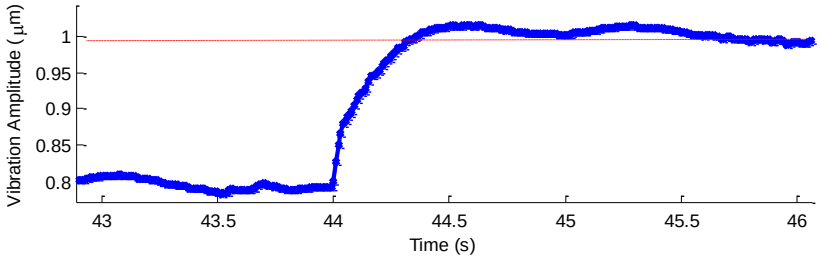

Figure 2-7: Measured response time to an amplitude command 1μm of the PI controller. A constant load of 0.5N is applied between the tactile plate and the finger. The tribometer arm is running back and forth, creating a variable damping effect that is compensated by the PI control loop.

2.3.2.4 Experimental Protocol

In order to assess the influence of all the main contributing parameters to the UL effect, multiple measures were done for each of the parameters and subjects. Following previous results with this setup [70], the aim was to explore in depth and on multiple subjects the effect of normal force, speed of exploration and amplitude of vibration on the evolution of UL.

Table 2: Summary of the participants for the in vivo friction measurements

Participant	p1	p2	p3	p4	p5	p6
Age	27	26	32	35	30	27
Sex	F	F	F	F	M	M

Table 2 summarizes the details of the participants for the in vivo friction measurements; all participants gave their informed consent. It should be noted that the measurements can be quite long and exhausting for a participant since completing a full 3D matrix for a range of velocities and normal loads takes a minimum of 5 h. To prevent any change in the finger pad characteristics and possible artefacts due to movements of the finger, the participants were only subjected to one parameter (velocity or normal force) for a given session. The finger to be studied was initially cleaned with a commercial soap and water and, after thorough rinsing with water, it was allowed to equilibrate for at least 10 min under ambient conditions of 16°C and a relative humidity of 50 %. The arm of the participant was positioned in the holder for the most comfortable position. The right-hand index finger pad was supported by the wedge support at 30º to the horizontal and additionally adjusted by using a tape on the second phalange to prevent any rotation of the finger under the high loads.

Each session was initiated by automatic load calibration after which standard calibrated weights were placed on the sensor/ultrasonic plate assembly for applying the required normal force. The vibrational amplitude was increased by a staircase function in steps of 0.1 - 0.2 µm, for every three full sliding cycles. Data associated with reversals of the sliding direction were not considered in the analysis; the effective working distance was estimated to be 65 % ± 5 % of the total sliding distance (60 mm). One measure of friction for a given load or velocity takes from 10 to 60 s. In order to control that no modification of the finger properties occurs during the measurements, a frictional hysteresis check was implemented for 30 % of the runs. This involved returning to zero amplitude after a full run; thus, allowing a comparison between the end and start dynamic friction. Results show that the friction coefficient with no vibration was reduced by a mean value of 8 % compared to the original friction observed. This discrepancy is due to the plasticization of the fingertip present with this setup, but the phenomenon is sufficiently small to be ignored in the first order model proposed in paragraph 2.3.3.2.

2.3.3 Evaluation of the Friction Reduction Results

This section describes the results of the experiments done to characterize the evolution of the frictional reduction when subjected to varying normal force, speed of exploration and amplitude of vibration.

2.3.3.1 Fine Amplitude Analysis

In order to provide a good repeatability of the experiment as well as a reduced discomfort for the subjects, the number of finger repositions was reduced to a minimum. The hand of a participant and the surface of the tactile plate were cleaned and positioned on the tribometer. Once the finger pad is positioned at the center of the stimulator, the experiment was started

and all amplitudes of vibrations were measured in one session. The beam of the tribometer was configured to cycle continuously while the amplitude of vibration command was slowly increased every three cycles (6 displacements in each direction). The half-cycles where the amplitude changed were not considered for the analysis. To avoid potential destructive vibrations, the maximum peak to peak amplitude was limited respectively to 3.5 and 2.5 µm for the aluminum and steel vibrating stimulators. Frictional forces for each half-cycle were averaged locally. This local dynamic friction coefficient was then calculated. Finally, the error propagation of the standard deviation of the dynamic friction coefficient was calculated as described in section 2.2.2.2.

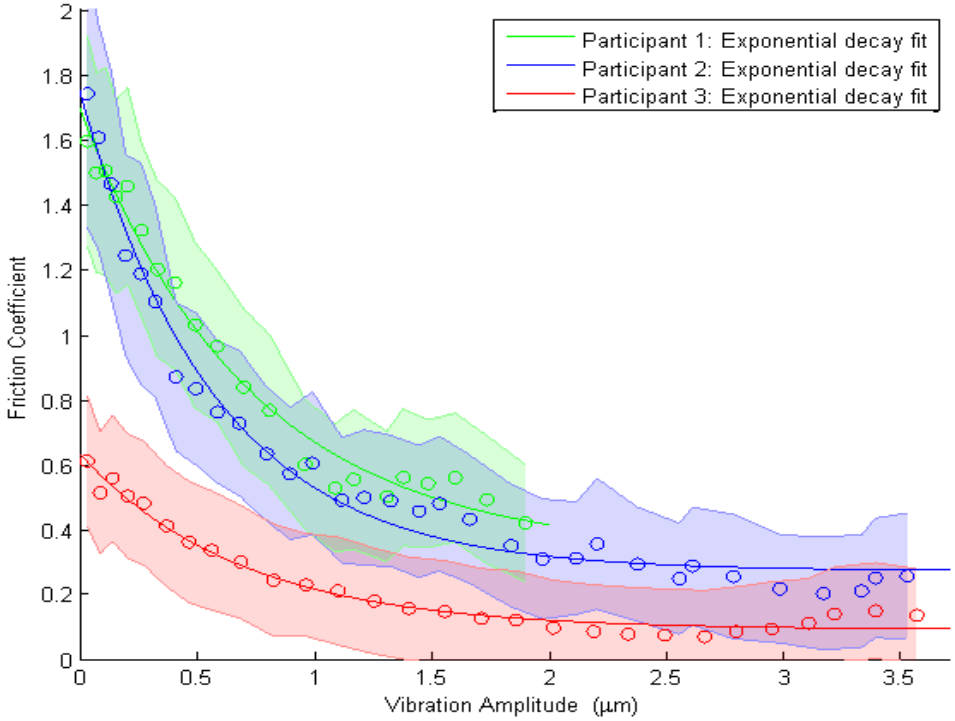

Figure 2-8: Friction coefficient as a function of vibrational amplitude for multiple subjects at the same normal load (0.1N) and speed of exploration (17 mm/s). Only three participants are shown for clarity. The data points represent the mean coefficient of friction calculated for three cycles at the same amplitude of vibration. Shaded areas correspond to the propagated standard deviation over stimuli. The curve shows an exponential decay fit for each participant.

Movements of the participants and so-called stick-slip effects [71] between the finger and the substrate were present on a significant portion of the measures (~ 40 %). In order to filter these measures, the mean Signal to Noise Ratio (SNR) of each run was calculated. This SNR level was then used as a threshold to exclude outlier points. Figure 2-8 shows an example of the friction coefficient as a function of the amplitude of vibration for 3 of the 6 studied participants. As highlighted in this figure, the measured dynamic friction coefficient with an unpowered device (null amplitude of vibration) is extremely variable between subjects. The three measures were done under the same conditions but for a different participant. The zero amplitude coefficients of friction are respectively 0.6, 1.6 and 1.7.

With define w as the amplitude of vibration. To compare the friction reduction from one user to the other, the relative friction coefficient $\mu' = \mu/\mu_0$ was calculated. With μ_0 representing

the base friction coefficient (no vibrations, $w = 0$) and μ the friction coefficient under vibration ($w > 0$). The relative friction coefficient behavior can be seen in Figure 2-9. We can observe that μ′ tends toward an asymptotic value, μ_1' as the amplitude of vibration increases above 2.5 µm.

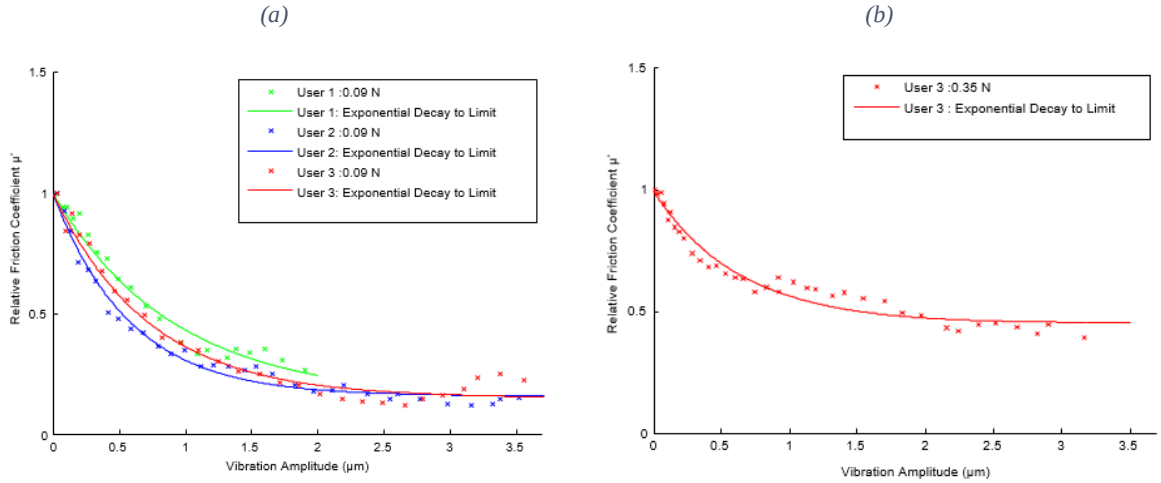

Figure 2-9: Relative friction coefficient as a function of vibrational amplitude at the same normal force for three subjects on an aluminum substrate. The normal load is 90 mN in case (a) and 350 mN in case (b). In both cases the data points represent the mean coefficient of friction calculated over three cycles and divided by the frictional coefficient at rest (amplitude = 0 µm). Each solid line represents the exponential decay fit

An exponential decay curve to an arbitrary limit can be fitted to the data with a mean square error of $R^2 > 0.98$ in most cases:

$$\mu'(w) = (a - c)e^{-w/\check{h}} + c \qquad (4)$$

The parameter a is the starting friction (with a value of unity when using the relative friction coefficient), $\check{h}$ is the characteristic amplitude and c is the limit of the friction reduction μ_1'.

2.3.3.2 Influence of the normal force and velocity on the reduction of the friction coefficient

In order to quantify the effect of the normal force and the velocity on the friction reduction, a series of measures were conducted while varying these two parameters. The steel stimulator presented in subsection 2.3.2.2 was used in these studies since it presents a larger width, which helps to reduce errors in the placement of the fingertip at the start of each experiment.

Data shown in Figure 2-10 were measured for a speed of 40 mm/s across all subjects and for a finger angle of both 30° and 45° with regard to the surface. After filtering the dataset as explained in 2.3.2.2, we obtain 44 points which give a large population of friction measures for the μ_1' limit as a function of the normal force. This indicates that μ_1' increases linearly with the normal force F_n with $\mu_1' = 0.153F_n + 0.27$.

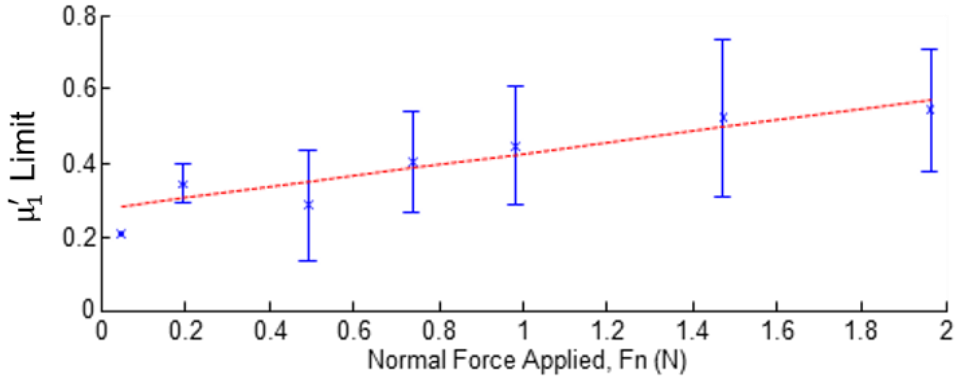

Figure 2-10: Evolution of the μ' limit ($\mu_1^{'}$) as a function of the applied normal force (6 subjects). The red line represents the linear trend.

Following the same method, a relationship between the speed of exploration V_l and the limit of the relative friction coefficient can be extracted. Figure 2-11 shows this evolution of the relative friction coefficient in function of the speed of exploration for one subject and a given normal load.

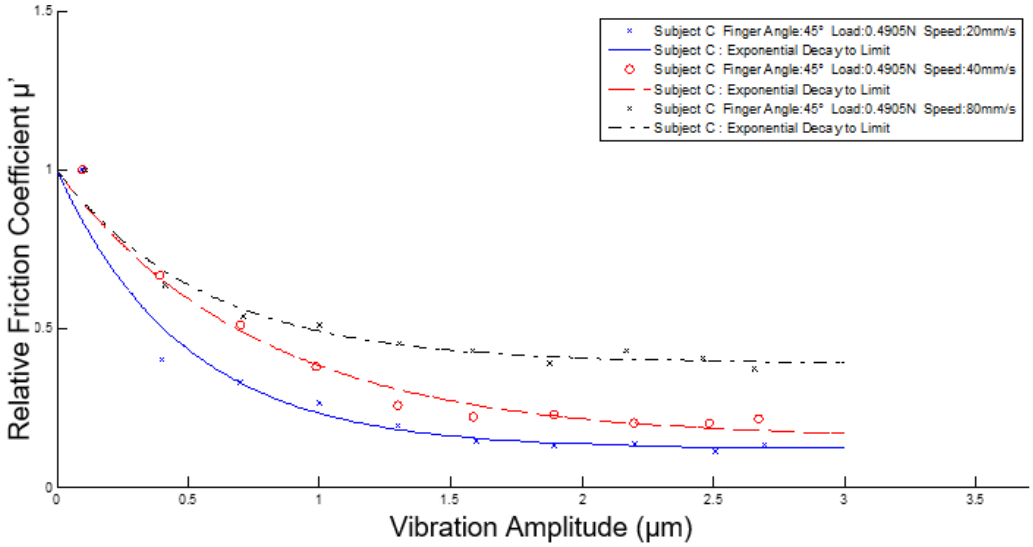

Figure 2-11: Relative Friction coefficient in function of the vibration amplitude for three speeds of exploration on a single subject. The solid lines represent the exponential fit to each set of data.

One sequence of increasing velocity measurements for one subject (male/30yr) was repeated three times. Figure 2-12 is a plot of these measures which shows a good repeatability and a clear linear relationship between velocity of exploration and the limit of relative friction coefficient with $\mu_1' = 0.0032V_l + 0.05$.

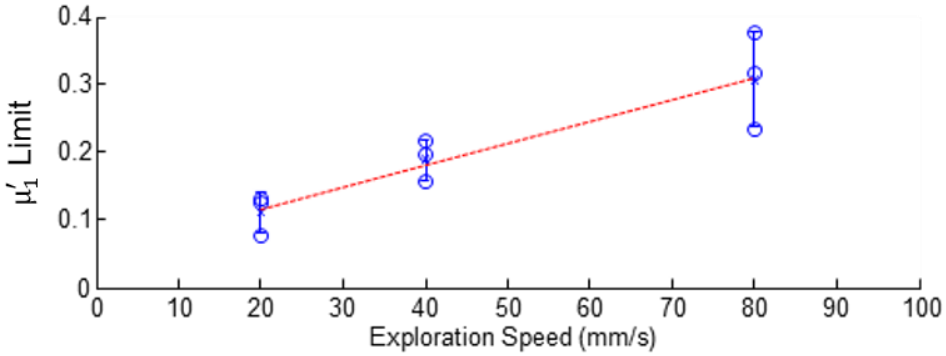

Figure 2-12: Evolution of the μ' limit (μ_1') as a function of the velocity of exploration (1 subjects) for a normal load of 0.49N. The red line represents the linear trend.

Subsequent measurements at different velocities and loads seem to confirm that the cross influence between the parameters is extremely limited. This hypothesis is also supported by a preliminary exploration of the effects of both parameters in [70]. With this hypothesis, it is then possible to propose the following equation to describe the relative dynamic friction mediated by UL as a function of both normal load and speed of exploration:

$$\mu'(w) = (1 - \mu_1')e^{-w/\breve{h}} + \mu_1' \qquad (5)$$

With $\mu_1' = 0.15F_n + 0.0032V_l$

Where V_l is the speed of exploration of the finger above the vibrating substrate. The value of the decay rate $\breve{h}$ did not correlate with the control parameters of the experiment and so is assumed to be mostly dependent on the properties of the fingers. The value of $\breve{h}$ is fitted to the experimental data to obtain the best match for each measure. A mean value of $\breve{h}$ = 0.6 µm is found. The parameters of equation (7) are valid for a steel substrate of roughness ~0.5 µm, it can be noted that the measurements presented above have also been conducted for the aluminum substrate and shows the same tendency [70]. This equation fits well with the measurements and provides an empirical way of estimating the reduction of the friction coefficient when applying ultrasonic lubrication.

2.3.4 Conclusion

The mechanical interaction between a finger pad and a flat ultrasonically vibrating surface has been measured. An empirical model based on the friction coefficient measurements was proposed and a general trend of the friction reduction is highlighted.

The limit of the achievable friction reduction, unpredicted by the classical “squeeze film” theory, may be useful in the design of new haptic stimulators. Indeed, this limit gives an upper bound to the amplitude necessary to achieve a maximum friction reduction and thus limits the energetic design constraint for the driver. This is especially important considering the portability required by the mobile platform industry.

2.4 Influence of the Resonant Frequency on Ultrasonic Friction Reduction Devices

2.4.1 Objectives of the Experiment

When designing an Ultrasonic Lubrication device, some critical parameters must be decided from the start. This is the case of the resonant frequency of the device. Typically, the choice of this frequency is impacted mainly by two constraints:

- The audio comfort of the users when the device is in operation.
- The homogeneity and strength of the UL effect across the device under consideration.
- The energetic cost which needs to be considered in a mobile UL device.

Making a plate vibrate freely in the air naturally generates sound that the user can potentially perceive if it is within its hearing spectrum. The commonly stated range of human hearing is 20 Hz to 20 kHz [72], though the amplitude threshold of perception increases sharply above 15 kHz in adults. Following this range, a requirement of minimum 20 kHz was selected to avoid the creation of a large audible speaker. Some of the first prototypes built around this rule were nevertheless perceived as noisy by the participants [73]. This noise is mostly due to the excitation of unwanted audible parasitic modes of vibration around the main resonant mode. Increasing the resonant frequency above 30 kHz seems necessary to reduce these parasitic modes and the sound perceived by users.

As said before, the friction reduction is perceivable for a given wave amplitude but also for frequencies above 10 kHz [35]. Finding a mode of vibration which provides a homogeneous amplitude across the whole surface of the screen can prove to be a challenge for certain geometries. Current mobile devices tend to use complex geometries of screen to attract new customers. These geometries with round corners and curved glass make the selection of modes of vibration hard for the ultrasonic haptic device designers. Standing wave resonant modes (when they exist) do not present the same homogeneity of amplitude of vibration that can be seen in simple rectangular screen. Typically, the resonant mode presents a high amplitude in the center of the screen that diminishes toward lower amplitudes on the corner or the edges of the devices. This phenomenon is especially present at “low” frequency of vibration, where the number of nodal lines is limited.

A third argument for choosing wisely the frequency of resonance in an ultrasonic device is the potential influence of the frequency on the friction reduction due to ultrasonic lubrication. This phenomenon was only succinctly explored by Watanabe & al. using a single plate with increasing the mode of resonance (with a different number of nodal lines). The results based on psychophysics were not conclusive [35].

This paragraph explores a novel approach to evaluate the effects of the resonance frequency on friction reduction devices independently of the mode’s shape and amplitude of vibration.

The first part presents the tribometer and probe used in this experiment. In a second part the effects of the frequency on the coefficient of friction are discussed.

2.4.2 Experimental Setup

This section introduces the specialized pieces of equipment required for the study; firstly, the ultrasonic friction reduction devices specifically developed are presented, then, in a second part the general experimental setup including a tribometer and the amplitude control system are shown.

2.4.2.1 Ultrasonic Friction Reduction Plates

For this study, five rectangular aluminum UL devices were built with increasing resonant frequencies. The plates have the same width and length of respectively 41 and 76 mm. The mode frequency of each plate was controlled by increasing the thickness from 0.8 to 2 mm. Exploring the effect of the frequency of vibration on the friction coefficient reduction is challenging. This is due to the mechanics of the resonant standing waves which impose a variable number of nodal lines when increasing the resonant frequency of the device. By simultaneously tuning the thickness, the same mode and the same number of nodal lines can be found on the plate, only the corresponding frequency is changed. All aluminum plates were cut from wrought 1050 aluminum alloy (69 GPa) to avoid any machining deformations. Each plate was finally covered with a polymer film to insure similar material properties, roughness and friction coefficient at rest.

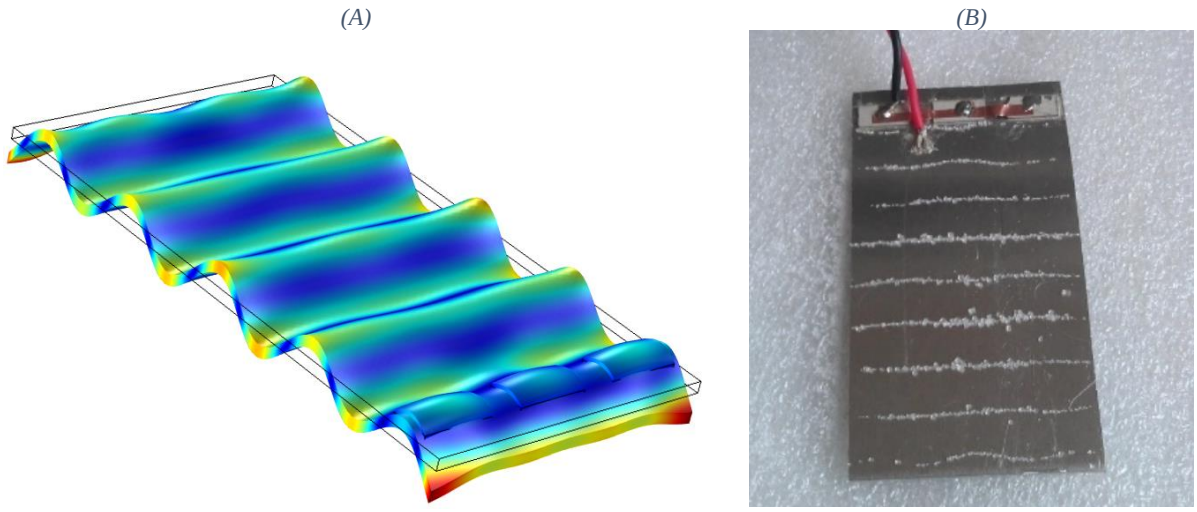

Figure 2-13. (A) Eigen mode simulation of the 2mm device (66kHz). (B) Mode verification using sugar powder (66kHz and 10 nodal lines)

Using SALOME-Meca finite element software, each device was simulated such that the same lamb wave resonant mode was present in the 20 to 70 kHz range studied (Figure 2-13 A). The chosen mode propagates along the long axis of the plate and presents 10 nodal lines (Figure 2-13 B). The devices incorporate one piezo-ceramic used as a sensor to measure the amplitude of vibration in real time. Each device was pre-calibrated with a vibrometer to extract the specific relationship between the measured voltage (V) and the amplitude of vibration (µm).

The relationship between the voltage applied to the ceramic transducer and the generated amplitude of vibration for the mode selected was calibrated by using an interferometer vibrometer (OV-5000, Polytech, Germany).

Table 3. Parameters of the UL devices

	1	**2**	**3**	**4**	**5**
Resonant frequency [kHz]	29.7	36.6	43.3	53.7	66.1
UL device thickness [mm]	0.8	1	1.25	1.6	2
Amplitude to Voltage ratio [µm/V]	0.0679	0.0696	0.0373	0.0246	0.0203

2.4.2.2 Tribometer and haptic probe

A tribometer (TRB, CSI, Switzerland) was used to measure accurately the friction coefficient between the vibrating plates and the haptic probe (Figure 2-14 A). This tribometer presents a static arm measuring the lateral forces exerted by the repetitive linear sliding of the sampled surface under it (Figure 2-14 A&B). The normal force applied by the arm on the surface can be adjusted by adding weights at the extremity of the arm.

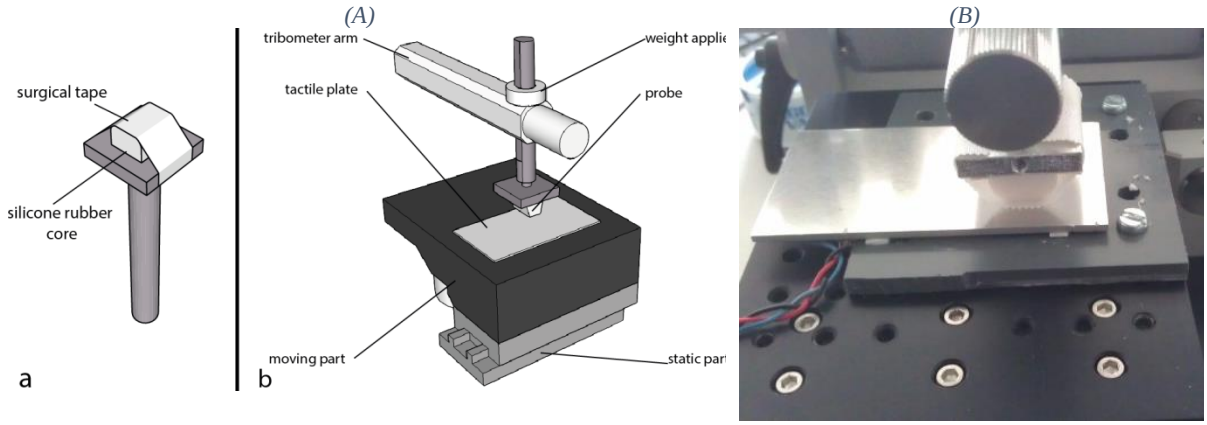

Figure 2-14. (A) Haptic Probe and General experimental schematics (B) Haptic probe and UL device 5 (2mm thickness)

The probe used is composed of an elastic silicon core covered with a surgical tape to reproduce the pattern and mechanical behavior of the fingertip in the ultrasonic domain. It has a silicone elastomeric core with dimensions 16 x 13 x 10 mm, a Young's modulus of 1 MPa and curved edges. The contacting region was covered with a surgical tape having mechanical properties (Young's modulus of ~ 20 MPa) and spatial periodicity similar to that of the fingerprint ridges [74]. To establish that the behavior of the probe is like that of a human finger pad, the tribometer, which is shown schematically in Figure 2-14 (A) was used to record the frictional modulation experienced by the probe sliding on the ultrasonic device at a peak-to-peak amplitude of 2.5 µm, a normal force of 0.5 N and an approximate sliding velocity of 17 mm/s. The probe similarity to the human finger when subjected to ultrasonic vibrations will be validated in paragraph 2.4.3.1

To prevent large modification of the friction coefficient, the tape was changed after all the measures on one plate were done. The data analysis after acquisition was performed through Matlab software in a process similar to the one presented in part 2.2.2.2.

2.4.2.3 Amplitude Control

As for the experiment presented in part 2.3.2.3, the plates need an active amplitude control to avoid large variations of the coefficient of friction during the measures. This numerical amplitude control loop is implemented in a STM32F405 DSP microcontroller in order to control the amplitude of vibration independently of the normal force or the position of the tribometer probe. The error between the requested vibration amplitude and the measured plate amplitude through the sensor was calculated in real time and fed into a PI controller at a frequency of 5 kHz. The necessary control frequency is higher in this experiment due to the variable damping created by the passage of the probe above the multiple nodal lines.

Once tuned with a Ziegler-Nichols method, this simple control system gave a good stability of the amplitude with less than 5 % overshoot for a time response of less than 100 ms. Similarly to the setup presented in section 2.3.2.3, the large response time of the control system is not a problem since the damping perturbation created by the movement of the tribometer is relatively slow. It should also be noted that the tribometer is acquiring data in permanent regime (no dynamic variation of the amplitude command) which reduces the need for an high frequency control system.

2.4.3 Evaluation of the Friction Reduction Measures

2.4.3.1 Validation of the probe friction coefficient in the ultrasonic domain

In order to assess the similarity between the probe and finger behavior to ultrasonic standing wave, the characteristics previously highlighted on the finger are checked with an artificial finger, called probe. This subsection validates that this probe presents a similar friction response to ultrasonic vibration than a natural finger.

Due to the configuration of the vibrating plates, the probe moved above nodes and antinodes of vibration. This caused the mean amplitude across the probe to change during measures. To insure a representative measure of the friction coefficient across the whole plate it was decided to calculate the friction mean across a large sample of each measure cycle periods (Figure 2-15 A). The lateral force variation due to the nodes is clearly visible in Figure 2-15 A. This is responsible for the high standard deviation seen in Figure 2-15 B.

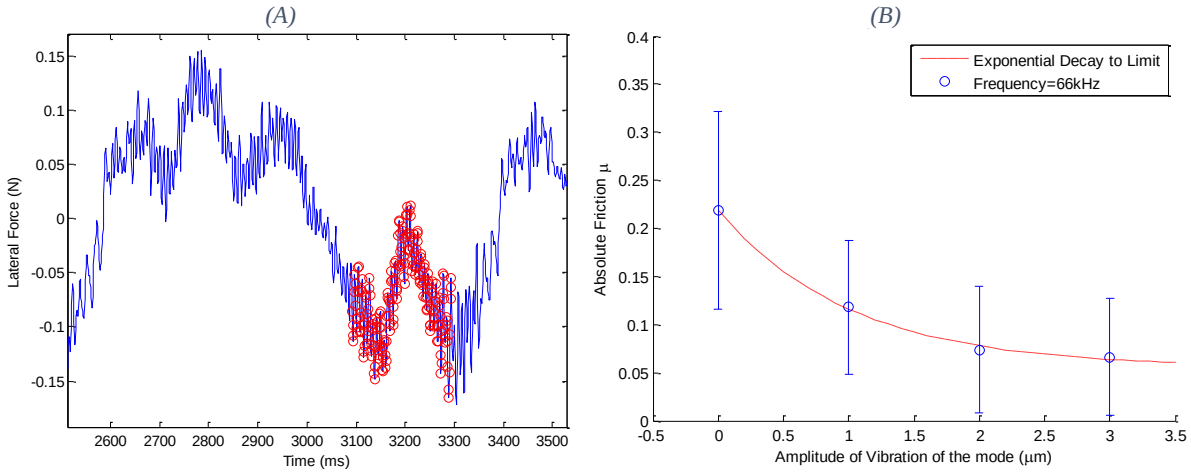

*Figure 2-15. **A** Measure of the lateral force and selected points (red). The lateral force goes from positive to negative following the direction of travel of the tribometer **B** Absolute friction in function of the amplitude of vibration for a speed of 30 mm/s and a normal force of 1 N on plate 5. Dotted line represents the exponential decay fit validating the probe response. Bars represent the standard deviation calculated for each point.*

As seen in Figure 2-15 B, the friction coefficient μ follows an exponential decrease in function of the amplitude of vibration. The friction coefficient tends toward an asymptotic value μ_1 for high amplitude of vibrations as seen on a real finger in section 2.3.3. Similarly, the evolution of friction in function of speed of exploration was measured using the same tribometer and haptic probe.

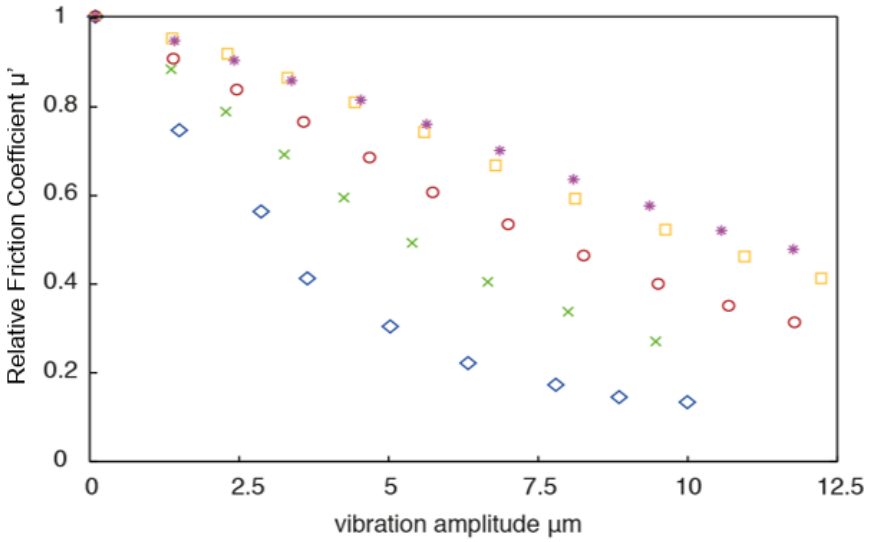

Figure 2-16: The relative coefficient of friction for the probe sliding on an ultrasonic vibrating plate as a function of the vibrational amplitude for an applied normal force of 0.5 N and vibrational frequency of 25.1 kHz. The exploration velocities are 10 (blue diamonds), 25 (green crosses), 50 (red circles), 75 (yellow squares) and 100 mm/s (purple stars) [75].

Figure 2-16 shows plots of the relative coefficient of friction as a function of the vibrational amplitude for exploration velocities in the range 25 – 100 mm/s and an applied normal force of 0.5 N. Again, the data exhibit the expected reduction in μ' with increasing amplitude. For a given vibrational amplitude, the value of μ' decreases systematically with decreasing exploration velocity and, for an amplitude of 3 μm, the reduction of the friction at a velocity of 25 mm/s is a factor of ~ 4 more than that at 100 mm/s.

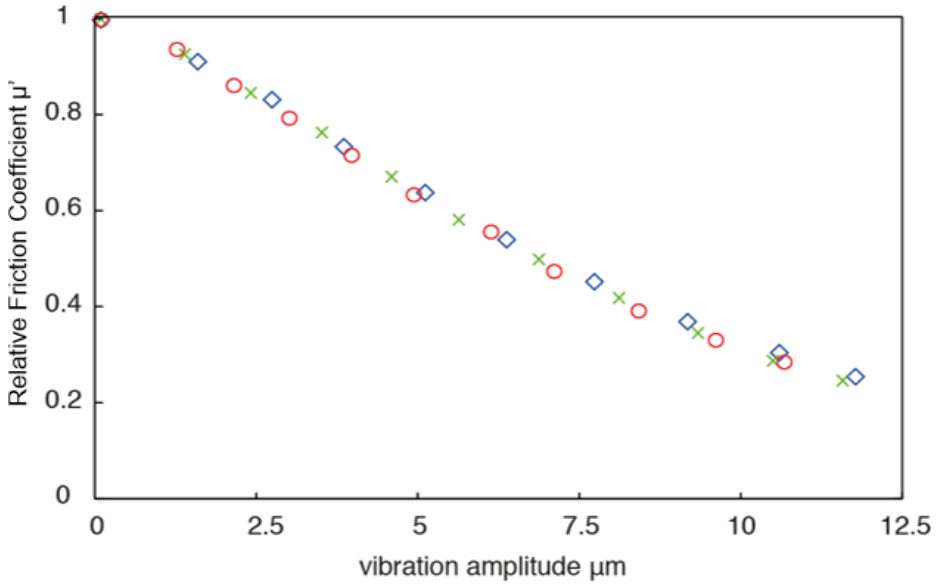

Figure 2-17:The relative coefficient of friction for the probe sliding on an ultrasonic vibrating plate as a function of the vibrational amplitude for applied normal forces of 0.25 N (blue diamonds), 0.5 N (green crosses), and 0.75 N (red circles). A vibrational frequency of 25.1 kHz and an exploration velocity of 50 mm/s were applied [75].

The last experiment was performed on the influence of the normal load. As can be seen in Figure 2-17, it does not seem to impact the friction reduction unlike what is described in part 2.3.3.2. This effect might be due to the lack of sudation on the probe and the homogeneous contact pressure across the sliding part of the probe, which does not occur on a natural finger.

Nevertheless, the probe presents the same pattern of friction reduction than that of a real finger in the ultrasonic domain as seen in section 2.3. Specifically, the reduction of the relative friction coefficient μ' in function of the amplitude of vibration and the velocity of exploration are the same. Following these results and despite the normal force influence, we can confirm that the probe acts as a good reproduction of the finger and follows the relations found in section 2.3.

2.4.3.2 Influence of the mode frequency on the friction coefficient

The lateral force in function of the amplitude of vibration was measured for each device at a normal force of 1 N and a speed of exploration of 30 mm/s. Each measure was acquired on 10 cycles of the arm to get an average of the friction coefficient μ. The procedure was then repeated for 4 amplitudes of vibration (at rest, 1 μm, 2 μm and 3 μm).

The friction coefficient at rest (no vibration) μ_0 was measured two times: first when setting up a new plate and a second time after all the cycles at different amplitudes were finished. Between the start and the end of the measures a diminution of approximately 2 % of the friction coefficient at rest μ_0 was observed. This low value confirms that the probe surface does not show a significant deterioration of its properties during this lime. The value of μ_0 used in the following results to calculate the relative friction coefficient μ' is an average of the start and end rest friction coefficients.

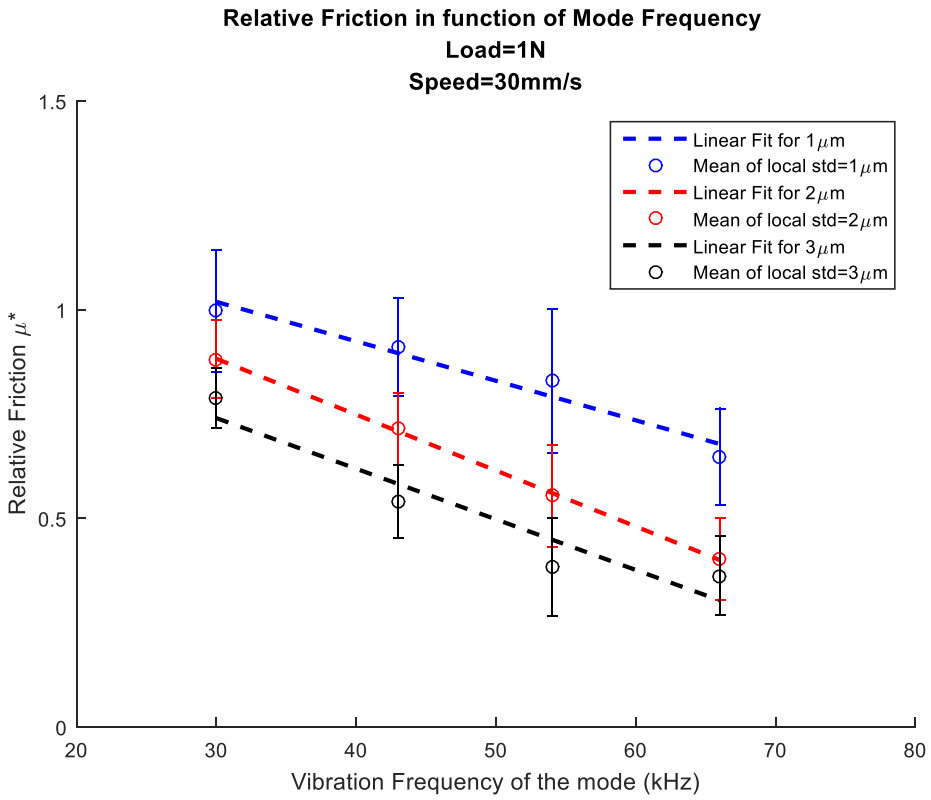

Figure 2-18. Relative friction coefficient in function of the mode's frequency (Normal load 1 N, Speed 30 mm/s).

Similarly to the observation of *in vivo* tissues in section 2.3.3.1, the asymptotic relative friction reduction μ_1' is reached for an amplitude of vibration above 2.5 µm (Figure 2-15 B) [70].

Due to partial ungluing of one piezoceramic, the plate 2 presented distortions of its mode of vibration. Measures were nevertheless possible up to 3µm of amplitude but presented a far lower friction reduction capability than the other plates. These results are excluded from the results displayed in Figure 2-18.

It can be noted from Figure 2-18 that the friction coefficient for each plate when an amplitude of 3µm is applied, decreases linearly with the increasing of the frequency of vibration. The value of μ_1' extracted from this experiment can be used to expand the empirical model presented in section 2.3.3.2 (equation 7) by adding the influence of the resonant frequency:

$$\mu'(h_r) = (1 - \mu_1')e^{-h_r/\check{h}} + \mu_1' \qquad (6)$$

With $\mu_1' = 0.15F_n + 0.0032V_l - 1.03\times10^{-5}F_r$

where F_r represents the resonant frequency in Hz of the device under consideration. This Equation has been valided for a range of resonant frequencies between 20 and 66 kHz.

2.4.4 Conclusion

Results shown in Figure 2-18 confirm that the designer of UL tactile devices should select the frequency of the resonance of their device with care. The linear reduction of μ_1' with the frequency suggests that the highest possible resonant frequency should be chosen to insure

the best reduction of friction. In practice, the choice of the resonant frequency is often constrained by multiple factors such as the control electronics' frequency, the amplifier gains and the power consumption in embedded tactile devices. Moreover, the proposed linear trend is only verified up to 66 kHz and further study should be done to understand the evolution of μ_1' above this frequency.

2.5 COMPARISON OF MEASURED DATA WITH EXISTING MODELS

2.5.1 Historical background on the Ultrasonic Lubrication

The physics underlying ultrasonic lubrication mediated by a flat surface have been subject to conjecture since the discovery of the phenomenon. As presented in Chapter 1, the first attempts of modelling haptic UL were made by Watanabe & Fukui in a paper describing the potential usefulness of friction reduction for haptic rendering [35]. This first study proposed a model derived from the Reynolds equations for fluid dynamics. This model is based on the squeeze film effect and was believed to be the main contributor to the reduction of friction between a finger pad and a flat surface. The squeeze film modelling has been further developed afterwards by Biet [38] and Winter [54].

In her PhD thesis, M. Biet also studied a second model based on Coulombic friction and intermittent contact [38] [76]. In this model a simplified mechanical model of the finger pad ridges is used to explain the change of the dynamic friction coefficient caused by the intermittent contact. But the model highly depends on the skin parameter values and the parameters considered in M. Biet PhD thesis led to the conclusion that intermittent contact could not be the origin of friction reduction. However, this mechanical model was recently expanded by E. Vezzoli & all in [77] and [75]. This new understanding of the physics behind Coulombic stick-slip mediated by intermittent contact is achieved through a finite element method optimization to gain a better knowledge of the finger pad material properties.

This part presents both models of the ultrasonic lubrication phenomenon and attempts to match them with our measures of the friction coefficient reduction μ' in function of different parameters as acquired in parts 2.3 and 2.4.

2.5.2 Evaluation of the Squeeze Film model

2.5.2.1 Description of the Model

This section describes succinctly the analytic model of acoustic levitation usually applied to haptic feedback through the squeeze film effect. As previously argued in [35] and [38], the vibration of a surface under a finger pad of a participant generates an ultra-thin film of air (air gap) in the contact region. Figure 2-19 shows a simplified geometry of the film of air. The film is subject to air compression and rarefaction at high frequencies in phase with the relative displacement of the surfaces.

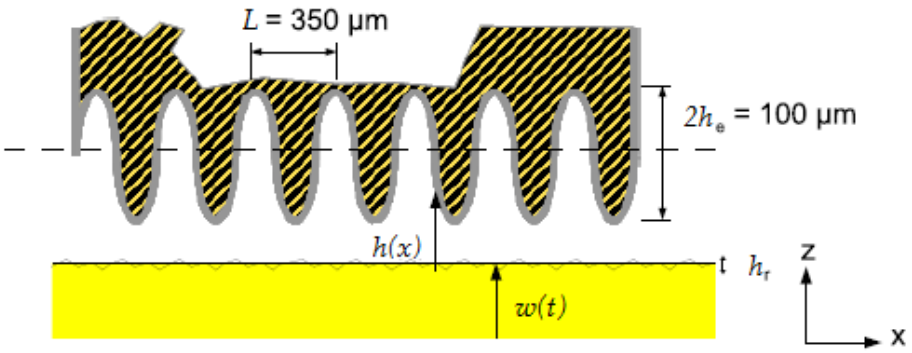

Figure 2-19: Approximation of the finger pad ridges [40].

The finger pad ridges are approximated by a cosine function and are considered to be rigid, or at least extremely stiff, at the vibration frequencies. With w being the amplitude of vibration and h_r the surface roughness, the thickness of the film can then be expressed by:

$$h(x,t) = h_r + w\,[1+\cos(\omega t)] + h_e\left[1+\cos\left(\frac{2\pi}{L}x\right)\right] \quad (7)$$

where the pulsation of the vibrating plate is given by ω. The relationship between the thickness, *h*, of the air-gap and the pressure, *p*, can be described by the Reynolds equations [16]:

$$\frac{\partial}{\partial x}\left(\frac{h^3\rho}{\eta}\frac{\partial p}{\partial x}\right)+\frac{\partial}{\partial y}\left(\frac{h^3\rho}{\eta}\frac{\partial p}{\partial y}\right)=6U\frac{\partial}{\partial x}(h\rho)+12\frac{\partial}{\partial t}(h\rho) \quad (8)$$

Here ρ and η are respectively the density and viscosity of air. The parameter *U* is the tangential velocity of the surface (exploration velocity of the participant finger). A normalized version of (8) is commonly used to describe the squeeze film effect. The new equation introduces the squeeze number Λ and the bearing number σ:

$$\frac{\partial}{\partial X}\left(H^3P\frac{\partial P}{\partial X}\right)+\frac{\partial}{\partial Y}\left(H^3P\frac{\partial P}{\partial Y}\right)=\Lambda\frac{\partial}{\partial X}(HP)+\sigma\frac{\partial}{\partial T}(HP) \quad (9)$$

$$\Lambda=\frac{6\eta U l_0}{h_0^2 p_0} \qquad \sigma=\frac{12\eta\omega_0 l_0^2}{h_0^2 p_0} \quad (10\text{ - }11)$$

with $X=x/l_0$, $Y=y/l_0$, $H=h/l_0$, $P=p/p_0$ and $T=\omega_0 t$. The parameter l_0 is the active length, h_0 is the mean air gap and p_0 is the ambient pressure. For a haptic device, the exploration velocity of the finger is usually assumed to be sufficiently slow that it can be neglected in the *x* and *y* directions (*U* = 0). We can then simplify (8) by reducing the system to one dimension and it becomes:

$$\frac{\partial}{\partial X}\left(H^3P\frac{\partial P}{\partial X}\right)=\sigma\frac{\partial}{\partial T}(HP) \quad (12)$$

This equation is solved in [54] with the assumption of a very large value of σ ($\sigma \to \infty$) by applying the previous mean amplitude equation (7) to this configuration. The resulting differential equation leads to the new local pressure P_∞ of the thin film (see [40] for full solution):

$$P_\infty = p_0 \frac{\left(1+\delta cos(kX)\right)\sqrt{\left(1+\delta cos\left(\frac{k}{2}\right)\right)^2 + \frac{3}{2}\varepsilon^2}}{\left(1+\delta cos\left(\frac{k}{2}\right)\right)\left(1+\varepsilon cos(T)+\delta cos(kX)\right)} \quad (13)$$

with $\varepsilon = \frac{w}{h_0+h_e}$, $\delta = \frac{h_e}{h_0+h_e}$, $k = \frac{2\pi l_0}{L}$

By integrating Equation (13) in time and position, the mean force applied to the finger pad by the squeeze film effect can be determined. F_s is the force applied per unit length in continuous mode.

$$F_s = \frac{1}{2\Pi}\int_0^{2\pi}\left(\int_{-\frac{1}{2}}^{\frac{1}{2}}(P_\infty - 1)dX\right)dT \quad (14)$$

The solution (12) assumed that σ tends toward infinity. Nevertheless, it is generally admitted that this condition can be restricted to σ > 10, which is applicable for a vibrational frequency superior to 25 kHz [40] (above the human maximum hearing range).

It is then possible to calculate μ', which is given by the coefficient of friction under actuation, relative to that at rest, μ_0.

$$\mu' = \frac{\mu}{\mu_0} = 1 - \frac{(P_\infty - 1)}{P_f} \quad (15)$$

With P_f the pressure applied by the finger pad. The parameters in Table 4 are then applied to calculate the relative dynamic friction coefficient, μ' , for the four normal forces applied to the vibrating plate.

Table 4: Squeeze Film Analytic model parameters

Amplitude of ridges	h_e	50 [μm]
Period of fingertip ridges	L	350 [μm]
Surface Roughness	h_r	1.2[μm]
Length of contact	l_0	1 [cm]
Normal force applied	F_f	0.1-0.5 [N]
Dynamic Viscosity of air	η	$1.85.10^{-5}$ [Pa.s]
Atmospheric pressure	p_0	0.1 [MPa]

As can be seen in Figure 2-20, this squeeze film model predicts a reduction to zero of the dynamic friction coefficient when the amplitude of vibration increases. We can nonetheless note that this is a simplified model, based on the assumption that the squeeze number is infinite for the frequency under study, which might not be totally true.

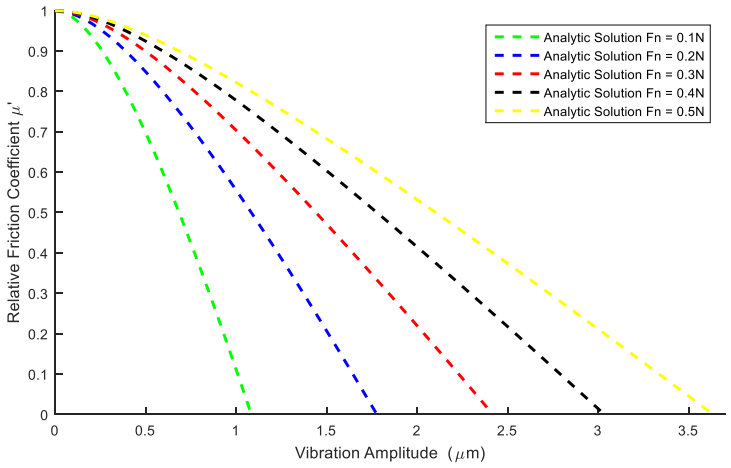

Figure 2-20: Modelling of the relative friction coefficient for different normal loads.

2.5.2.2 Comparison with measured data

The squeeze film model presents a relative friction coefficient that reduces faster for an increasing amplitude of vibration as can be seen in Figure 2-20. Measuring the overpressure generated in the air-film can be difficult (see [69]) and thus the relative friction coefficient $\mu' = \mu/\mu_0$ is used as a way to compare the resolution of the squeeze film model (15) with experimental data.

There is a lower limit to the friction reduction as a function of the vibrational amplitude when the amplitude of vibration increases (Figure 2-21). This phenomenon was observed for all the friction measurements. This seems to contradict an underlying principle of the squeeze film model regarding high amplitudes of vibration. Figure 2-21 shows an attempt to compare the actual tribological data to the squeeze film analytic model presented in section 2.5.2. Multiple mismatches between the model and measurements can be highlighted. First, while for small amplitudes, the model and the experimental data are relatively similar, there is a clear discrepancy between the predicted and observed friction reduction for amplitudes greater than a few micrometers. A second discrepancy is that the relative coefficient of friction, μ', tends towards an asymptotic value, μ_1'. The friction does not reduce to zero as predicted and instead, tends toward a lower limit when the amplitude of vibration increases above 2.5 μm.

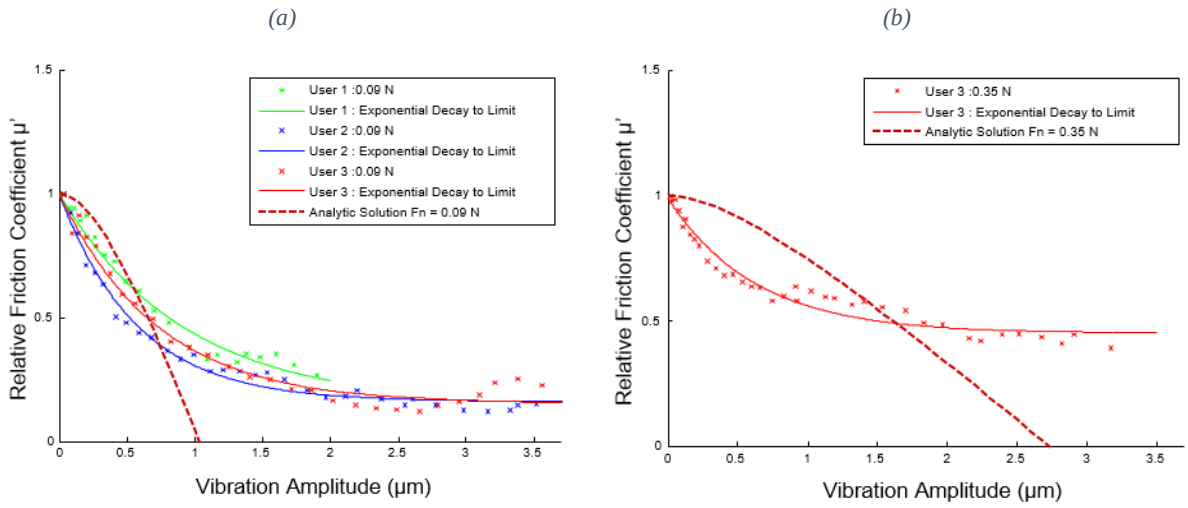

Figure 2-21: Relative friction coefficient as a function of vibrational amplitude at the same normal force for three subjects on an aluminum substrate. The normal load is 90 mN in case (a) and 350 mN in case (b). In both cases the data points represent the mean coefficient of friction calculated over three cycles and divided by the frictional force at rest (amplitude = 0 µm). Each solid line represents the exponential decay fit and the dashed line shows the calculated predicted friction reduction from the analytic squeeze film model at an averaged normal load.

2.5.3 Evaluation of the Intermittent Contact Spring Model

2.5.3.1 Description of the Model

The second common model to explain ultrasonic lubrication is not based on fluid mechanics but relies on intermittent contact. The intermittent contact model applied to tactile conditions was first explored in [38]. The mechanical principle underlying the reduction in friction in this case is interpreted using a simplified elastic model based on a Coulombic slider attached to lateral and normal linear springs, with a stiffness of k_l and k_n respectively as schematized in Figure 2-22. As proposed in [77] and [75], the slider represents a single fingerprint ridge that is attached to a rigid finger pad. The finger pad is considered rigid since vibrations applied to the fingertip show a large damping of ultrasonic vibrations [78]: the finger behaves like a low pass filter. When vibration is applied by the surface on the Coulombic slider, a rapid compression and decompression happens on the k_n spring. The static compression of the normal spring is assumed to be less than that of the vibrational amplitude. If the slider has a finite mass, this coupled spring system requires a numerical solution method such as finite element analysis as covered in [77]. However, a simplified model is sufficient to provide a qualitative interpretation that facilitates an explanation of the underlying physics. Thus, it is sufficient to treat the slider as having zero mass, which only influences the second order effects of damping and overshoot.

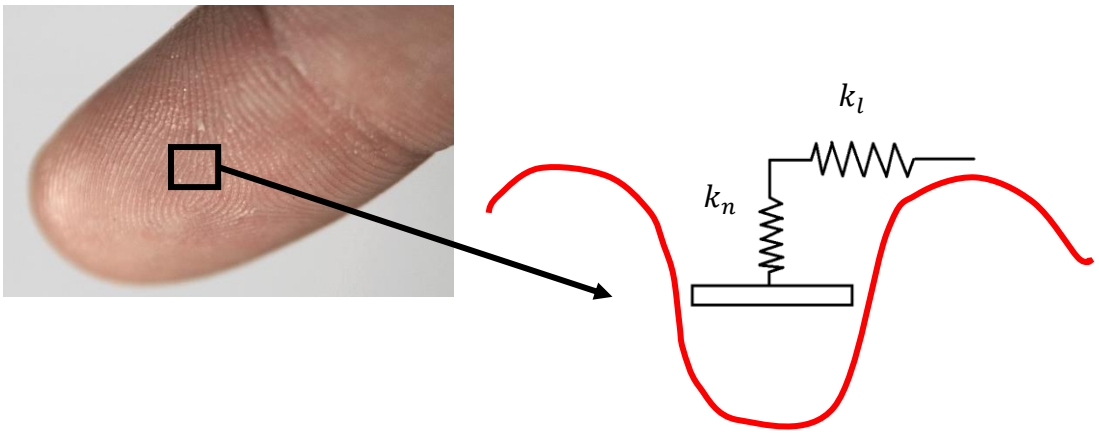

Figure 2-22: Representation of the fingerprint ridge as a Coulombic slider attached to two springs

The normal preloading distance Δy created by an applied normal force F_n, can be calculated as:

$$\Delta y = \frac{F_n}{K_n} \quad (16)$$

When the plate is vibrating with a sinusoidal profile, the amplitude of vibration, w, must be greater than the preloading Δy to induce detachment of the spring. It is then possible to define a critical vibrational amplitude of detachment, w_c , corresponding to a normal force F_{nc} :

$$w_c = \frac{F_{nc}}{k_n} \quad (17)$$

As long that $w < w_c$, the spring and the plate are in full contact over the whole vibrational period, whereas for a higher amplitude of vibration $w > w_c$ the contact is intermittent.

At equilibrium, the integral mean of the forces applied by the normal spring and the total reaction force of the plate must be equal to each other over one entire period of vibration T.

$$\int_t^{t+T} F_{reac}(w)dt = \int_t^{t+T} F_{reac}(0)dt = F_n T \quad (18)$$

The lateral forces applied to the slider during this period of vibration T can be separated into 3 time slices (Figure 2-23):

- First, in the case where no contact exists between the plate and the slider, the coefficient of friction and the lateral force F_l are equal to 0.
- In a second time slice, the contact is re-established. Initially, the lateral displacement of the plate is accommodated by the compression of the lateral spring and thus the lateral force will increase linearly with the compression.
- Finally, once the spring force is equal to the frictional force, the slider starts moving across the surface. Let us define t_s the time at which the slip occurs. For any given sliding velocity, U, the coefficient of friction is equal to μ_0 when contact is made.

The slip time t_s will occur at a critical compression, Δx_c:

$$\Delta x_c(\mathrm{w},\mathrm{t}) = \frac{\mu_0 F_{reac}(w,t)}{\mathrm{K_l}} \quad (19)$$

For a given vibrational amplitude, the time at which the slip occurs, t_s, can then be defined as:

$$t_s = \frac{\Delta x_c(t_s)}{U} \quad (20)$$

For a given total contact time t_c , we have $t_c > t_s$, and it is possible to calculate the lateral frictional force as function of time, $F_l(t)$, for each complete vibrational period T:

$$F_l(\mathrm{t}) = \mathrm{U}t k_l \quad \text{if} \quad 0 < t < t_s \quad (21)$$

$$F_l(\mathrm{t}) = \mu_0 F_{reac} \quad \text{if} \quad t_s < t < t_c \quad (22)$$

$$F_l(\mathrm{t}) = 0 \quad \text{if} \quad t_c < t < T \quad (23)$$

The preloading of the lateral spring k_l is dissipated when it detaches from the plate at $t > t_c$ and thus it is fully unloaded when contact is re-initiated. Figure 2-23 shows a visualization of this simple model for an established intermittent contact.

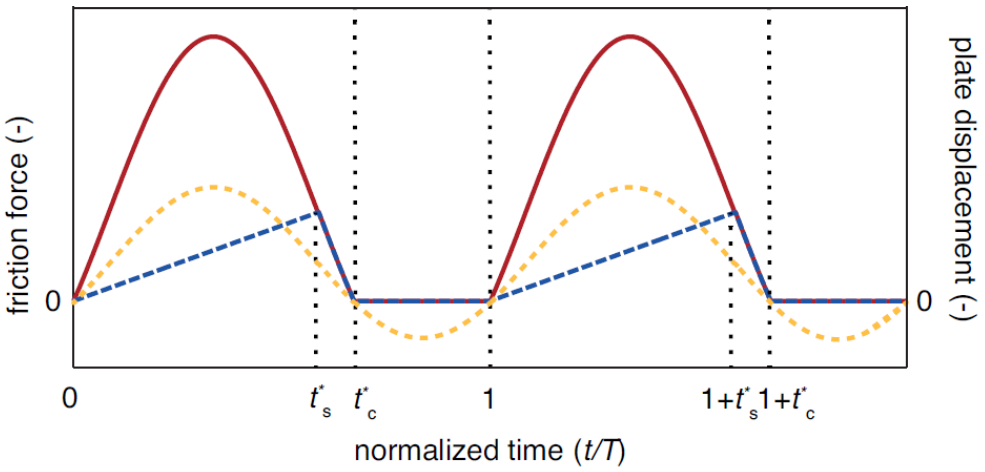

Figure 2-23: Explanation of the reduced friction of an elastic body periodically in contact with a vibrating plate; the frictional force as a function of time was calculated using the spring-slider model where $t_s^* = t_s/T$ and $t_c^* = t_c/T$. The continuous red lines are determined by $\mu_0 F_{reac}$ i.e. the frictional force that would be generated if Coulombic slip occurred throughout each cycle. The dashed blue lines correspond to the lateral force on the elastic body at the interface with the vibrating plate. The dotted black vertical lines denote the times at which Coulombic slip is initiated.

This model emphasizes the importance of intermittent contact to explain the friction modulation observed in ultrasonic devices. This phenomenon is analogous to a frictional ratchet presenting periodic engagement and escape. This latching mechanism is induced by the normal vibration and displacement of the slider which is initially accommodated by compression of the lateral spring so that the frictional force is less than the sliding value. The spring-slider model is assessed by the finite element simulation done in [77].

In summary, the friction increases in proportion to the compression of the lateral spring but the maximum force that can be generated depends on the frictional mobilization time, t_s,

which depends on the duration of contact, t_c. A few consequences can be extrapolated from this simple model:

- The frictional force decreases with increasing frequency due to the reduction of t_c and the resulting decrease of the preloading time (load, unload tension of the lateral spring).
- The frictional force increases with increasing sliding velocity since the lateral deformation rate, and hence that of the lateral force, increases.
- The friction decreases as μ_0 increases since the time to satisfy the slip condition increases.
- Finally, μ is reduced compared to μ_0 due to the lower lateral force present during the loading period.

2.5.3.2 Comparison with measured data

In vivo data measured in the previous experiments are presented in Figure 2-24 (a) for one participant (p4) with an applied normal force of 0.5 N, and a vibrational frequency of 25.1 kHz for three exploration velocities of 20, 40 and 80 mm/s. The reduction in the friction is systematically greater with decreasing exploration velocity. An important point about Figure 2-24 (a) is that normalization results in an approximate superposition of the data.

Trends for the dependency of the vibrational frequency shown in Figure 2-24 (b) show the same increase in reduction that was found in the experiment of section 2.4. This dependence cannot be explained by the squeeze film model only.

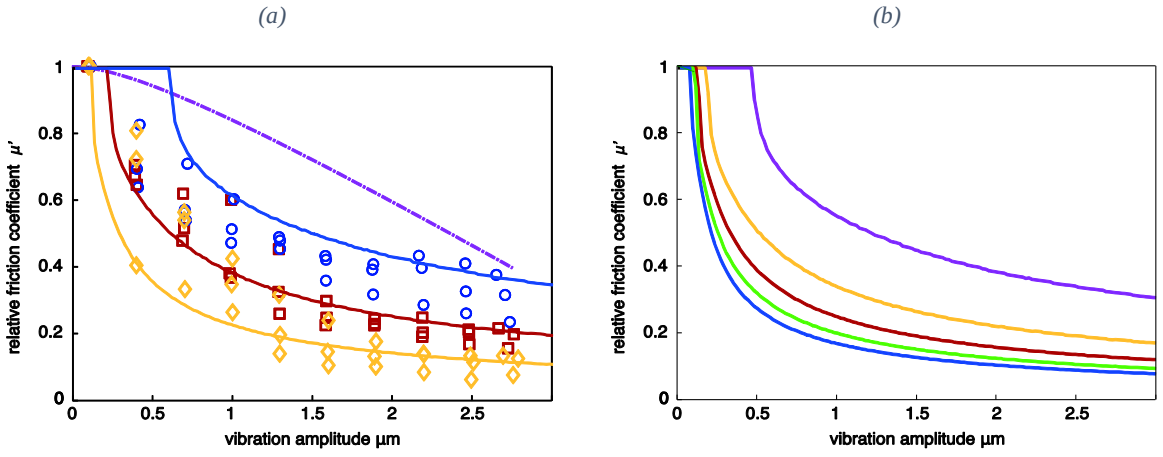

Figure 2-24: Calculated reduction of friction using intermittent contact modelling with the input parameters for the humid case [77] (a) The relative coefficient of friction for p5 as a function of the vibrational amplitude at a frequency of 25.1 kHz, an applied normal force of 0.5 N and the following exploration velocities: 20 (yellow diamonds - dashed line), 40 (red squares – continuous line) and 80 (blue circles – dotted line) mm/s. Solid lines were calculated using the intermittent contact model, the purple chain line was calculated using the squeeze film model [40]. (b) Relative friction coefficient for different resonant frequencies:100 kHz (purple), 80 kHz (Yellow), 60 kHz (red), 40 kHz (green), 20 kHz (green)

As can be seen in Figure 2-14, no friction reduction is predicted by the intermittent contact model for low amplitude of vibration. This lack of reduction is an artifact of the simplified nature of the model, at low amplitude of vibration w_c is not reached and thus the skin does

not detach from surface. In reality, the gradient of forces applied by the pulp of the fingerpad and fingerprint ridges insures that F_{nc} is always reached somewhere, and thus w_c. The model is nevertheless showing a good superposition with the experimental data at higher amplitudes. These artefacts are not visible in the finite element model used to validate the phenomenon [2].

The mean values of the relative coefficient of friction as a function of the vibrational amplitude for all participants are presented in Figure 2-25. There is not a systematic dependence on the applied normal force for the range examined.

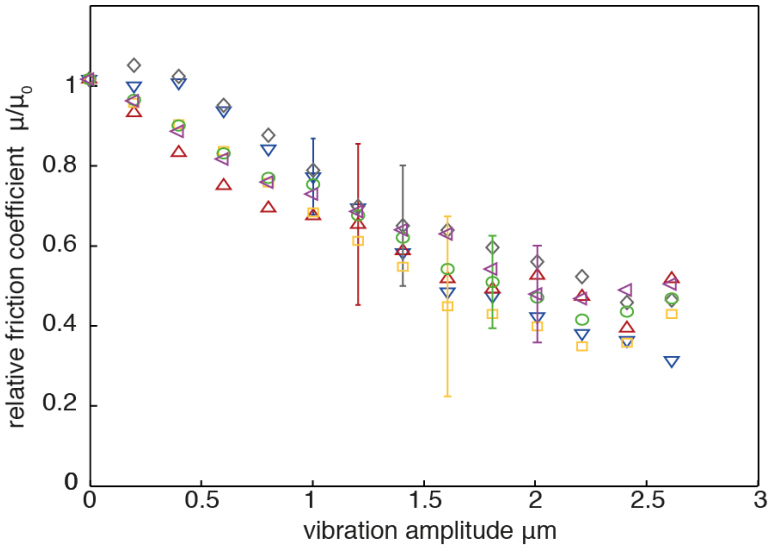

Figure 2-25: Mean relative coefficient of friction for all participants (p1 - p6) as a function of the vibrational amplitude for the following applied normal forces: 0.2 (blue down triangle), 0.5 (red up triangle), 0.75 (grey diamonds), 1.0 (yellow squares, 1.5 (green circles), and 2 N (purple left triangles). An exploration speed of 17 mm/s and resonant frequency of 25.1 kHz was applied in all cases. The error bars indicate the mean standard deviation between the participants.

2.5.3.2.1 Introduction of the dimensionless group data superposition method

A dimensionless group is useful for summarizing the governing parameters of a system and allowing data superposition. It is not possible to write a closed-form solution for the current system and thus any dimensionless group that is derived will provide only first order data reduction.

A necessary condition to obtain a reduction of the friction coefficient - or μ' < 1 - is that there exists a time when the finger pad is out of contact with the plate. This can be written $t' < 1$ where $t' = t_c/T$. Then μ' depends on the ratio t_c/t_s such that μ' $= 0$ when $t_c = 0$ and μ' $= 1$ when $t_s = 0$ in the first period or $t_s = (n-1)T$ in the nth period, where $t_c \sim \left(\frac{F_{reac}}{k_n w}\right) T = \frac{F_{reac}}{k_n w f}$ and $t_s \approx \frac{F_{reac}\mu_0}{k_l U}$. Thus the dimensionless group $\Psi = t_c/t_s$ may be written as:

$$\Psi = \frac{F_{reac}}{k_n w f} \cdot \frac{k_l U}{\mu_0 F_{reac}} = \frac{k_l U}{k_n w f \mu_0} \qquad (24)$$

Since for a finger pad, a common contact area is involved, (24) may be written as:

$$\Psi = \frac{G_{sc}U}{E_{sc}wf\mu_0} \sim \frac{U}{wf\mu_0(1+v)} \quad (25)$$

$$\text{And } G_{sc} = \frac{E_{sc}}{2(1+v)} \quad (26)$$

with E_{sc} is the Young modulus of the *stratum corneum*, G_{sc} the shear modulus, and v the poisson modulus of the ridges.

Finally, the dimensionless group can be better shown with an exponential function for data superposition:

$$\mu' = [1 - \exp(-\Psi/\Psi^*)] \quad (27)$$

where Ψ^* is the characteristic value of Ψ. Eq. (27) satisfies the boundary conditions $\mu' = 0$ at $\Psi = 0$ (tc=0) and $\mu' = 1$ at $\Psi = \infty$ (ts=0).

It has been shown that a minimum gross damping is required for artificial probes to reproduce the reduction in friction observed for human finger pads [24]. The current proposed mechanism of friction modulation is consistent with this observation since it depends on the unloading of the finger pad being much slower than that associated with the vibration. This is required to ensure that the static normal compressive displacement is less than that of the amplitude of vibration of the external layers of the skin.

2.5.3.2.2 Dimensionless group matching with measured data

The analytic intermittent contact model presented in the previous section was validated based on FE modelling [77]. In both models, it is argued that the reduction in friction for ultrasonic haptic displays could be ascribed to a ratchet mechanism in which engagement induces lateral deformation of the fingerprint ridges until the frictional mobilization criterion is satisfied. Thus, during any vibration cycle, the friction is either (i) zero when there is a loss of contact or (ii) less than the slip value.

The model was evaluated in the current work by calculating the influence of the vibrational amplitude for a range of exploration velocities and normal forces on in vivo frictional data. The calculated values are compared with the experimental data in Figure 2-24 and the trends in the numerical values are reasonably like those measured despite the model being relatively simple. The values of the relative coefficient of friction calculated using the squeeze film model [40] are also shown in this figure. The experimental data fit less closely with these friction coefficients and the model cannot account for the friction being a function of the exploration velocity. Thus, these findings are consistent with the observation that the friction reduction does not seem to be influenced by a reduced ambient pressure [75], which would be expected if squeeze film levitation was significant.

Another way to highlight the self-consistency between the experimental data and the ones predicted by the modelling, involving all the parameters' influence is to use the dimensionless

group. The comparison is done in Figure 2-26 for study-case with a natural finger: the reduced variables plot of the in vivo data show a reasonable data superposition for amplitudes of > 1 µm with the exponential function (27) with $\Psi^* = 4.69 \pm 0.32$. However, it may be noted that, in this case, only a small range of the dimensionless group could be fitted, because for amplitudes lower than 1µm, the intermittent contact is not established. In comparison, using the probe, it is possible to achieve data superposition for a range of vibrational frequencies, exploration velocities and applied normal forces as well as vibrational amplitudes (Figure 2-27) In this case, the value of Ψ^* is 0.70 ± 0.04.

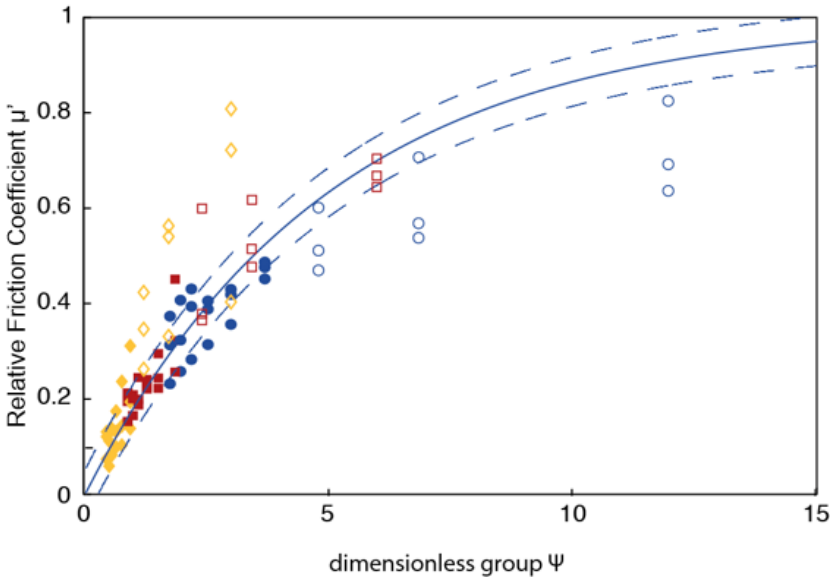

Figure 2-26: Relative friction for participant p5 with an exploration velocity of 20 (yellow diamonds), 40 (red squares) and 80 mm/s (blue circles) as a function of the dimensionless group; the data are taken from Figure 2-24(a). The full line is the best fit of the filled points to Eq. (27) and the value of Ψ^* is 4.69 ± 0.32; the open points correspond to w > 1 µm and were not included in the fit. The dashed lines show the RMSE variation of the fit.

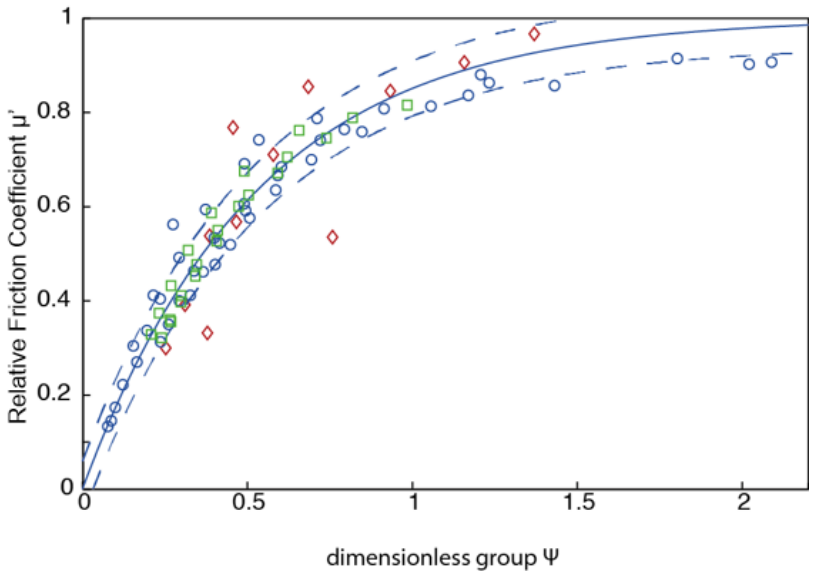

Figure 2-27: The relative coefficient of friction as a function of the dimensionless group for the probe sliding on an ultrasonic vibrating plate with a range of vibrational frequencies (red diamonds), exploration velocities (blue circles) and applied normal forces (green squares) the data are taken from Figure 2-18 respectively. The full lines are the best fits to Eq. (27) and the value of Ψ^* is 0.70 ± 0.04; the dashed lines correspond to the RMSE variation.

Actually, *in vivo* data are considerably more scattered and less reproducible as exemplified in Figure 2-28 for two of the participants and a range of applied normal forces. A possible contributory factor is that the finger pads exhibited a wide range of Young's moduli so that not all the data corresponded to the intermittent contact being sufficiently well developed. In such cases, the reduced variables approach becomes inapplicable at smaller vibrational amplitudes. However, by taking mean values of the data for all participants (Figure 2-25) and fitting to the exponential function, mean values of Ψ^* as a function of the applied normal force were obtained (Figure 2-29). The figure shows the best fit to a linear relationship with a slope of -0.094 with 95 % confidence bounds of -0.49 and 0.30 and an intercept of 1.80 with 95 % confidence bounds of 1.34 and 2.27. Thus, it may be concluded from these data that Ψ^* is not a strong function of the applied normal force and that the mean value of Ψ^* is reasonably consistent with that of the numerical data for which $\Psi^* = 2.38 \pm 0.21$ [77].

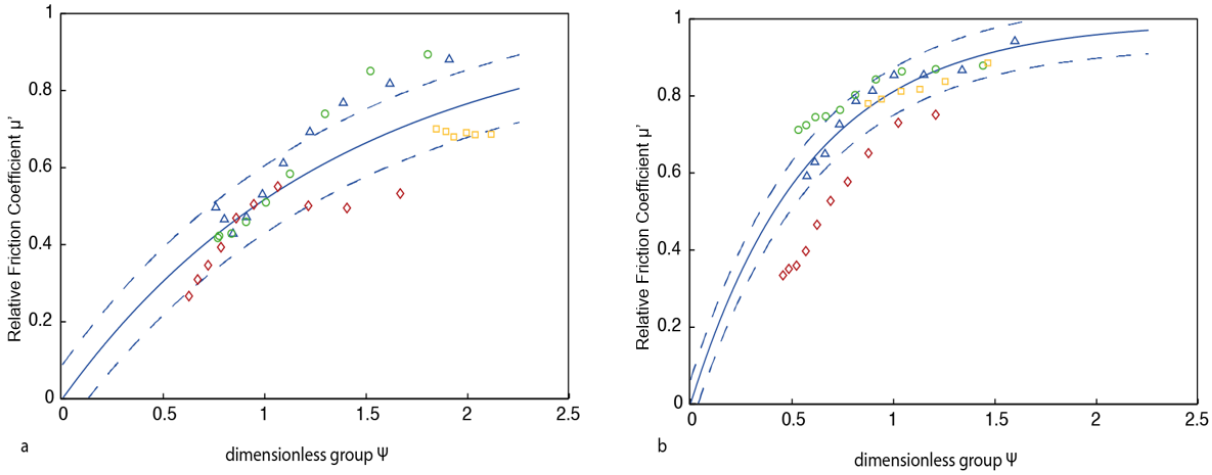

Figure 2-28: The relative coefficient of friction as a function of the dimensionless group measured for two participants with an exploration velocity of 40 mm/s and a range of normal forces. (a) p2: 0.75 (red diamonds), 1 (blue triangle), 1.5 (green circles) and 2 N (yellow squares). (b) p3: 0.2 (red diamonds), 0.75 (blue triangle), 1 (green circle), and 2 N (yellow squares). The full lines are the best fits to Eq. (27) and values of Ψ^* equal to 1.89 ± 0.18 and 0.78 ± 0.046 respectively; the dashed lines correspond to the standard deviation of the fit to the exponential function (27).

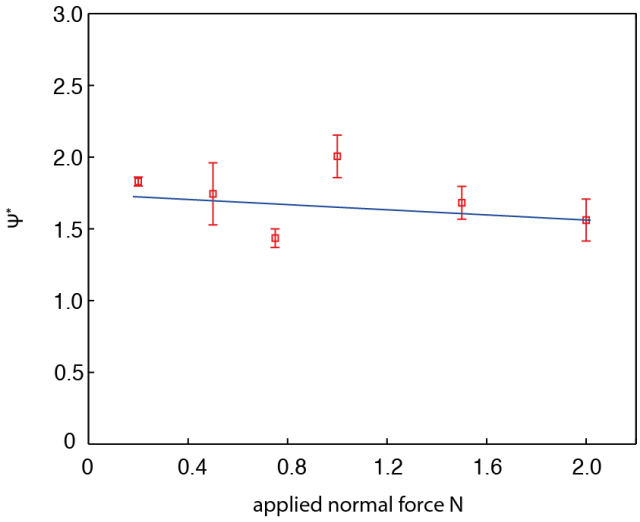

Figure 2-29: The characteristic value of the dimensionless group as a function of the applied normal force calculated by fitting Eq. (27) to the data in Figure 2-25. The line is the best linear fit to the data.

It can be noted that the reduction of the friction coefficient in function of the amplitude of vibration does not seem to be a strong function of the normal load applied. The low influence of load in the experimental data seen in paragraph 2.3.3.2 might thus be due to an increase of the contact area when applying higher normal loads. This increase of the area could cause an increase of the friction coefficient due to the non-homogeneous amplitude of vibration across the short axis of the experiment devices.

2.5.4 Conclusions

The current experimental data are consistent with the analytic model presented in paragraph 2.5.3.1 and the data superposition scheme derived in that work. Thus, the proposed ratchet mechanism is a satisfactory explanation for the friction modulation of ultrasonic displays and squeeze film levitation does not seem to make a significant contribution. The friction modulation depends on the exploration velocity, it is relatively independent of the applied normal force and it does not diminish to zero, which is contrary to the predicted behavior based on squeeze film levitation. Data reduction using an exponential function of a dimensionless group requires that the vibrational amplitude must be > 1µm for the range of frequencies examined here. This is because the intermittent contact must be sufficiently well developed, which was the case for the measurements with the probe. However, a smaller range of amplitudes was employed for the in vivo measurements to be consistent with those in current practice. Coupled with the inherent variability of such measurements, it is only possible to obtain approximate data reduction. While there is an upper limit on the amplitude at which vibrations will be sensed by a user, the performance of existing displays could be enhanced by increasing the vibrational frequency.

A reliable theoretical model of the friction modulation for ultrasonic devices will have implications for control, energy consumption and performance optimization.

2.6 List of Requirements for an ULD and Design Rules

This chapter explored the influence of relevant parameters on ultrasonic lubrication. Measurements were done to assess the effect of normal load, velocity of exploration and frequency of vibration. Strong of this dataset, a correlation was done on two different models of the ultrasonic lubrication effect. It was found that the so called “squeeze film” effect does not predict reliably the reduction of the friction coefficient. This is not the case for the second model explored which is based on intermittent contact of a Coulombic slider.

The large amount of detailed data and the analytic model allow us to redefine the necessary requirements for the optimal design of tactile display based on ultrasonic lubrication.

2.6.1 Amplitude of Vibration

The amplitude of vibration reachable by the UL HMI has the most impact on the haptic feedback given to the users. This chapter completes the psychophysical studies that have been conducted to assess the influence of this parameter [38] [63] [68]. As seen in section 2.3.3 a previously unknown phenomenon about maximum friction reduction was highlighted. This limit after which an increase of amplitude does not have any effect on **the friction reduction seems to appear above 2.5µm for all users.** This establishes an upper bound to the amplitude necessary to achieve a maximum friction reduction and thus limits the energetic design constraint for the driver.

2.6.2 Frequency of the resonant mode

The choice of the vibration frequency is originally one of the less constraining parameters in the design of UL tactile device, the only limits being the range of human hearing and the need for a squeeze number above 10. These limits pushed the resonant frequency above 25 kHz but did not give more cues on the optimal frequency range a designer of UL devices should select. The experimental data acquired in chapter 2.4 **show that increasing the frequency further could improve the range of friction reduction achievable with a tactile device.** This finding is confirmed by the analytic intermittent contact model presented in section 2.5.3. Increasing the vibrational velocity is both a constraint and a benefit for the design of the electronic components. The impact of these benefits and constraints on the integration of this technology in future mobile devices will be explored in the chapter 3.

2.6.3 Rise time of the Vibration Amplitude

While not physically measured in this chapter, one more factor, the bandwidth of modulation of the friction coefficient, should be added to the guidelines pertaining to the design and development of UL display. This factor is fundamentally linked to the human perceptions limits but has a significant impact on the geometry of the resonating plate and on the design of the electronics of the amplitude control loop. It should thus be factored in at the first stage of the design.

As seen in chapter 1 the human mechanoreceptors can perceive vibration until ~500 Hz. In order to stimulate the fingertip on its whole range of sensation a tactile device should offer control vibration up to this limit. In the case of ultrasonic lubrication, the vibration of the mechanoreceptors is created by alternating states of high and low friction coefficients. To generate this effect, the whole surface of the device must go from static to high amplitude of vibration quickly enough (similarly the damping needs to be sufficient to ensure that the surface stops vibrating in time). The minimal rise time in the case of a square modulation can be estimated using the following relation:

$$T_{rt} = \frac{0.35}{Bw} \quad (28)$$

Where T_{rt} is the rise time and Bw the frequency bandwidth of the signal. This estimation is calculated by approximating the highest sinusoidal wave frequency needed to get a specific rise time as can be seen in Annex A.

In our case, equation (28) necessitates a minimal rise time of 700 µs to obtain a bandwidth of 500 Hz. This rise time value is small compared to most previous prototypes of ultrasonic display [48] [79]. It suggests that these displays did not have the capability of stimulating the whole range of sensation of the human fingertip. As a matter of fact, this limit is also present on the measurement devices presented in this chapter, for example the steel plates presented in section 2.3 present a rise time above 500 ms even with the PI control system. The second set of devices presented in section 2.4 would be little more usable for modulation purpose since they possess a rise time of ~100 ms.

While a rise time of 700 µs is necessary to stimulate the whole perceptive bandwidth, it can be difficult to reach this value. To lower the constraints associated with the time rise, we propose a maximal bandwidth of 150 Hz, corresponding to the point of maximal perception for the SA II mechanoreceptors as was presented in chapter 1, Figure 1-8. A value of 150 Hz is also the point of inflection after which the global psychophysical amplitude perception threshold increases again. With this value, we can propose that **the rise time of ultrasonic display shall be under 2.3 ms.** The rise time of the vibration will be studied deeper in Chapter 4 using psychophysical methods.

2.6.4 Conclusion

To summarize, the experimental and model findings presented in this chapter concur to point the following design rules for improved sensations on ultrasonic tactile devices.

- To reach the best friction reduction, the device shall reach a vibration amplitude of at least 2.5 µm. However, if we consider that an amplitude of vibration of 2 µm is enough to achieve at least 95% friction reduction, this value offers a good alternative that is less energetically expansive, improving the integrability potential of UL technology.

- The vibrational velocity of the resonant display shall be as high as the embedded electronics' control allows (typically above 70 kHz)
- The rise time of vibrating screen shall be under 2.3 ms to be able to stimulate all the mechanoreceptors, and reach the fingers frequency of maximal sensibility.

It is to be noted that the new design rules highlighted in this chapter only have the objective of increasing the haptic feedback given to the user by the ultrasonic vibrating display. These optimizations, while quite effective in this aspect, will impose a higher power consumption to these devices. The dimensions and energy consumption of the piezo-ceramic driver are especially important considering the level of integration and portability required by the mobile platform industry.

These three design rules will be applied in the next chapter to present the design process of optimized UL tactile displays. Psychophysical evaluation in chapter 4 will then be applied to demonstrate that this higher power consumption can be partially compensated by a more intelligent and human-based control software.

3 DESIGN AND DEVELOPMENT OF OPTIMIZED TACTILE DEVICES INTEGRATING HAPTIC AND VISUAL FEEDBACKS

Summary

3.1 INTRODUCTION

Tactile friction modulation has large potential in multiple fields of human-machine interfaces (HMI), this effect can be used on its own (for example to help visually impaired user) but would find a significantly larger market by its implementation on ubiquitous mobile devices. As described in chapter 1, combination of ultrasonic friction modulation and visual feedback has been previously prototyped [80]. However, one issue with this integration is that it imposes multiple constraints on the HMI design, which then proved to impact negatively the usability of these first designs [81]. These issues are centered on the size of the dead margin of the screen, the high excitation voltage of the actuators, and the size of the piezo ceramics' driver.

Using the new design rules presented in chapter 2, the design of the actuator for transparent display was rethought, to optimize both visual and haptic feedbacks. These optimizations are concentrated on the improvement of the choice of resonant frequency, rise time and vibration amplitude.

The first section of this chapter presents three HMI prototypes developed to explore the optimization and the industrialization of transparent ultrasonic friction modulation. The first two implementations are based on discreet piezoelectric actuators. They offer design improvements to increase the vibration amplitude and reduce the rise time. The third HMI device explores the possibility of using thin-film actuators to reduce the voltage needed to actuate the glass, and facilitate integration into thin devices.

Moreover, to optimize the haptic feedback generated by UL, it is necessary to improve the driving algorithm controlling the amplitude of vibration. In a second section, such optimization is presented and applied to the design of an advanced piezoelectric driver, used to control the previously described HMIs.

3.2 COUPLING VISUAL AND TACTILE FEEDBACKS

3.2.1 Engineering challenges of coupling UL and visual feedbacks

This first section introduces the challenges inherent to the utilization of discreet piezoceramic actuators and to the design of the transparent UL plate with a large amplitude of vibration is described.

3.2.1.1 Integration issues related to discreet piezo ceramic actuators

As seen in chapter 1, all the historic ultrasonic lubrication prototypes are actuated using discrete ceramics that were glued separately on the resonant surface. The process is similar for transparent and opaque demonstrators, with the exception that transparent demonstrator needs the integration of a common ground shared between the ceramics for proper excitation, because glass is an insulator, and a specific location of the ceramics to keep a transparent area. In devices where the amplitude control or measure is important, an additional piezoelectric ceramic is used as a sensor.

Discreet piezoelectric ceramics are historically used because of their simplicity of manual integration. They are nevertheless constraining when industrialization is the objective. Two main issues can be identified: first, a difficulty of integrating discreet ceramics into an industrial device due to the high failure rate of the glue and the necessity to pick and place each ceramic independently. Wiring the independent ceramics automatically in a reliable manner also poses problems.

The second issue lies with the high voltage necessary to actuate such piezo ceramics up to the required amplitude of vibration. As seen in Chapter 1, to obtain the required amplitude of vibration across the resonant device, it is necessary to increase the maximum deflection achieved by the piezo ceramics. This deflection is intrinsically linked to the electrical field applied across the electrodes of the piezo ceramic actuators, as presented in equation (1). High voltage differential has multiple negative effects on the design and operation of consumer tactile device. Firstly, we need to consider its impacts on the driving electronic. Designing a piezoelectric driver able to sustain actuation above 200 V imposes the use of large components able to resist to the thermal load and high voltage transient during commutation. The size of the capacitors is also severely impacted by the excitation voltage. Finally, large voltages create the problem of a potential ‘fear’ felt by some users; most people when first presented with the UL technology are enthusiastic, however they emit reserves when familiarized with the voltage needed to actuate the piezo ceramics. These reserves are like the remarks made about electro-vibration based friction modulation where high voltage must be applied a few µm away from the user’s skin.

As presented in equation (1) for a given amplitude of vibration w, the main parameters affecting the voltage to apply across the piezoelectric ceramics are the thickness of the actuators h_p and its ratio with the thickness of the resonant device itself. Reducing the

thickness of the ceramics under 0.5mm is difficult due to a reduction in the polarization of the ceramic piezoelectric material.

3.2.1.2 Challenges inherent to the combined integration of both visual and haptic feedbacks

The design of a transparent UL device is quickly confronted to the problem of the lack of place available for the piezoelectric actuators. Since actuators are not transparent, they need to be positioned on the outside of the central space of the plate, occupied by the visual screen. The lateral zones used for the placement of ceramics are referred as “dead zones” in reference to similar emplacement used to fix the protective glass screen on first generations of smartphones.

A second issue appears when trying to combine visual and haptic feedbacks; due to the necessity of vibrating the top surface in contact with the fingers, it is impossible for this glass to be into contact with the underlying layers. An air gap must thus be preserved at all time between the resonant layer and the visual screen, the depth of this air gap must be enough to accommodate for the deflection of the glass under the pressure of a finger (1 to 2 N max). However, the air gap cannot be too large due to its strong negative impact on the visual quality of the screen, caused by parallax effects and reflectivity problems. This air gap problem is the big limiting factor for the size of UL stimulators in the future.

This problem is even compounded if we envisage the future integration of UL stimulation to new industrial smartphones; indeed, since a few years, the manufacturer uses a layer of glue between the “protective” screen and the underneath layers to create a full lamination of the stack. This process has a twofold benefit for the manufacturer: first, the glue is chosen for its optical properties to reduce reflectivity and increase color contrast. The second advantage is the strength of the final laminated screen, which is required by all car and mobile phone manufacturers. These problems while potentially solvable (by increasing the power or laminating transparent thin-film actuators) are beyond the scope of this study.

3.2.2 Optimized Transparent UL Stimulator: Discreet Piezoelectric Actuators

In this section, two demonstrators are realized combining visual and tactile feedbacks. Their design requirements are based on the proposed optimum UL stimulation parameters found in Chapter 2. These new devices are designed to include visual feedback as well as UL tactile feedback.

The first part studies the new requirements of the design and proposes an overall architecture that will be applied to both demonstrators. In a second part, a first actuator setup, aiming to increase amplitude of vibration while reducing the size of the actuators is described. The last subsection presents the E-ViTa, a demonstrator built specifically to produce an extremely reduced rise time for future psychophysical studies.

3.2.2.1 Optimization of Previous design combination of UL Haptic and Visual feedback

The set of rules defined at the end of Chapter 2 are used for these two demonstrators to ensure optimum tactile feedback capabilities: The amplitude should reach at least 2.5 µm to ensure a maximum friction reduction. The frequency should be above 60kHz to improve the tactile stimulation, and a rise time at least under 2.3ms to offer a minimum bandwidth of 150 Hz. In the case of a device combining haptic and visual feedbacks, two more constraints can be found:

- The central surface of the haptic device must be transparent to allow direct interaction with the virtual objects
- The latency between the detection of the position of the finger and the application of a tactile stimulation should be kept to the minimum to reduce the feeling of lag by the user

Considering these constraints, it was decided to build the architecture of the device around a cheap embedded Linux computer (BananaPro), this computer can be simply extended with a 5-inch LCD screen including a capacitive touchscreen. A UL resonant glass is placed on the top of this computer to provide tactile feedback. The architecture uses an optimized driver that will be presented in detail in section 3.3.

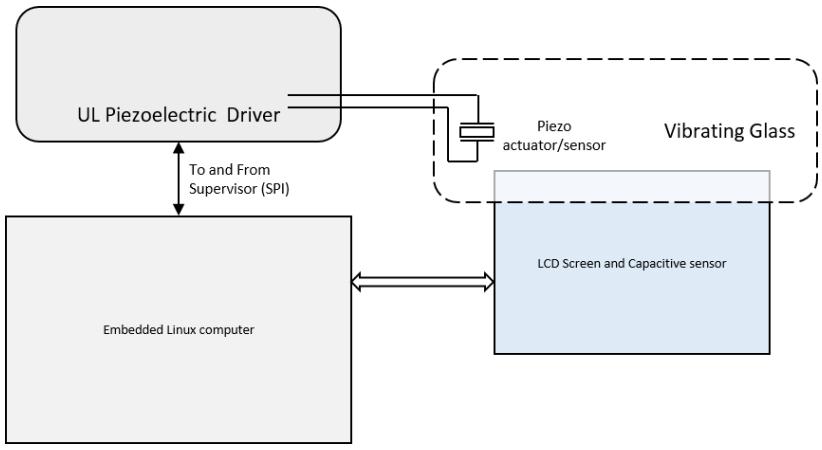

Figure 3-1: Proposed overall architecture, Including the driver developed in section 3.3.

3.2.2.2 Implementation of "winglets" type of actuation

3.2.2.2.1 Design of the transparent UL actuator

To actuate a homogeneous lamb wave across a flat square surface, the designer must place the piezo ceramic actuators on a position optimizing the electromechanical coupling. This type of electromechanical couplings' enhancement to provide higher amplitudes of displacements is common in "bender" actuators. These bender actuators use the extremely high force provided by the piezo ceramic actuators to compensate for their small range of movement.

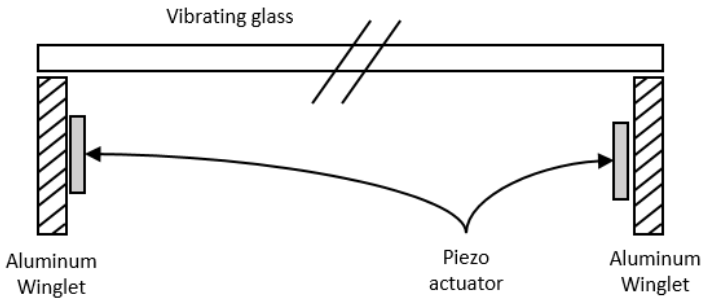

Figure 3-2: Schematics of the winglets and ceramic placement

A similar solution was proposed by M. Amberg to implement this concept to the actuation of UL devices [82]. As shown Figure 3-2 the piezoelectric ceramics are reported on two metallic bands (here Aluminum) that are each one glued to the extremities of the resonant surface. This approach proved its ability to enhance the voltage to displacement ratio and thus insure higher achievable amplitude of vibration for a given driving circuit. An iterative optimization of the ceramic placement and length of the aluminum resonator is done as detailed in Chapter 1. The material properties used are recapitulated in the following table (the glue is considered perfect).

Table 5: Material properties of the Aluminum, Glass and the piezoelectric PZT

Material	Young's modulus (GPa)	Poisson's ratio	Density (g/cm^3)
PZT ceramic	80	0.33	7,9
Glass	73.6	0.23	2.38
Aluminum	75	0.33	2.8

In Figure 3-3, the amplification effect can be seen on the Eigen simulation of the resonant mode; indeed, while a large even displacement if found across the surface, the bending radius on the metallic band is extremely reduced.

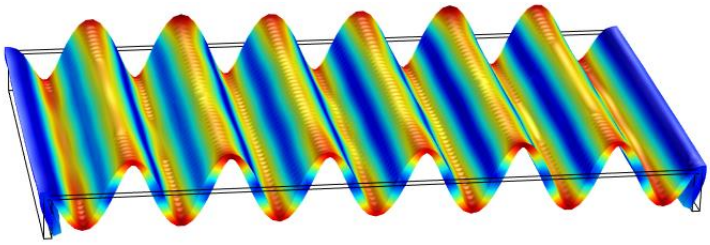

Figure 3-3: Eigen mode simulation in a free-floating configuration for a glass surface with 2 aluminum resonators at the extremities. Resonant mode is found at 23493 Hz

This actuation solution also brings multiple advantages compared to simple actuator deposition on the surface of the screen:

- The lateral dead zones are reduced to a minimum, allowing the creation of smaller device.

- The low displacement seen at the corner at the gluing point is also a good candidate for simple fixation of the screen since it would only affect minimally the resonant mode.
- High rejection of parasitic modes of vibration due to the large metallic band reducing the possibilities of torsion in other axis than the length of the plate.
- Deported winglet actuators provide an easier manufacturing method, simpler to automatize. The metallic substrate of the winglet provides an easy bottom electrode that can be used to power the ceramics.

Due to these advantages, the winglet actuator type was chosen to create the UL effect on the demonstrator. To comply with the requirement, a high resonant frequency was searched. As can be seen in in Figure 3-5 (b) a prototype was built on this concept. The size of the glass resonator is 128 x 75 x 0.8 mm, with winglet of 75 x 9 x 1.5 mm to be able to position a 5-inch (12.7 cm) LCD screen underneath.

The electromechanical coupling on a range of frequencies of the realized device was measured using a BK Precesion Mdel 891™ RLC meter.

(a) *(b)*

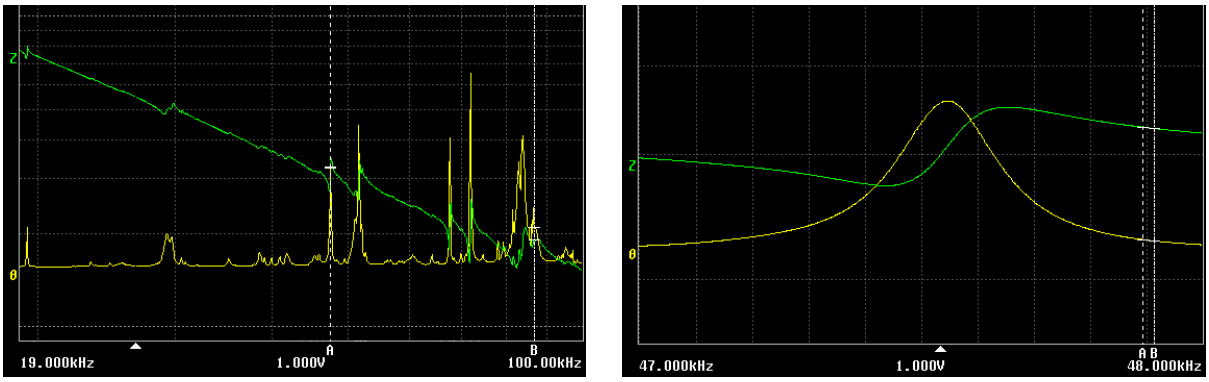

Figure 3-4: Impedance meter measurement of the electromechanical response of the winglet plate. (a) Broad exploration of the spectrum from 19 kHz up to 100 kHz. (b) Zoom on the clean resonant mode identified at 47560 Hz.

As it can be seen from Figure 3-4 (a), the number of strong modes present on the large spectrum of 20 to 100 kHz is low. This phenomenon is due to the large filtering of the lateral metallic bands that preserve almost only the sinusoidal standing wave resonant modes along the length of the plate. The chosen mode frequency (~47 kHz) is not the mode with the stronger mechanical coupling as seen in Figure 3-4 (a), but higher resonances presented close parasitic modes that could affect the stability of the waveform when subjected to damping. Figure 3-4 q (b) shows the selected resonant mode, presenting a good resonant mode with no parasitic mode of vibration at a close frequency.

For the chosen mode, the performances of the simulation compared to the realized device can be seen in Figure 3-5. The actuation of the actuator was done using a function generator (33250A) and an amplifier (FALCO). The nodal lines are found to check the shape of the mode

using sugar powder. A small discrepancy of 0.5% can be seen between the simulated and measured frequency: respectively 47770 Hz and 47560 Hz. Probably due to manual manufacturing defaults. The deformation of the device under resonance was then observed using a laser vibrometer (POLYTEC©). This system uses interferometry to measure the velocity of the point under the vibrometer. With a voltage to amplitude ratio of 0.042 µm/V, the maximal useful amplitude of 2.3 µm peak-to-peak was reached with only 55 V AC.

(a) *(b)*

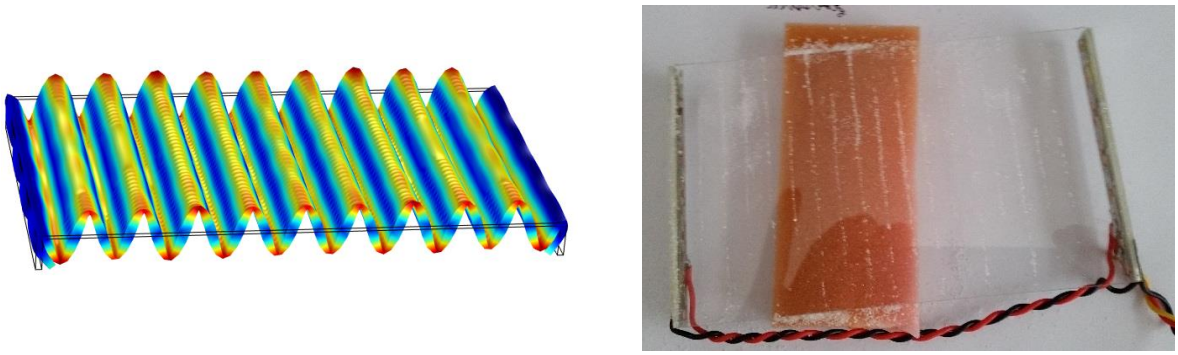

Figure 3-5: (a) Eigen mode simulation in a free-floating configuration for a glass surface with 2 aluminum resonators at the extremities. Resonant mode is found at 47770 Hz.

The corresponding resonant mode in the physical device is confirmed using sugar powder to mark the nodal lines. A resonant frequency of 47560 Hz is found at 21°C.

3.2.2.2.2 Implementation of low Latency control system on the final assembly

As described in subsection 3.2.2.1 the completed system integrates a Linux computer controlling a 5-inch LCD screen and a capacitive sensor. The haptic feedback is provided by the integration of the high speed piezoelectric driver that will be developed in section 3.3. The resonant glass with lateral winglet actuators is put on the top of the whole system in a free configuration (hold in place by foam tape on the edges of the nodal lines). The CAD exploded view of the device can be seen in Figure 3-6 (a). The external connections of the BananaPro embedded computer are left apparent to connect different peripherals. Figure 3-6 (b) shows the realized final product with its black 3D printed casing. The embedded computer and the piezoelectric driver are powered using a common 5V DC external supply.

(a) *(b)*

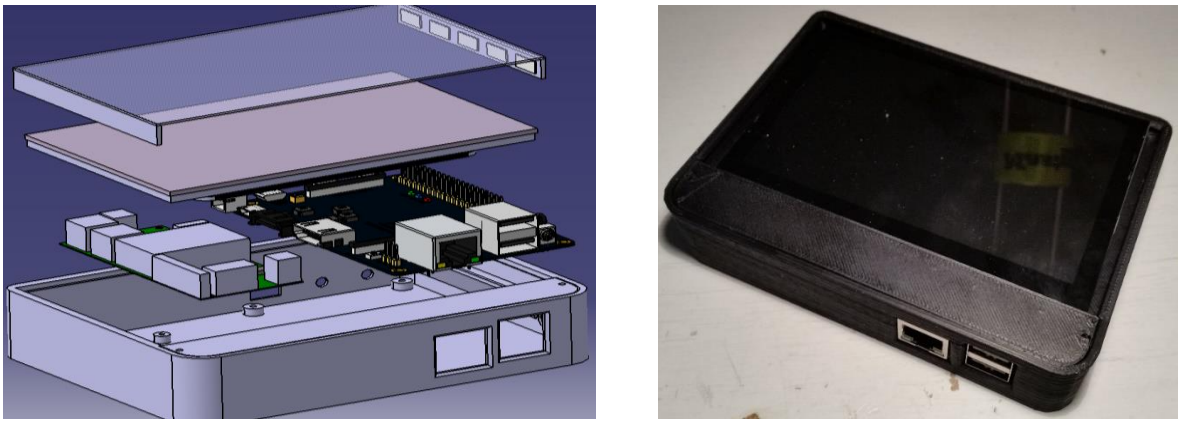

Figure 3-6:(a) Components of the demonstrator fitting into the 3D printed enclosure. The transparent plate with its amplifying winglets can be seen on the top. The UL driver developed in section 3.3 and the BananaPro Linux computer can be seen.

(b) Final realized device integrating all components.

The latency of the finalized system is affected by multiple components. Since the architecture is built around a central processing unit, multiple communication delays occur at different stages, and were to be handled:

- Acquisition of the position by the capacitive sensor
- Maximum update frequency of the position to the embedded computer
- Processing of a potential event (for example a click in the GUI)
- Transmission of command to the low-level system
- Rise time of the UL Device (dependent on the control frequency and intrinsic rise time of the resonant plate).

This prototype and the associated basic Graphical User Interface (GUI) demo interface, was delivered to a partner company Hap2U® for testing and demonstration purposes in 2016.

3.2.2.2.3 Conclusion

A HMI device integrating haptic and visual feedbacks was designed and built. The realized device is a standalone interface that can be used to showcase and test multiple scenario of friction modulation. The UL feedback given by the device is optimized compared to previous generations due to the use of new design rules amplifying the strength of the friction modulation effect.

3.2.2.3 Implementation of a high frequency transparent stimulator: E-ViTa

Another transparent configuration, named E-ViTa is described here as it will be used for the psychophysical evaluation presented in Chapter 4. It has been mainly designed by E. Vezzoli [2] and partly within the present work for the control aspect. Indeed, to measure the limits of human perception, the tactile feedback device must present signals with a lower than average rise time and higher frequency of modulation. First, the general experimental system is

described and then the UL resonator that was specifically developed to provide high modulation frequencies, is detailed.

3.2.2.3.1 Global System Description

This specific UL stimulator was designed to deliver controlled and repeatable stimulations. The architecture is like the winglet device presented in paragraph 3.2.2.2. The system architecture presents the same embedded computer board communicating directly with a low level piezoelectric driver, which is based on phase shifted transformer technology. To control the modulation frequency at high frequency and the vibration amplitude of the haptic plate, a new device was specifically developed. The main difference can be seen in the topology of actuation used to deform the resonant plate (Figure 3-7)

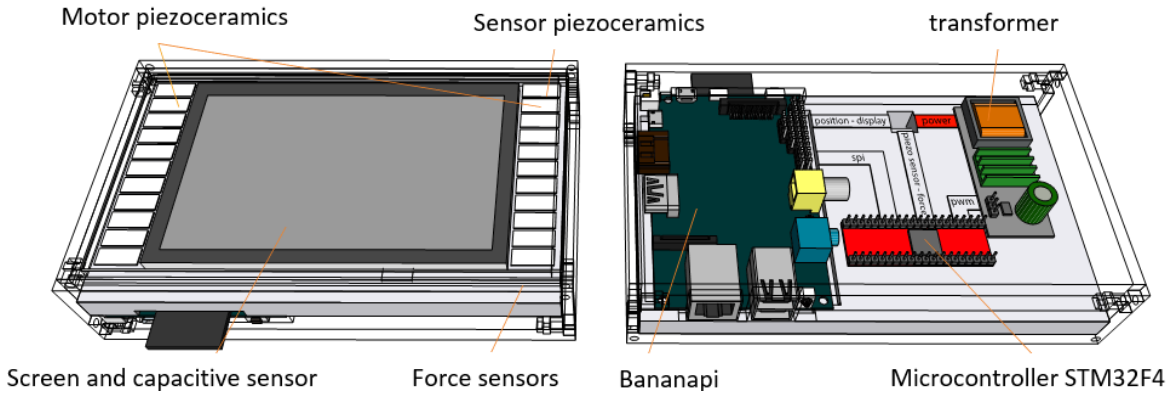

Figure 3-7: Device architecture [83]

Moreover, this system includes both visual and haptic feedbacks. Computation and control of the experiment is separated in two parts: a “high level” signal using the Banana Pi (Shenzhen LeMaker Technology Co. Ltd, China) single board computer featuring a 1 GHz ARM Cortex-A7 dual-core CPU with 1 GB of ram. A “low level” signal generation is implemented in a separate DSP microcontroller (stm32f4, STMicroelectronics, France) running at 164 MHz. In this setup “high level” computing refers to the display of the instruction to the user, selection of the haptic signal commands and storage of the results. The signal generation microcontroller applies commands from the board computer to create the necessary waveforms for the friction modulation. The communication between the microcontroller and the single board pc is provided by an SPI bus working at 10 kHz.

As in the device presented in paragraph 3.2.2.2, the single board computer is connected to a 5 inches’ flat capacitive touch screen (Banana-LCD-5"-TS, Marel, China) providing the finger position input and display output, where the sampling frequency of the finger position is 62 Hz.

3.2.2.3.2 Ultrasonic Vibrating Plate

The ultrasonic vibrating plate implemented in the device is specifically designed to provide the best modulation bandwidth [83]. The glass plate measures 154 x 81 x 1.6 mm^3, resonating at

60750 Hz, where the half length of the vibration mode is 8 mm. 22 piezoceramics, 14 x 6 x 0.5 mm^3 are mounted at the side of the plate along the extremum of deformation, 20 used as motors and 2 as vibration sensors. To cope with the isolating function performed by the glass, their unglued electrode was cut along the nodal line and each side connected to the amplifier to create a virtual mass on the glued face of the ceramic. The cartography of the vibration amplitude of the plate is reported in Figure 3-8.

A closed loop control is implemented in the microcontroller; it is acquiring the amplitude of vibration using 2 piezoceramic sensors. Tuned with the Ziegler-Nichols method, this controller exhibits a bandwidth of 400 Hz at 2 µm. The closed loop control generates an amplitude stability within a tolerance of 50 nm, for a normal force applied by the fingertip lower than 3 N (Figure 3-8).

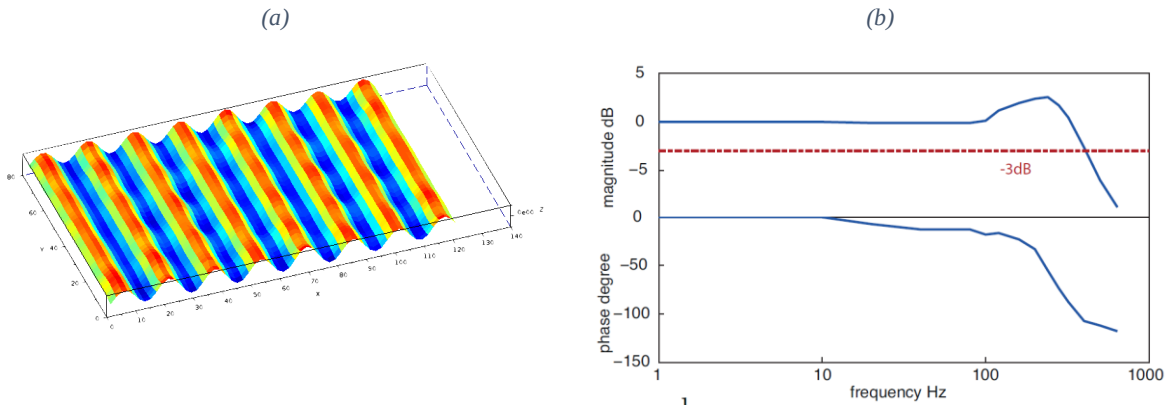

Figure 3-8: Dynamics of the resonator. (a) Cartography of the ultrasonic vibrating plate. (b) Bode diagram of the vibration response of the plate. The dashed line at -3 dB indicates the bandwidth of the plate up to 400 Hz

This device is usually operated with a vibration amplitude of only 1.5 µm peak to peak, which is lower than the optimal levels found in Chapter 2. Nevertheless, due to the high frequency of resonance (60 kHz) participants report a strong tactile feedback.

3.2.3 Optimized Transparent UL Stimulator: Thin Film Piezoelectric Actuators

This section presents a technological alternative to discrete piezo ceramics by relying on the deposition of thin film piezoelectric material using process commonly used by silicon chip manufacturers. The development and characterization of a transparent proof-of-concept prototype based on this technology is described and characterized. This work was done in collaboration with Francois Bernard and Fabrice Casset with the support of MINALOGIC FUI project *TouchIt.* My work was centered around the mechatronic integration of the control system, and the low-level code associated with it.

3.2.3.1 General advantages of Thin Film Technology

Thin film piezoelectric-ceramics technologies present multiple advantages for an UL device. The first of these advantages is the extremely reduced thickness of the ceramic. As seen previously, this reduction in thickness is directly correlated with a decrease of the voltage needed to create the same electric field across the poles of the piezo ceramic. As will be seen later in this chapter, this reduced excitation voltage has a significant impact on the dimensions of the components of the piezoelectric driver.

A second advantage of using thinner piezoelectric ceramic actuators and sensors is a simplification of the manufacturing process. Depositing single ceramic actuators one by one is a complex and time intensive process. When discussing with companies like Microsoft and Samsung they mentioned difficulties in getting a reliable gluing process that will withstand the stress of high frequency vibrations on glass surfaces. Common modes of failures of this process includes ungluing (delamination) and breaking of the piezo-ceramics. Thin film actuators can be deposited with a totally different process: Direct Deposition or Roll-to-roll. Direct deposition is the process of depositing and engraving the contacts and the piezoelectric ceramics directly on the vibrating substrate (in our case the transparent glass) using standard photolithographic methods of the semiconductor industry. In a roll to roll process, the electronic devices are created on a roll of flexible material (polymer or metal) and then cut to size and glued to the vibrating surface. This method could allow the fabrication of many devices at a fraction of the cost of traditional semiconductor methods.

The extremely reduced thickness of the actuators (from 500 nm to 2 µm) also presents two potentially important benefits to the manufacturing and integration process. First, the integration of the technology in mobile platforms is made easier by having thinner components (smartphones and tablets tend to have thinner and thinner profiles to satisfy consumers). Second, this thinness could be exploited in the future to create fully transparent actuators and sensors directly deposited on the transparent part of the vibrating screen. Transparent thin film piezo-ceramics would further reduce the size of the screen by removing the need for dead zones around the screen which normally house the ceramics. Moreover, the opportunity to place ceramics across the surface of the vibrating plate would increase

once again the achievable amplitude of vibration for a given excitation voltage as seen in [38] [84].

3.2.3.2 Development of a Touchpad type device integrating the Aln Actuators

The next subsections introduce a device created as a proof of concept of the Thin-Film technology application in UL devices.

3.2.3.2.1 General design of the demonstrator

The device presented in this section is a demonstrator created to prove the effectiveness of the thin-film piezoelectric technology in the creation of ultrasonic lubrication display. If successful, this technology will bring many improvements to the actual implementation of UL displays as detailed in the previous section.

As a first proof of concept, the new device was built mainly around the requirement of generating haptic tactile cues. To this end, it was decided to create a touch-pad type device like the first generation of Stimtac [84]. A touch-pad architecture simplifies the design constraints to allow more focus on the UL tactile screen itself. It was also intended to keep the design of the UL display as modular as possible to integrate more capabilities in the future

A set of requirement was proposed before the design phase to insure the Touch-Pad testability and its future modularity:

- The tactile interface integrated in the device must create a minimum tactile cue that can be perceived by the user. This minimum perceptible cue was defined by the TouchIt partners as an amplitude of vibration of 1 um for a frequency above 20 kHz. These values where selected to match previously design functional devices such as [84] and [80] and before the recent optimizations highlighted in the previous chapter.
- The device shall have a transparent display for a possible future integration with a visual feedback system. This is made possible using a totally transparent glass screen with 4 inches (10.16cm) diagonal display as can be found in current industrial smartphones.
- To act as a Touch-Pad display, it is necessary to integrate a system to measure in real time the position of the user's fingers. This was made possible using a dedicated capacitive touch sensor embedded on an independent electronic board provided by STMicroelectronics.
- To provide the ability to change the tactile feedback in reaction to a user's action, the device must possess a low latency and bidirectional interface with a standard personal computer.
- The device shall be able to generate its high own modulation signal to avoid artifacts caused by variable latency between the PC and the Touchpad (~150 Hz).

3.2.3.2.2 FEM design of the vibrating surface and positioning of the actuators

To satisfy with the requirement of a central transparent surface like a mobile device, a square area of 88.55 x 49.8 mm² is kept clear of any Thin-Film actuators. This area corresponds to a standard mobile phone screen of 4 inches at a 16:9 ratios. The geometry of haptic device glass substrate itself was increased to a dimension of 110 x 65 mm² to leave place for the dead zone and its non-transparent actuators. The screen was designed by F. Casset and F. Bernard using an iterative method combining the Eigen modal simulation followed by harmonic simulations to design the actuators leading to the highest substrate displacement amplitude as presented in Chapter 1. The material properties used in the FEM simulation are summarized in Table 6, the AlN properties were measured using picosecond acoustics as described in [61]. The reinforced glass used is a commercially available product sold by EAGLE XG© for mobile phone application.

Table 6: Material properties of the Glass and the piezoelectric AlN [60]

Material	Young's modulus (GPa)	Poisson's ratio	Density (g/cm^3)	$e_{31,f}$ (C/m^2)
AlN	300	0.3	3.27	-1.1
Glass	73.6	0.23	2.38	-

It was decided to implement thin-film piezo ceramics on multiple position of interest to test the potential of each position and arrangement on the final electromechanical coupling between the actuators and the vibrating glass. The width and position of these actuators were determined using the same iterative harmonic simulation. The actuators can be powered using three main arrangements relatively to the AC1 actuator line: In phase, Out of Phase and Extremum ventral positions. The final optimized position of each actuator can be seen on Figure 3-9 as green squares.

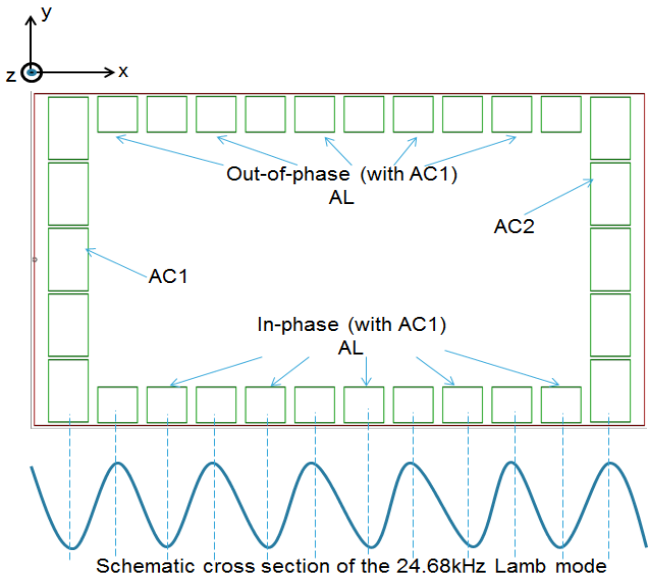

Figure 3-9: Final geometry of the optimized device and its actuators for a 24.68 kHz resonant Lamb mode. [60]

The deposition of the thin-film actuators was done at the CEA LETI in Grenoble. The devices were realized on a transparent reinforced glass substrate produced by EAGLE®. The process of deposition is shown in details in Annex B and described in F. Bernard Thesis [59]. The contacts for each Aln Thin Film actuators are reported away from the actuators themselves. Using these deported contacts, flexible connectors made of a Kapton substrate with copper tracks were specially designed and fused directly on the glass substrate. Fusing this flexible Kapton PCB is done with a conductive glue (type ACP HENKEL©) under a temperature gradient. It can be noted that each ceramic on the long axis possesses its own contacts to test multiple actuator and sensor excitation configurations.

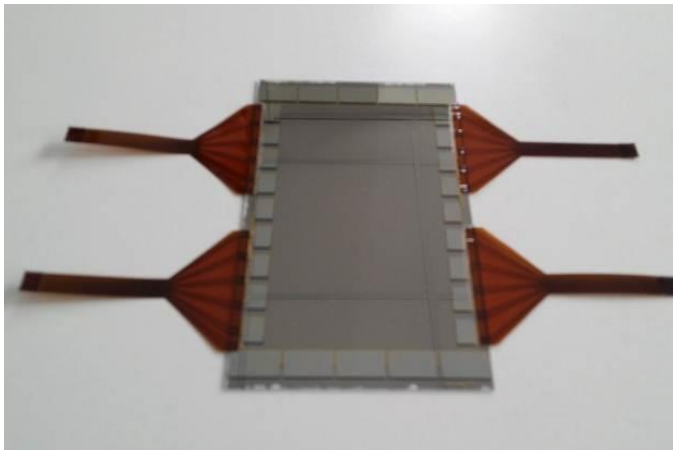

Figure 3-10: AlN-on-glass individual haptic plate with flexible electrical connectors. [59]

Flexible connector is useful for this application since they don't add significant mass to the resonant system and present a minimum damping to the resonating plate.

3.2.3.2.3 Integration of the electro-mechanic system

The resonant glass thus created was connected to a specifically developed interface Printed Circuit board. This new PCB purpose offers a plug for the flexible connectors' interfaces and a set of switches to choose the configuration of each thin film piezo ceramic: actuator, sensor or unconnected.

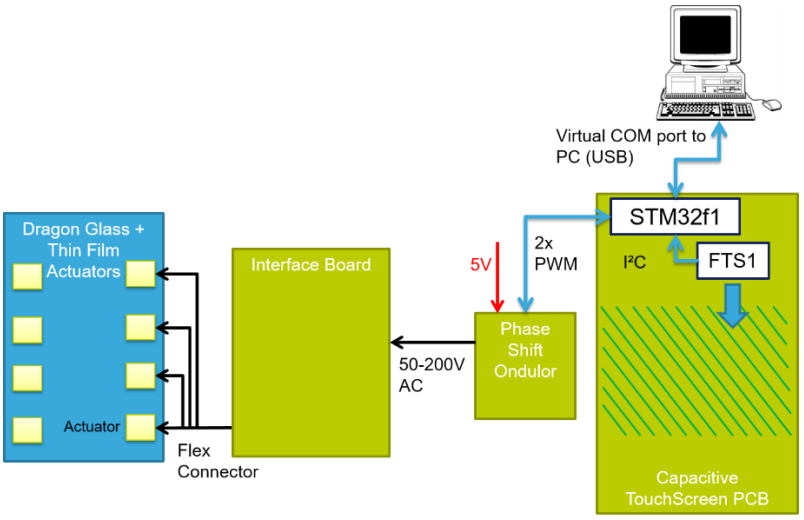

Figure 3-11: Functional Schematics of the interfaces and protocols used in the Thin-Film Haptic Touchpad

a Digital Signal Processor (DSP) is usually used to control the piezoelectric driver. In the case of this touchpad demonstrator, it was possible to use directly the microcontroller (STM32F1) present on the capacitive touchscreen PCB for this modulation function. Moreover, the touchscreen Printed Board Circuit (PCB) integrates an USB connector and direct Digital Input Outputs, necessary for the simple connection with the computer (Figure 3-11). The communication to the computer through the USB connection is done by a virtual COM port, simulating a simple serial protocol. These available external connections are used to meet the Touchpad requirements defined in section 3.2.3.2.1. The Interface PCB and the Capacitive sensor PCB can be seen in Figure 3-12 (a) and (b).

(a) *(b)*

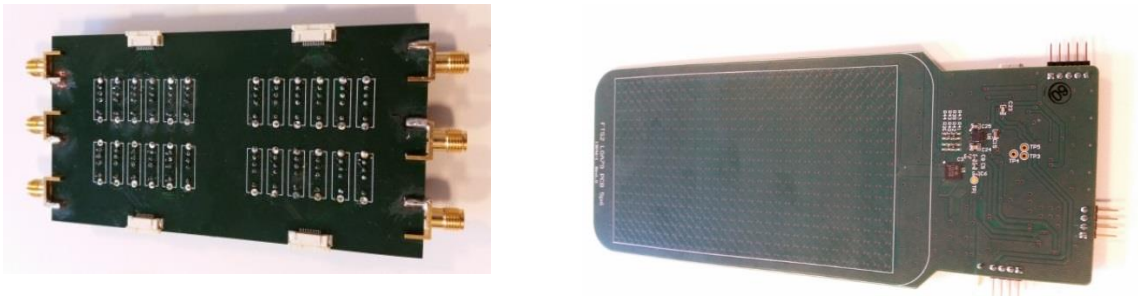

Figure 3-12:Electronic boards developed to control the thin-film touchpad (a) Interface PCB, include the flex connectors and SMA connector for external test purposes. (b) STMicroelectronics FTS1 capacitive touchscreen demonstrator used as a control board in this application.

As can be seen in Figure 3-11 the touchpad uses an external piezoelectric amplifier based on the principle of the phase shift amplifier that will be described in part 3.3.3.1. This solution was selected since it presented a simple way of amplifying the modulated signal with a known voltage ratio. The amplifier is fed with a low tension of 5 V and a current under 500 mV, this power can be directly provided by the computer and its USB connection. The library used to modulate the friction reduction is like the ones described later in paragraph 3.2.2.2.2, a simple porting of the code from the original STM32F4 to a STM32F1 was done. Using this library, it is possible to apply a square and triangular modulation of the excitation amplitude on a range of frequencies from 1Hz up to 200Hz.

The final system is integrated in a 3D printed frame supporting the glass, the PCB interface, the piezoelectric driver and the capacitive touchscreen PCB. The fully integrated system can be seen in Figure 3-13.

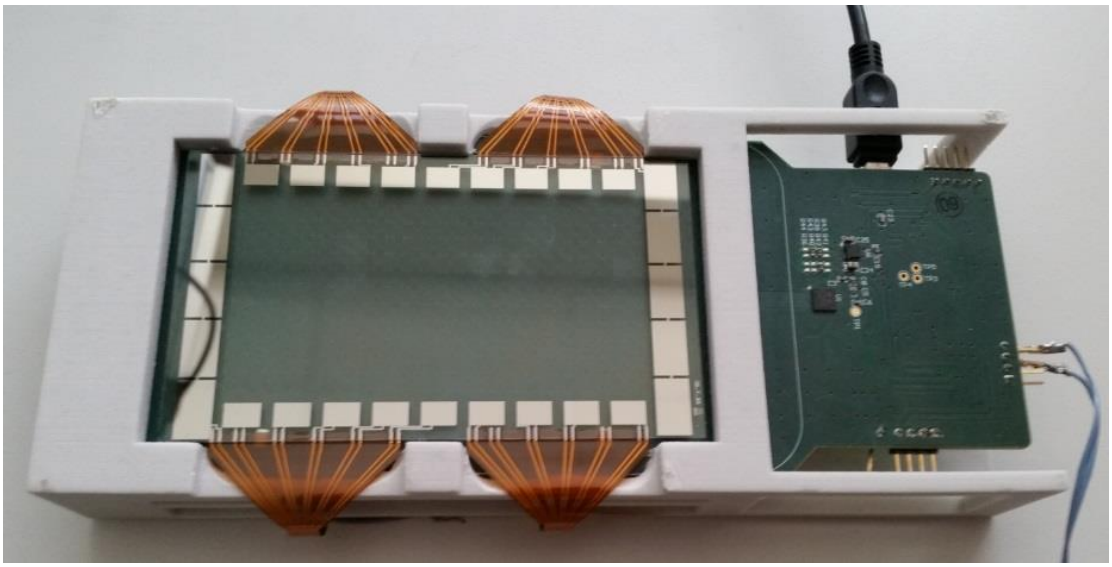

Figure 3-13: AlN-on-glass 110 × 65 mm² haptic plate reported on a mechanical carrier and flexible electrical connectors connected on a PCB.

3.2.3.3 Characterization of thin film Touchpad demonstrator

In this part, the realized Touchscreen device based on thin film actuators is analyzed, first the characteristics of the newly developed actuator are shown and then the comportment of the device under friction modulation is evaluated.

3.2.3.3.1 Characterization of thin film piezo ceramic actuated UL device

The quality of the thin film piezoelectric AlN layer was characterized to check the validity of the deposition process on such glass substrate (The technology stack was initially developed and tested on silicon substrate) [61]. To this end, we measured the capacitance (parallel capacitance Cp) versus frequency of one actuator (5 x 5 mm² and 2.2 µm thickness) across a range of frequencies around the resonant frequency of the screen (from 10 to 100 kHz). The actuator was found to have a constant capacitance of 1.12 nF and a dielectric constant of 10 across the measured frequency spectrum [61]. These values agree with the expected characteristics of the Thin-Film AlN material.

Figure 3-14 (b) shows the nodal lines (zone of low deformation) of the haptic plate under actuation using sugar powder. This method was used to quickly confirm that the expected shape of the vibrational mode was the correct one for a given frequency. This resonant mode was found at a frequency of 23.02 kHz which exhibits a discrepancy of 6.7 % compared to the simulation. This discrepancy can be explained by the variability of the sawing process used to shape the devices from the finished wafer.

(a) *(b)*

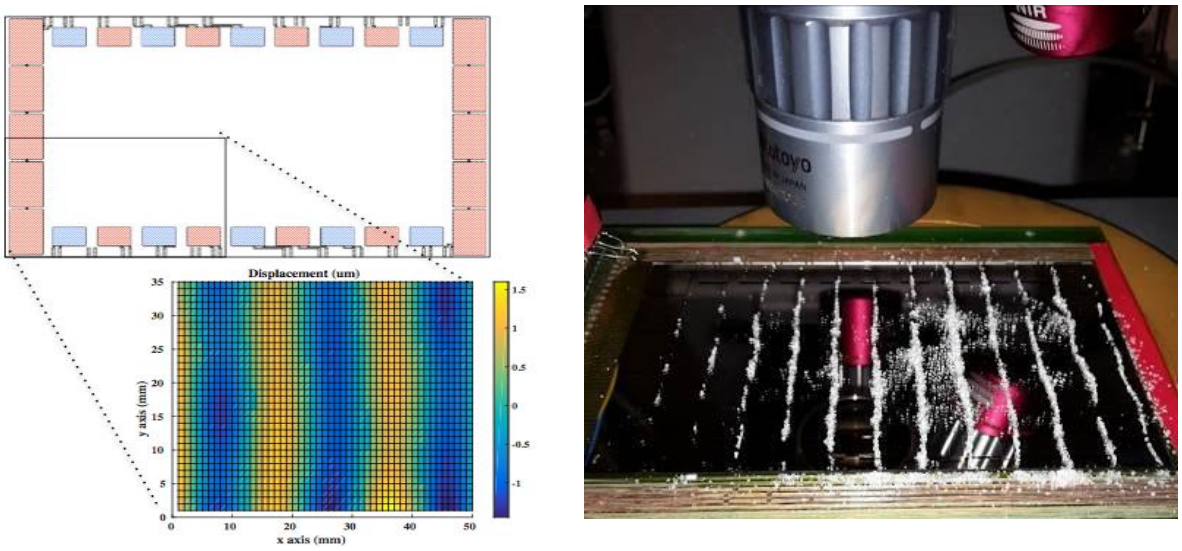

Figure 3-14:(a) Scan of the normal surface displacement under vibration using a vibrometer. [59] (b) Highlight of the vibration mode shape on the AlN-on-glass plate using sugar. [60]

The deformation of the device under resonance was then observed using a laser vibrometer (POLYTEC©). This system uses interferometry to measure the velocity of the point under the vibrometer. Using a 2-axis robotic system this measure is repeated to create a map of the resulting deformation as can be seen in Figure 3-14 (a). The harmonic measurement associated with this resonant frequency is reported in Figure 3-15 (a).

To excite the in and out of phase actuators of the device, two function generators (33250A) and two amplifiers (HAS4011 and FALCO) were used. The maximum displacement of the plate was measured under a tension of 60 V_{AC}, different actuator configurations were then tested at this excitation level. As can be seen in Figure 3-15 (b) 60 V_{AC} is sufficient to obtain a displacement above 1 µm in most cases, an acceptable agreement is observed between simulation and measurement (discrepancy ranging from 6 to 20 %).

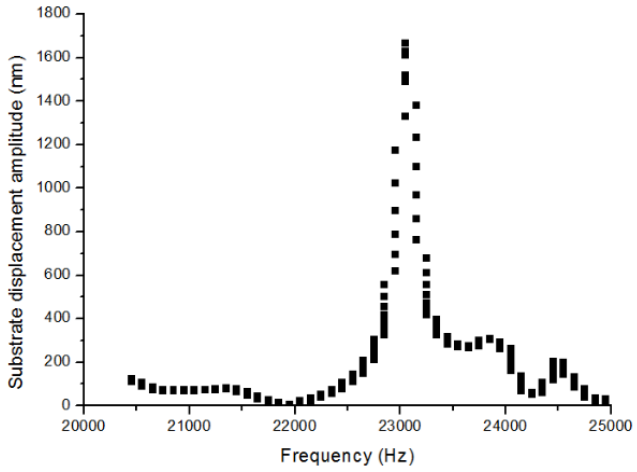

Figure 3-15: (a) Harmonic measurement on the 110 × 65 mm² plate to determine the resonant frequency of the Lamb mode (+60 V applied to AC1 and AC1-in-phase AL actuators and -60 V applied to the AC1-out-of-phase actuators). [60]

Finally, the power consumption of thin-film AlN actuators was studied at 60 V_{AC} using a current probe. A power consumption of approximately 1 W was measured on the AC1 and on the AC2 columns whereas 0.5 W was measured on the AC1-In-phase or on the AC1-out-of-phase AL actuators. The use of all the actuators on the plate thus consumes 3 W of power under a tension of 60 V_{AC}. The power consumption for most actuator configurations is below the 2.5 W limit provided by a typical USB2 connection (5 V and 0.5 A) and thus fits the established requirements. An interesting property of the different actuation configurations is the variation of their respective power and surface efficiencies. The ratio of amplitude reached in function of the power consumption and of the area of thin-film actuator used is shown in the following table. An actuation scheme based on long lateral actuators at the end of the vibrating surface should be selected to provide the best power and surface efficiency use.

Table 7: Amplitude of vibration vs Surface of actuators and Power consumption

Configuration	AL in phase	AL in & out phase	AC1	AC1+AC2	AC1+AC2+AL in phase	ALL
Surface (mm²)	179.4	358.8	430.5	861	1040.4	1219.8
Amplitude vs surface ($\mu\boldsymbol{m^{-1}}$)	1.135 $\times 10^{-6}$	1.397 $\times 10^{-6}$	1.520 $\times 10^{-6}$	1.504 $\times 10^{-6}$	1.435 $\times 10^{-6}$	1.387 $\times 10^{-6}$
Amplitude vs Power (µm/W)	0.407	0.501	0.654	0.647	0.597	0.563

3.2.3.3.2 Evaluation of the friction modulation characteristics of the demonstrator

As seen in Chapter 2, a haptic system based on ultrasonic lubrication requires an ability to modulate the friction reduction effect on a range of frequency adapted to the human finger. One of the open questions relative to this Thin-Film demonstrator during its conception was its ability to modulate the friction reduction effect at a sufficiently elevated frequency. Indeed, the Thin-Film piezoelectric deposition directly on the screen results in a resonant mode with a large quality factor compared to similar system using discreet actuators [59]. To measure the modulation bandwidth of the Touchpad demonstrator, a sinusoidal burst of 200 cycles at the mechanical resonance (f_r=19362 Hz) is generated and applied to the actuators. The voltage amplitude applied during this burst is setup at 10 V_{AC}. The resulting displacement of the device is measured using the previously described laser vibrometer, at the central position of the bottom AC1 actuator (Thus corresponding to a local maximum of displacement). The results of these measures are shown in Figure 3-16.The rise time corresponding to 95 % of the maximum amplitude is reached under 2.3 ms. Similarly, the falling time after the stop of the actuation takes an average of 2.3 ms. This timing be used to approximate the bandwidth of the system as seen in Chapter 2. Using an average of the rising and falling times, the actual modulation bandwidth of the system is estimated at 150 Hz which is the minimal bandwidth proposed in section 3.2.3.2.1.

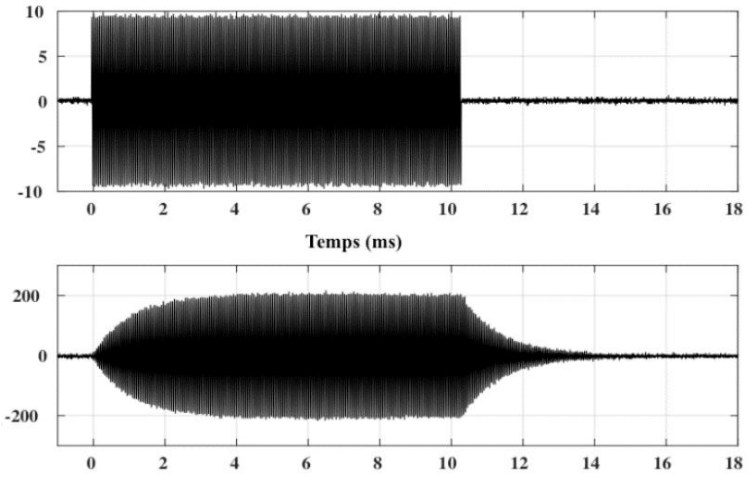

Figure 3-16: Resonant wave establishment time under a pulse exitation of 10V at the mecanical resonant frequency [59]

3.2.3.4 Conclusion

A proof of concept of a transparent tactile interface based on ultrasonic lubrication and using AlN-actuators deposited above a glass substrate was performed. The final device measured 110 × 65 mm² with a 4-inch transparent area. FEM simulations of the system show low discrepancy with the actual amplitudes and damping measured on the Touchpad device. The minimal requirement of 1 µm necessary for a just perceivable UL tactile feedback was achieved, as predicted, for a much lower voltage than the one necessary using discreet actuators glued to the surface. The Touchpad also successfully meets the required specification of low power consumption and a significant bandwidth of modulation.

However, using an actuation voltage of 60 V_{AC} , an extremely small tactile stimulation was perceptible by participants. Indeed, as specified in Chapter 2, higher amplitudes of vibration are needed to provide a strong perception for all user (especially at these low frequencies as seen in Chapter 2). These larger amplitudes were made impossible due to unforeseen limitations during tests at higher voltage. Above 70 V_{AC} an electrical breakdown phenomenon was observed which always resulted in the destruction of the piezo ceramic actuators. As seen in the previous section, the AlN piezoelectric properties are within the specification, which should insure a breakdown voltage of the actuators above 400 V_{AC}. After analysis of the cross section (see Annex B), it is postulated that the low breakdown voltage might be due to a design problem of the top electrode that encourages electrical breakdown in the external passivation layer. The electric arc then propagates and destroys the rest of the actuator. Due to this limitation, the Touchpad device cannot provide a strong tactile feedback but was nevertheless successful as a proof of concept for the application of thin-film technology to UL based tactile feedback. This technology promises a simpler integration of UL devices in the future and might reduce the power constraints within the limits of current mobile devices.

3.3 DESIGN OF A CONTROL SYSTEM ADAPTED TO OPTIMIZED UL FEEDBACKS

This section presents the design and realization of a piezoelectric driver adapted to an optimal UL tactile stimulation. The optimization of the control of the piezoelectric ceramics is presented.

3.3.1 Description of the goal of a piezoelectric driver and its constraints:

To promote the ultrasonic lubrication effect, piezoelectric actuators are almost universally used. They are particularly adapted due to their extremely large bandwidth (above Megahertz) and deformation force, necessary to put a surface under ultrasonic vibrations. Creating the deformation of a piezoelectric material is done through the application of an electric field across its electrodes, the field characteristics can then be tuned to modify the distance and direction of deformation.

Nevertheless, the out of plane amplitude of vibration across the UL plate is proportional with the in-plane displacement imposed on the actuator. This in turn imposes generally a large voltage differential between the actuators' electrodes, in the case of discreet piezo ceramic, as shown in section 3.2.2.

Since one of the main applications of tactile device is found in mobile platforms, the global efficiency of the UL tactile stimulation is paramount in the design. To this end, the signal generated by the driver needs to reduce the electric loss due to resistive effect to the minimum. This means that a proper matching of the driver impedance with the impedance of the driven actuators must be ensured.

The second constraint is the frequency of modulation necessary to generate tactile feedback to a user. As seen in Chapter 1, an optimal bandwidth of 500 Hz should be selected to stimulate the whole range of mechanoreceptors present in the human hand. As it will be seen later in this chapter, the control of the amplitude with this bandwidth has a significant impact on the design of the real-time amplitude control system.

3.3.2 Power inverter and amplifier dedicated to UL stimulation

The frequency at which the piezoelectric element vibrates most readily and most efficiently, to convert the electrical energy input into mechanical energy, is the resonance frequency. Since this frequency is defined by the geometry of the plate, the optimal frequency of the driver can be setup to match the resonant frequency of the resonating device. The electrical behavior of the piezoelectric transducer around the selected resonant frequency is presented in Figure 3-17 [54]. The frequencies f_1 and f_2 correspond respectively to the serial and the parallel mechanical resonances. If we ignore the resistance caused by mechanical losses, f_1 and f_2 can be described as follow:

- The minimum impedance frequency, f_1 , approximates the series resonant frequency, at which impedance an electrical circuit describing the element is zero.

- The maximum impedance frequency (minimum admittance), f_2 , approximates the parallel resonance frequency, at which parallel resistance in the equivalent electrical circuit is infinite.

Maximum displacement response from the piezoelectric actuator will be at a point between f_1 and f_2.

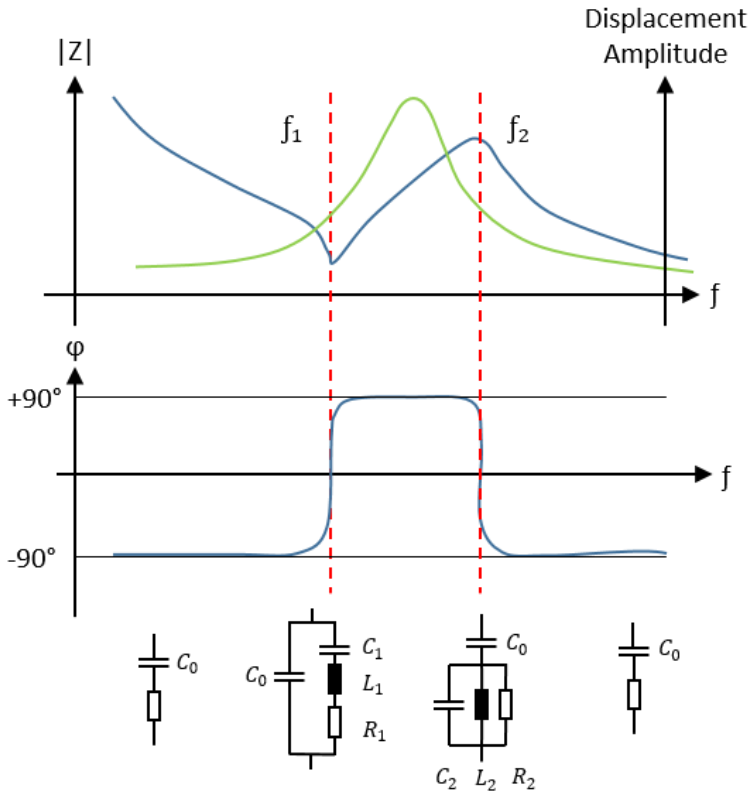

Figure 3-17: Equivalent electrical schematics of Ultrasonic display at resonance

Independently of the actuation frequency relative to the mechanical resonance, the main capacitance C_0 stays relatively constant. It is possible to compensate the reactive power produced by C_0 using a simple serial or parallel inductive compensation (Figure 3-18).

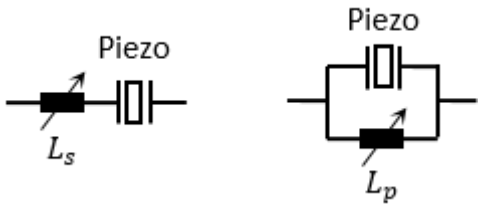

Figure 3-18: Serial (Left) and Parallel (Right) inductive compensation schemes

The serial compensation presents the advantage of maximizing the impedance value at the mechanical resonance, which reduces the intensity of the driving current. For a tuned resonance f_r between f_1 and f_2, the value of the matching inductance L_s is given by:

$$L_s = \frac{1}{4\pi^2 f_r^2 C_0} \quad (29)$$

The mechanical resonance of an UL device is slightly variable during its lifetime due to variable damping and temperature. Since the final integrated version of this driver would be mass produced, it would be impossible to tune perfectly each inductor L_s to perfectly match the mechanical resonance of the plate at all time. These limitations prevent the use of more advanced impedance matching schemes that would ultimately prove inefficient with a variable resonant operating frequency. A simple serial matching as presented previously, is slightly less efficient but provides a larger efficient bandwidth.

3.3.3 Topology of piezoelectric driver

As described in the previous part, driving the piezoelectric actuators generally involves creating a large alternative tension and applying it to the poles of the actuators at the right impedance. Since the voltage in a mobile platform typically comes from a DC source (battery, charger), an inverter is required to obtain an AC source. The voltage then needs to be amplified to the correct level.

Multiple types of amplifiers can be used in UL piezoelectric application. The advantages and limits of the two principal architectures are described in this section. The capacitive nature of piezoelectric actuators loads orients the choice of architecture toward a solution that includes integrate inductances susceptible to offer a simple impedance match.

3.3.3.1 Phase shift power inverter with transformer

Power inverter based on the use of a H-bridge inverter followed by a transformer was the first to be implemented into UL tactile devices. This is still the case today as most new prototypes apply this technology. As seen in Figure 3-19, this system is advantageous for prototyping since it is extremely simple to wind a new transformer fitted to a specific resonator. The output voltage is simply dependent on the ratio of turns between the primary and the secondary inductors of the transformers. Moreover, matching the impedance of the amplifier output to the impedance of the piezoelectric actuators can be done easily by adjusting the insulator gap between the ferrites of the transformer.

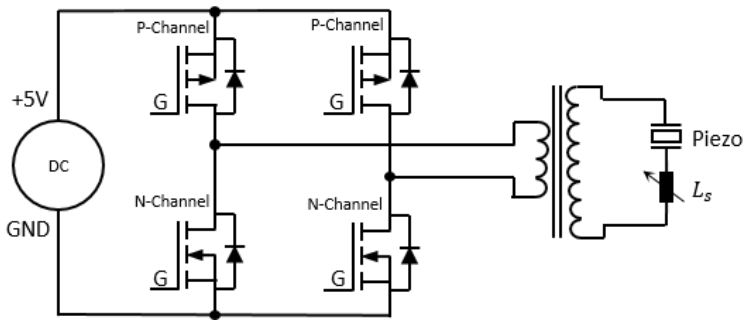

Figure 3-19: General electronic Schematics of Phase Shifted H-bridge amplifier

With all its advantages for prototyping, this type of inverter topology is nevertheless difficult to integrate and produce in an industrial way. The difficulty lies with the transformer component. While it is possible to order custom made transformers with the correct winding ratio and current capabilities, these are prohibitively expensive. Moreover, transformers tend to be big components since they need to handle the relatively large current load of UL applications (up to 5W), and thus necessitate large winding diameter. Finally, the last issue is the inability to order of-the-shelf transformers with a secondary winding impedance pre-calibrated. The circuit using such component would then be bulky (minimum 1 cm thickness), expensive, and necessitate additional components to match the impedance.

3.3.3.2 Pre-boosted H bridge resonant amplifier

The second simple architecture keeps a similar inverter design, but uses a different amplifier stage. Figure 3-20 describes this architecture; the original DC power source is first fed into a standard DC-DC boost amplifier before going through the H-bridge inverter. The final matching of the output impedance with the capacitive piezoelectric load is done by the addition of a separate inductance.

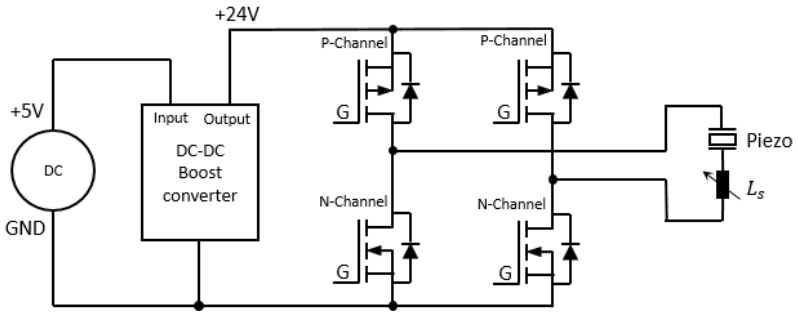

Figure 3-20: Electronic Schematics of a pre-boosted H-bridge amplifier

This design offers the simplicity of reducing the number of components compared to the transformer solution. The impedance matching can be done easily with cheap off-the-shelf components. The use of a separate impedance also offers the possibility of dividing it into multiple small impedances. The resulting footprint is reduced for a same total inductor and thus, fits more easily into mobile devices. Finally, a drawback can be identified with this architecture, indeed to reach high voltages the boost ratio of the DC-DC convertor needs to be high. Since high ratio DC-DC boost convertor tends to be less energy efficient, this can affect the final efficiency of the architecture.

3.3.4 Description of the design of simple H bridge piezoelectric amplifier:

With the objective of designing a system simplifying the integration of UL technology into mobile platforms, a pre-boosted resonant H-bridge architecture is chosen. As previously described, this architecture is composed of a DC-DC boost converter independent from the H-bridge inverter. A third part of the design, the DSP microcontroller, is added to fill the need

for a high-speed control of the amplifier. This last part will be described in the next section. The three-part design can be seen in Figure 3-21.

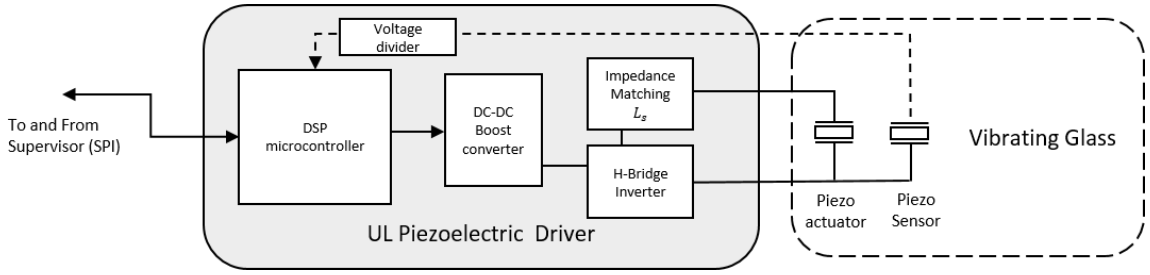

Figure 3-21: General design of the UL piezoelectric Driver

The amplifying capabilities of the selected architecture are limited by the ratio and power limits of the DC-DC boost amplifier. In our case, given the complexity of implementing a high efficiency boost converter, we decided to use an off-the-shelf component provided by TRACOPOWER©. One advantage of this choice is that this amplifier line shares a similar footprint (31.8 x 20.3 x 10.2), giving the ability to swap the booster to adapt to difference in damping from one design to another. The modules possess an internal EMI filter and can handle up to 10W continuous power.

Table 8: Available DC-DC boost converter with the same form factor

	THM 10-0511WI	THM 10-0513WI	THM 10-0515WI
Output Tension	5VDC	15VDC	24VDC
Maximum current	2000mA	670mA	416mA

To create the H-bridge itself, it was decided to use a single chip since these devices are now available for automotive purposes. This all integrated H-bridge chip, L6201PS, is advantageous compared with separate MOSFETs, since it provides a better management of dead time and integrated protection against electrical shortcuts and thermal runaway. The chip can handle a supply voltage of up to 48 V (important in a pre-boosted design) with a continuous current of 1 A and peak of 5 A.

Tuning the resonance of the driver to match the mechanical resonance of the plate is done by the selection of a proper inductance to compensate for the reactive power of the actuators, as shown in equation 1. A simple matching of the impedance focusing on the mainly capacitive load of the piezoelectric actuators was selected. To provide a modular system, the emplacement for 2 large current inductances is added to the PCB.

3.3.5 Low level signal generation and control system

Multiple schemes help with the control of the inverter to provide an optimal control of the voltage waveform applied to the actuators. This section first presents the low-level

modulation schemes used to optimize the quality of the sinusoidal waveform created and to reduce its distortions. In the second part, the concept of amplitude control used in Chapter 2 is expanded and detailed.

3.3.5.1 PWM generation of sinusoidal excitation

The voltage applied across the load can be reversed by switching the 4 MOSFETs present in H-bridge on and off with the correct pattern. This simple switch of the current going through the load only produces a square voltage waveform when not coupled to a filtering load (transformer or RLC circuit). The adjunction of an inductive load smooths the voltage waveform and eliminates parts of the harmonics. Figure 3-22 presents the results of a simple phase shifted square wave modulation on a transformer type amplifier. A large distortion is observable compared to an optimum sinusoid, this distortion is especially visible on Figure 3-22 (b) which presents small angle of phase shift.

(a) *(b)*

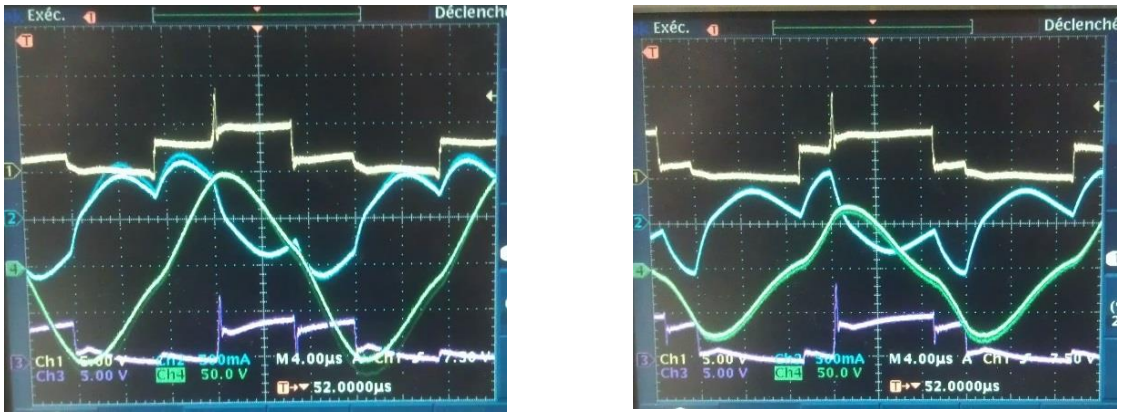

Figure 3-22: Example of the voltage and current waveforms taken on an H-bridge followed by a high ratio transformer (1:30). Yellow and violet lines represent the voltage on both side of the transformer primary. Green and Blue are respectively the output voltage and current of the secondary winding.

(a) shows a square wave modulation (90° phase shift in bridge control, to get the maximum voltage amplitude) (b) shows a smaller phase shift (~20° phase shift). Even after the filtering of the primary and secondary winding a large distortion from a perfect sinusoid is visible.

This distortion is due to the presence of harmonics created by the simple switch of the voltage waveform. It is possible to calculate the Total Harmonic Distortion (THD) of the modulated signal using Fourier analysis. This can be done by calculating the square root of the sum of the harmonic voltages divided by the fundamental voltage:

$$THD = \frac{\sqrt{V_2 + V_3 + V_4 + \cdots + V_n}}{V_1} \quad (30)$$

Figure 3-23 presents the harmonics calculated for different modulation schemes using Matlab. As described in Figure 3-23 (a), the analysis of the Fourier transform shows that the simple square wave modulation contains only odd harmonics (The 3rd, 5th, 7th etc.). It is nevertheless possible to add a step at zero-voltage, to remove the harmonics that are divisible by three, this leave the 5th, 7th,11th etc. (See Figure 3-23 (b)).

(a) *(b)*

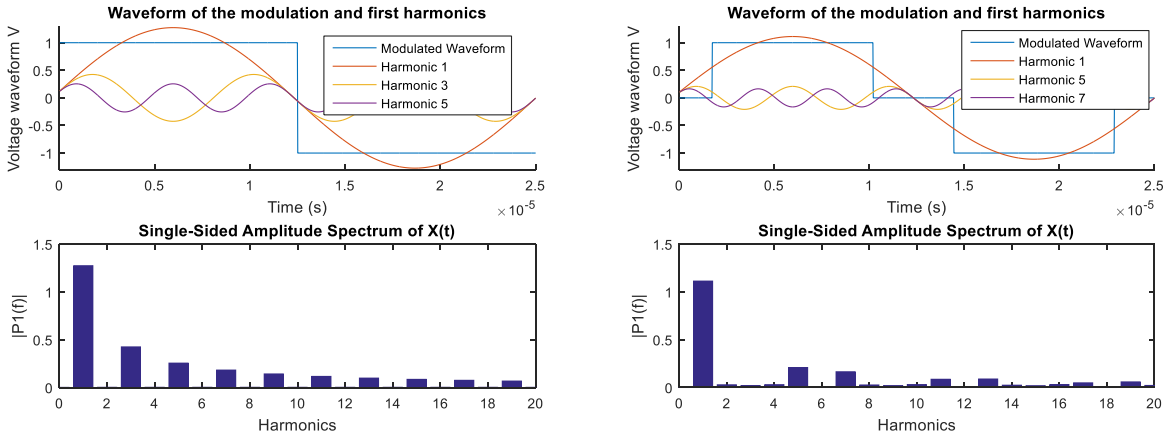

(c)

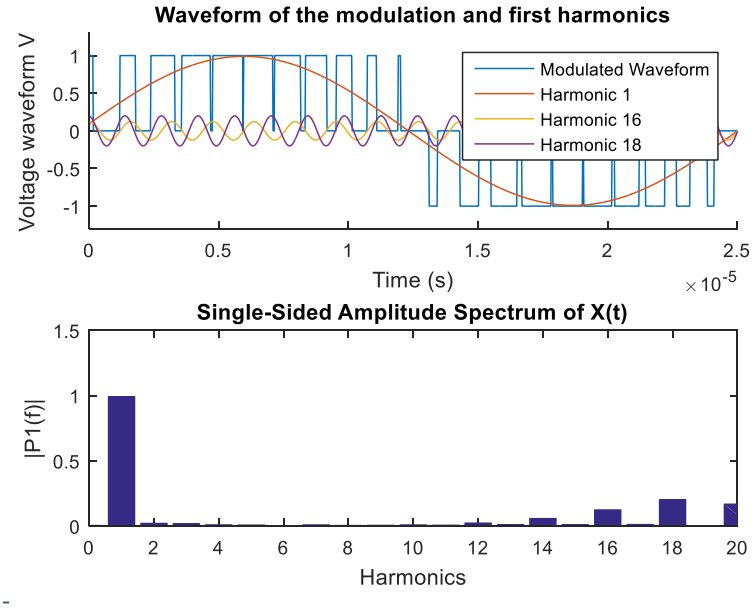

Figure 3-23: Creation of a sinusoid at 40kHz with PWM at different carrier frequencies. The three first main harmonics (above 0.1 amplitude) of the signal are shown. (a) Simple square PWM, only the odd harmonics are expressed(b) Square PWM with zero level, the harmonics divisible by 3 are also removed (c) High speed PWM, all harmonics before rank 16th are rejected, distortion is kept to the minimum.

Adapting the square wave modulation in this manner is called Pulse-Width Modulation or PWM. Reducing the harmonics and the distortion of the output of the inverter is critical to the control of UL based tactile feedbacks. Indeed, large harmonic distortion imposes rapid strains on the piezoelectric ceramics which reduce their life time and increase the chance of ungluing. Moreover, these harmonics can excite unwanted mode of resonance of the device and reduce the overall quality of the stimulation.

The elimination of harmonics can be easier achieved at higher frequency, where the filter components can be much smaller and less expensive. The frequency of the pulse-width modulated signal is called the carrier frequency. Due to the easier reduction of the harmonics

it is thus usually more efficient to increase the number of pulse-width to the maximum achievable by the controller. As seen in Figure 3-23 (c), once implemented, high speed PWM control schemes on the inverter can be used to generate a large range of output voltage and frequency adjustments in real time while reducing distortion to the minimum.

The implementation of high speed PWM control requires heavy load on the control microcontroller. This is a constraint that needs to be factored in the choice of the DSP microcontroller included in the piezoelectric driver PCB. A second potential drawback of high speed PWM compared to simple square wave is the reduction of the power sent to the fundamental signal. As shown in Figure 3-23, the amplitude of the fundamental signal is 1.3 for a square wave and only 0.9 using a cleaner fast PWM.

3.3.5.2 Amplitude control system

The control of the friction reduction in an ultrasonic device is achieved by modulating the amplitude of the vibration developed. Usually, this control is done by changing in open loop the amplitude of the sinusoidal tension applied to the piezoelectric actuators. This simple approach has the drawback of not controlling the variable damping effect imposed by the finger, when it moves across the vibrating surface. Usually the variable damping is dependent on the force applied by the finger and its position relative to the nodes of vibration (a finger on a node will have less damping effect than a finger placed between 2 nodes). While this variable damping is not necessarily an issue in haptic devices, it does have a large impact when making precise friction coefficient measures. This effect was particularly visible in the first tribology experiments detailed in the previous chapter. These first experiments didn't include any amplitude control system, which created large noise and uncertainty on the vibration amplitude applied to the finger.

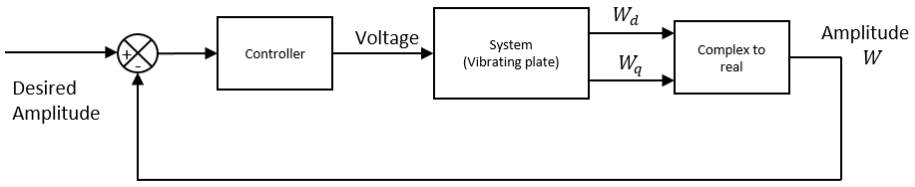

Figure 3-24: Amplitude Control System

Subsequently to these first measures, a control system was implemented in all measurement setups. This control system is similar to the ones proposed in [85] by W. Ben Messaoud; composed of an amplitude measurement and a closed loop numerical Proportional/Integral (PI) control system, as seen in Figure 3-24. The amplitude of vibration is measured in real time by a piezoceramic glued on the vibrating device. The vibration amplitude can be expressed as follow:

$$w = (W_d + jW_q)e^{j\omega t} \qquad (31)$$

Where W_d and W_q are respectively the real and the imaginary parts of the vibration. ω is the pulsation frequency with $\omega = 2\pi f$ where f is the excitation frequency. The geometry of the

frame d, q is chosen so that the voltage supply vector V is along the q axis. V can be expressed as:

$$V(t) = \mathrm{A}\sin(\omega t + \varphi) \quad (32)$$

where φ is the phase shift. A is the voltage amplitude and is having a linear influence on the vibration amplitude under static damping conditions. Once the resonance is reached we have $W_q = 0$. Then the aim of the control system is to keep W_d constant by acting on the voltage amplitude A. We know that, at the resonance, W becomes equal to W_d and a first order transfer function can be found between W and V [79]. Using the Laplace transform, it can then be written:

$$\frac{W(s)}{V(s)} = \frac{G}{1 + \tau s} \quad (33)$$

with $G = \frac{N}{ds\omega_0}$, $\tau = 2m/ds$ with ds, c, m and N being material properties and geometries of the resonant device. The parameters of this function for the specific device under consideration can then be found by applying voltage steps and measuring the resulting vibration amplitude. Once found, it is then possible to implement and tune the closed loop Proportional Integral controller.

If it is necessary to tune multiple devices and if the response quality of the controller is not critical, it is then possible to tune the PI manually, using the Ziegler-Nichols method. The control system can improve significantly the tactile feedback perceived by the user when applying a modulation. In this scenario, the control loop insures that the raise time of the amplitude of vibrating plate stays low independently of the damping applied. Recent experiments involving this type of device were found to elicit a similar level of feedback to user for lower voltage of actuation.

Last, it may be noted that the control described in [85] assumes the tracking of the resonant frequency simultaneously with the vibration amplitude control thanks to the voltage level tuning.

3.3.6 Final realization and integration of the optimized piezoelectric driver

The result of the driver is shown in Figure 3-27. The final dimensions of the completed piezoelectric driver are 33.8 x 74 x 11 mm^3. These dimensions are still too large to be integrated into a mobile device, but propose an improvement compared to the previous non-integrated solutions.

(a) *(b)*

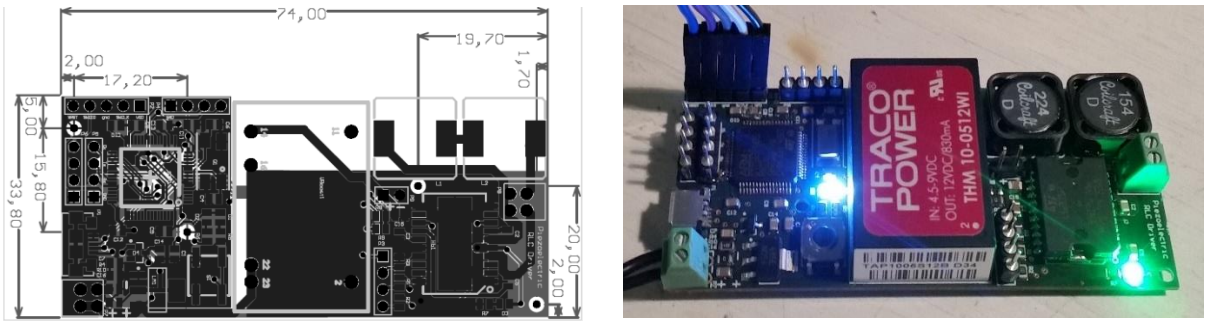

Figure 3-25: (a) Gerber file of the finalized piezoelectric driver (b) Photo of the assembled PCB and components, the left part encompasses the logic part of the driver with its STM32F446 DSP microcontroller, the DC-DC booster is visible in the middle in red and the Inverter plus impedance matching shown on the right.

The STM32F446 was chosen because of its high operation frequency (up to 180 MHz), necessary to run the High speed PWM and amplitude control loop detailed in subsection 3.3.5 and 3.3.5.1. Due to limitation in the frequency of commutation of the H-bridge (due to thermal load), a carrier frequency of 500 kHz is used as a maximum limit (10 commutations per period for a 50 kHz fundamental signal). The resulting PWM signal and voltage across the piezoelectric actuators in an application at 56 kHz can be seen in Figure 3-28. Little to no distortion of the sinusoidal voltage applied to the actuator is visible compared to the square wave modulation of Figure 3-22.

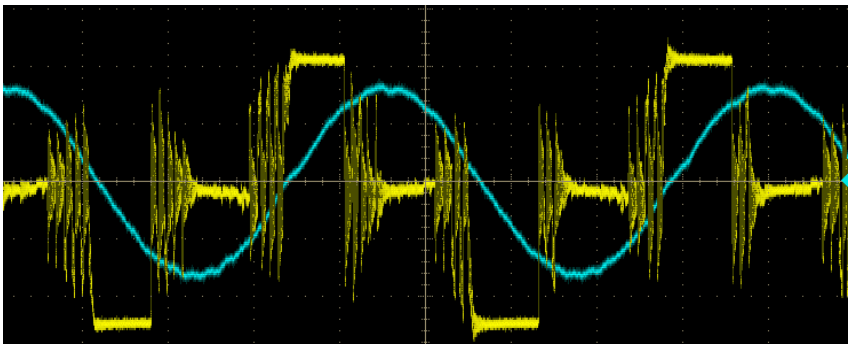

Fi Figure 3-26: High Speed PWM (yellow) and Output Voltage (blue) waveforms generated across the piezoelectric actuator by the realized driver. (The PWM commutation shown here in yellow is filtered by the inductance Ls, explaining the fuzziness of the commutation)

3.4 CONCLUSION

In this chapter, the tools available to the designer of devices based on ultrasonic lubrication were explored.

Two transparent demonstrators using the new design rules found in Chapter 2 were realized. These devices, built around a similar control architecture, can generate a strong tactile feedback combined with a complete computer based, visual feedback system. These new devices demonstrate the feasibility of creating a “tablet” type platform implementing powerful and high frequency friction modulation capabilities.

Finally, a third demonstrator, built as a Proof of concept, was presented. Using Thin-film actuator technologies to generate an UL based tactile feedback, it offers a large potential for future industrial application. While limited by unforeseen defect of the deposited actuators, the demonstrator proved the validity of the technology and its large potential for the integration of friction modulation in smartphones and tablet computers.

Finally, the problematics attached to the development of an efficient piezoelectric driver where then showed, and such an optimized driver was finally realized. The clean control of the amplitude of vibration necessitates the use of high frequency PWM and control loops, housed in a fast DSP microcontroller.

With newly created tactile devices producing a strong and low rise time UL feedback, it is possible to study, not only the friction reduction but also the effect of friction modulation on the Human perception. In Chapter 4, the question of how to create the best modulation to elicit the strongest sensation to the user will be answered.

4 PSYCHOPHYSICAL STUDIES OF MULTI-SENSORIAL INTERFACES

Summary

4.1 INTRODUCTION

When the UL effect was discovered, it was first believed that the typical stimulation should be done by applying a specific amplitude of vibration that the user would then perceive as a specific friction coefficient [35] [63]. This approach proved difficult due to the lack of precision of the human mechanoreceptors, unable to determine the absolute stretching applied to the fingertip. Indeed, due to their evolution as texture sensor and grip solidity detector, the mechanoreceptors offer multiple channels of stretch frequency detection [86], as seen in Chapter 1. With the availability of new finger detection methods (e.g. optical, resistive and capacitive sensors), it became possible to simulate textures [87]. In consequence, most UL control scheme today use friction modulation, in one form or another, to create feedback and reproduce textures.

Due to the importance of friction modulation schemes, it becomes important to analyses their characteristics and limits. In this chapter, different friction modulation methods are analyzed to determine the limits of perception of human users. This study aims to offer the most meaningful stimulation while reducing unnecessary “on” time, to reduce to the minimum, the power consumption of the devices.

It is interesting to note that the study of friction modulation is transposable to all technologies creating an effect of friction modulation: ultrasonic lubrication of course but also electrovibration stimulation [88] [89] and lateral stretch of the finger pad via low frequency displacement [90]. We chose an UL device to implement this study due to two main factors. First, power consumption studies are simplified since UL devices present higher power draw in active state than electrovibration devices for a similar form factor. This is mostly due to the continuous damping of the air against the vibrating plate [79]. A second important factor is that electrovibration screens create a perception degradation when repeated slidings of the finger are performed. This negative effect is caused by the deposition of sweat that shields the finger from the electrical field [91]. It can prevent meaningful psychophysical measures of the threshold of perception.

This chapter presents three different studies that were performed to measure the human perception of friction modulation. The experiments and their analysis were conducted in collaboration with David Gueorguiev from the University Catholique de Louvain and Eric Vezzoli from Lille1 University. A first experiment was conducted to determine the capacity of participants to distinguish differences in the duration and rise time of a single tactile stimulation. The second experimental protocol aimed to measure the achievable duty cycle reduction for a range of modulation frequencies. Finally, the last section will present preliminary measures with the objective of compensating, on a perception level, a reduced amplitude of vibration or rise time of the resonating plate.

4.2 METHODOLOGIES

The experiments and measurements presented in this chapter were conducted using a single setup designed in collaboration with Eric Vezzoli at the University of Lille1. The device, Called E-Vita was previously in Chapter 3.2.2.3. This section presents the psychophysical methods used to determine the perceptive thresholds of human participants in this chapter

4.2.1 Introduction to the psychophysical protocols and analysis

This subsection presents the experimental protocol and the psychophysical method used to determine the Just Noticeable Difference (JND) of the different stimuli studied in this chapter.

4.2.1.1 Just Noticeable Difference (JND)

Due to its extensive use in this chapter, a short description of the JND is done in this paragraph. In psychophysics, the JND expresses the amount a stimulus must change in order to be detectable at least half of the time by the human participants. The type of stimulus can be of many sensory modalities and over a wide range of stimulus magnitudes sufficiently far from the upper and lower limits of perception. The JND can be expressed as a fixed proportion of the sensory level used as reference. The ratio between the JND and its reference is more or less constant. This relation can be written as follow:

$$\mathrm{k} = \frac{\Delta I}{\mathrm{I}} \qquad (34)$$

where I is the reference intensity of a stimulation and ΔI is the necessary variation required for the change to be perceived (the JND). The constant k is called the Weber constant in reference to Ernst Heinrich Weber (1795–1878), an anatomist and physiologist, who applied this concept in experiments on the perception thresholds of lifted weights. The constant nature of k remains approximately true for many but not all sensory dimensions. A common example of this relation can be found when calculating the JND of different light and audio stimulus. The Weber constant is true for the intensity and the pitch of sounds, and also for the brightness of lights. However, it does not remain true for the wavelength of light.

The JND is by its nature a statistical tool. The difference that a given person notices will vary slightly, and it is therefore necessary to conduct many trials to determine the threshold. The JND is usually reported when participants statistically detect a difference between the reference and the stimulus on more than half of trials.

4.2.1.2 Design of the Psychophysical Protocol

An experiment dedicated to measure the JND of a sensory dimension needs to be carefully prepared. Indeed, the protocol must ensure that the range of stimulus presented to the participants is large enough to determine the threshold with which the participant goes from a state of perception, to a state of indistinguishability compared to the reference. If this is done correctly, it will then be possible to fit the psychophysical curve to the acquired data. To obtain a precise value of the JND, it is of course also important to make sure that the final

protocol gives regularly spaced measurements during the transition from perception to indistinguishability of the difference.

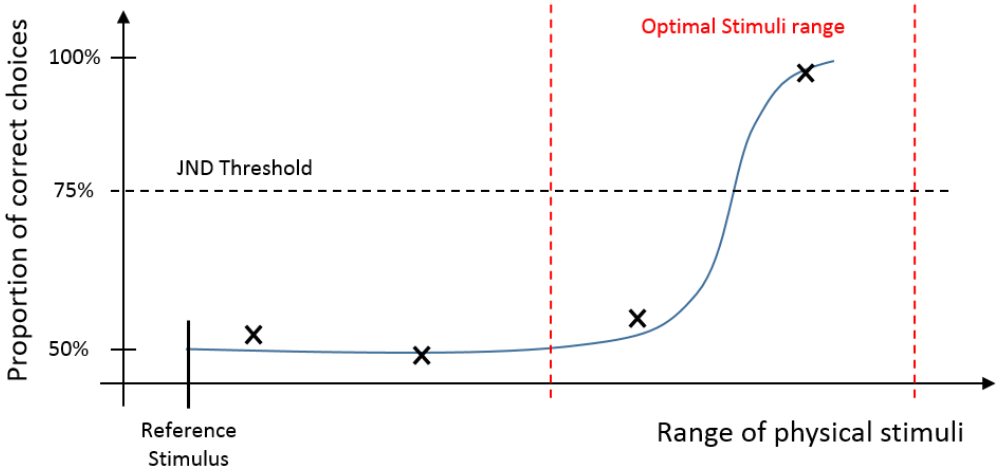

Figure 4-1: Selection of the optimum measurement range necessary to obtain a precise psychophysical curve and JND extrapolation. The black crosses are the measurement stimuli that the participant must differentiate from the reference. The blue line represents a fit of the psychometric function on the preliminary measurement points.

To insure the correct range of data for the main psychophysical experiment, a preliminary study is generally prepared with a lower number of participants. In this preliminary study, an arbitrary range of signals is presented to measure the approximate range of the JND transition. An example is shown in Figure 4-1; in this fictional case, participants must compare two stimuli to a reference and select the one they believe is the "strongest". On the left the participant are not able to distinguish the difference between the two signals (50% correct answers), and on the larger stimuli on the right of the figure, they tend toward a perfect distinction (100% correct answers). For a forced choice task with two alternatives, the JND is typically set as 75 % of correct answers (this corresponds to a statistical detection of a difference half of the time). We can observe that the range of the preliminary experiment is too large on the indistinguishability side, and too short on the other side to ensure 100% detection. The optimal range of measures to be done in the full study is highlighted in red in this case.

This simple protocol is necessary to reduce the experiment time for both the participants and the researcher. Nevertheless, it should be noted that in often it is not possible to extend the range of signal proposed due to physical limitations (e.g. impossible to create a large enough amplitude of stimulation or a short enough pulsation).

4.2.1.1 Experimental protocol

This subsection presents the general setup of the psychophysical measures presented later in the chapter. As detailed in the introduction, three main psychophysical studies were conducted and will be presented in this chapter. In all experiments, the participants were interacting with the E-VITA described in the previous chapter, section 3.2.2.3. The first two experiments presented (section 4.3 and 4.4) uses a large pool of 12 participants aged between

25 and 40 (10 males and 2 females as detailed in Table 1). The last experiment in section 4.5 is preliminary, and thus utilizes a smaller sample of subjects that will be described there.

Table 4-9: List of the age, sex of the participants

Participant	P1	P2	P3	P4	P5	P6	P7	P8	P9	P10	P11	P12
Age	27	26	28	25	28	27	29	29	27	40	29	26
Sex	F	F	M	M	M	M	M	M	M	M	M	M

The UL tactile interface sometimes makes a slight noise when alternating active and passive states. Therefore, to prevent any influence of this noise on the participant's perception, the subjects had to wear noise reduction headphones and a white noise (rain sound) was also diffused in the room during the experiments (see Figure 4-2). For each trial, the participants had to move their finger from left to right on the screen, which generates a stimulation. They were free to choose the normal force to apply and the speed of exploration. The participants had to totally lift their finger from the plate after each sliding on the plate to be able to generate the start of the generation of the next stimulation.

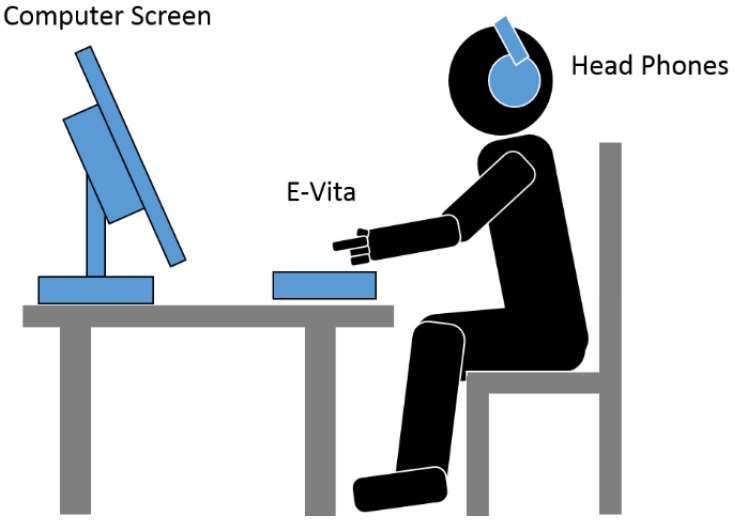

Figure 4-2: Schematics of the installation of the participants and of the experimental setup

The LCD display present on the E-Vita is used to give visual confirmation of the experiment goals during the measures. A second visual system using a computer screen is used to display comfortably the control of the experiments to each participant.

The fittings of the psychometric curves to the experimental data presented in this chapter were implemented by using the version 1.81 of the Palamedes toolbox [92] (Kingdom & Prins). This toolbox provides reference tools based on scientific literature specifically developed for the analysis and plotting of psychophysical curves.

4.3 PERCEPTIVE THRESHOLDS ASSESSMENT OF THE UL SINGLE PULSE MODULATION PARAMETERS

This section presents two psychophysical experiments aiming to assess the minimal perceptive threshold of single pulse UL modulation event: the perception of the time rises and the signal duration. These experiments use the experimental setup described in the previous section.

4.3.1 Introduction and psychophysical protocol

The simplest form of friction control can be created by modulating the friction coefficient in order to generate a single pulse of vibration on the resonating device. If the user is moving its finger while this simple stimulation is applied, a clear event is perceived by the participants. These events are usually described as like a “bump” or irregularity in the surface of the device. The two experiments presented in this section aims to quantify the minimum perception threshold associated with such a simple stimulation. As seen in Figure 4-3, for a constant amplitude of vibration, the two main parameters driving the sensation of a single event stimulation are its rise time and its length.

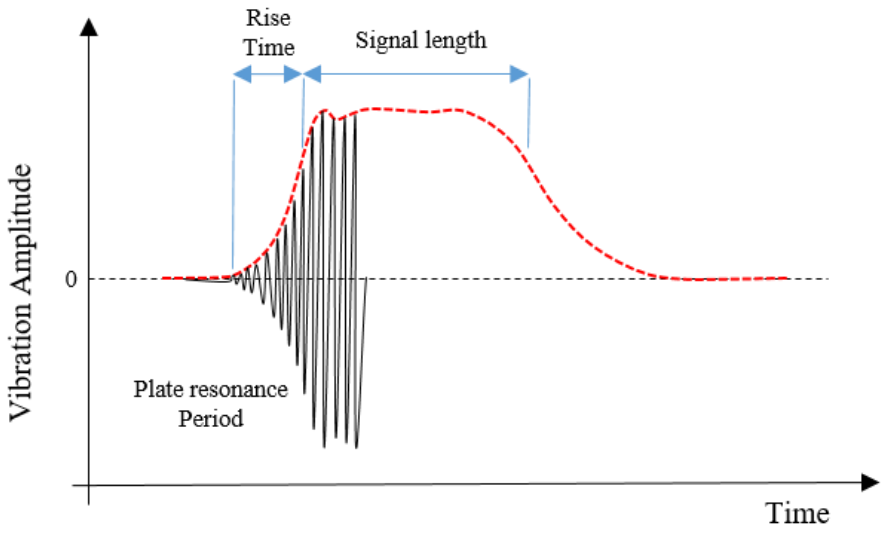

Figure 4-3: Voltage amplitude of the signal duration experiment

The first experiment uses the device and psychophysical protocol highlighted in section 4.2 to measure the minimum perceptible change in rise time for a single event. The second measure presented in this section uses the same means to quantify the influence of the signal length variation.

4.3.2 Minimal perceptible signal duration

The aim of the minimal signal duration discrimination experiment was to determine the capacity to perceive differences in the time length of the friction reduction. From this psychometric function, it was then possible to extract the just noticeable difference (JND) of signal duration for humans interacting with the UL tactile device. The experiment was based on a forced choice task with a constant pool of stimuli (constant stimuli method). The

participants had to compare the length of two stimuli, displayed in sequential order. A reference value of signal duration was always randomly set as one of the two stimuli presented in the discrimination task. The other stimulus was a test value to compare against the baseline. The participants explored the two stimuli up to 3 times and were then asked to report which stimulus offered the “shortest” stimulation. They had to choose one of the signals even if not sure of the answer.

Test signals were presented in a pseudorandom order where one of the signals was always the baseline and the other selected from a list of five signal lengths calibrated in advance. A first preliminary experiment (as described in subsection 4.2.1.2) allowed us to select an optimum range of stimulus for the fit of the psychometric function. The possible time durations selected were 1.6, 2.4, 3.2, 4 to 4.8 ms to be compared with a baseline of 0.8 ms. The experiment was stopped after a signal of each length had been presented 10 times against the reference. Each of the subjects was thus presented to a total of 50 signal comparisons.

Results from the 12 subjects described in Table 1 are presented here. All the answers from the twelve participants were averaged together and the standard deviation calculated. The difference proportion of correct response in function if the difference between the test signals and the baseline are shown in Figure 4-4.

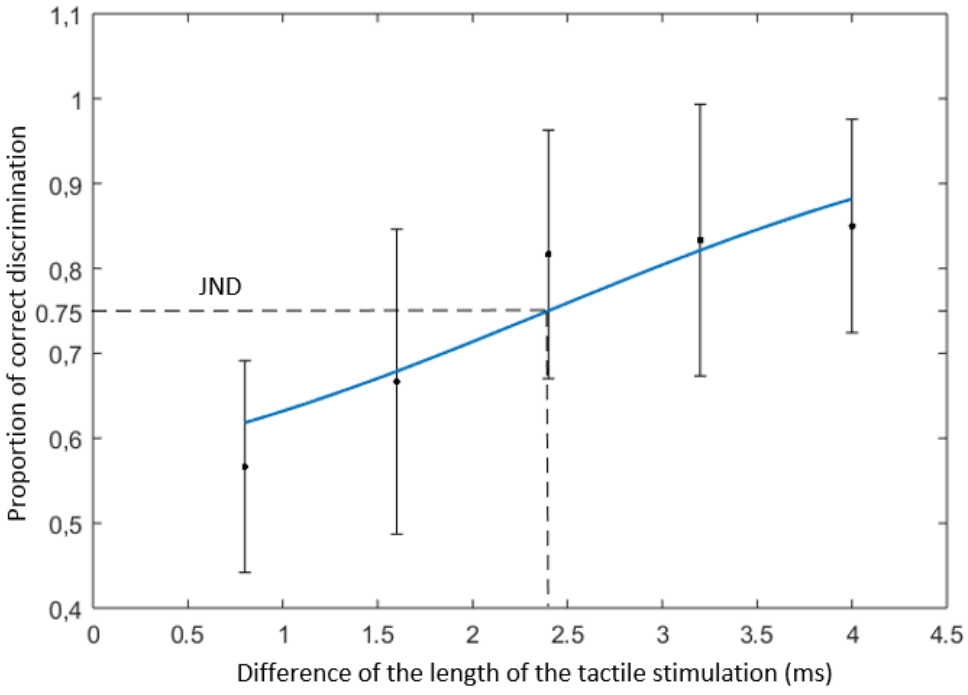

Figure 4-4: Just noticeable difference of signal length. Error bars represent the standard deviation and blue line is a fit of a logistic psychometric function to the result plot.

To compute the just noticeable difference (JND), which represents the minimum signal length difference that can be reliably discriminated, the percent of the time that the participants responded correctly as a function of the difference in the signal length was calculated. A

logistic psychometric function bounded between 0.5 and 1 was fitted to the resulting plot. A value of 0.5 on the Y axis represents a situation where the participant performs at chance level. On the contrary a value of 1 represents 100 % correct discrimination from the participant.

The overall JND for the twelve participants was estimated by interception of the psychometric function at Y = 0.75 as described in subsection 4.2.1.2. The JND of 2.45 ms means that extremely short pulse signals are indistinguishable by users for all values under 2.45 ms. It is thus possible to reduce a single pulse stimulation to its shortest value (which depends on the rising time of the devices; here 0.8ms) without any difference for the final tactile users. This limit could be used to reduce the power consumption in specific usage cases such as singular “bumps” or clicks”.

4.3.3 Minimal perceptible response time

The minimal response time (or rise time) discrimination experiment aim was to determine the capacity to perceive differences in the time taken by the resonating plate to reach its maximal amplitude. As previously the psychometric function was measured on the setup and with the participants presented in section 4.2. From this psychometric function the JND of rise time for humans interacting with the UL tactile device was extracted. The experiment was based on a forced choice task with a constant pool of stimuli (constant stimuli method).

Differences in rise time change the time it takes to reduce the friction coefficient, this phenomenon creates a difference in sensation, independent of the duration of the signal. To quantify this change in perception, we asked the participants to compare the sharpness of two stimuli, displayed in sequential order. A reference value of sharpness was always randomly set as one of the two stimuli presented in the discrimination task. The other stimulus was a test value to compare against the baseline. The participants explored the two stimuli up to 3 times and were then asked to report which stimulus offered the “sharpest” stimulation. They had to choose one of the signals even if not sure of the answer.

As for the previous experiment, the test signals were presented in a pseudorandom order, where one of the signals was always the baseline and the other selected from a list of five signal rise times calibrated in advance. The total signal presented was always 10ms, the possible rise time were selected after a preliminary experiment at 0.8, 1.2, 1.8, 2.6 and 4.4 ms to be compared with a baseline of 0.4 ms. The baseline is the absolute minimum rise time that can be generated with the E-Vita in this configuration. A pre-calibrated open loop voltage profile was used to reach this low rise time. The experiment was stopped after a signal of each length had been presented 10 times against the reference. Each of the twelve subjects was thus presented to a total of 50 signal comparisons. Figure 4-5 presents the results from the 12 subjects described in Table 1. All the answers from the participants were averaged together and the standard deviation calculated.

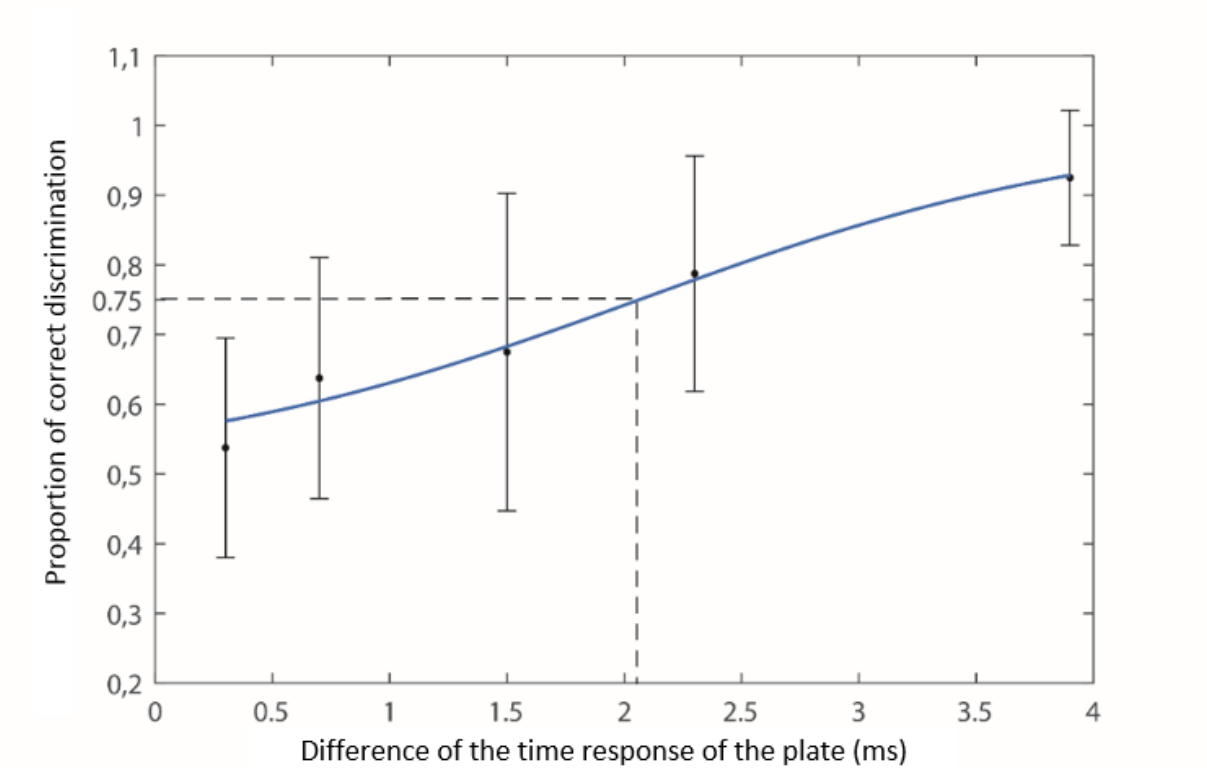

Figure 4-5: Just noticeable difference of time response of a single pulse modulation. Error bars represent the standard deviation and blue line is a fit of a logistic psychometric function to the result plot.

The JND was then calculated as a percent of the time that the participants responded correctly as a function of the difference in the signal length. This JND represents the minimum rise time difference that can be reliably discriminated from a small 0.3 ms reference rise time. A logistic psychometric function bounded between 0.5 and 1 was fitted to the resulting plot as previously. With a threshold set at 75 % of correct answers the overall JND was therefore estimated at a 2.1 ms rise time difference.

The indistinguishability of the rise time of signals under 2.1 ms confirms the bandwidth assumptions made in Chapter 2 for single pulse modulation. When applying a tactile feedback consisting of a single pulse stimulation, there is no need for the response time of the resonant plate to be under 2.1 ms since the difference will not be perceived. This limit is useful to reduce the constraints associated with the creation of an UL device that would be mainly used in single pulse type of stimulation.

It should be noted that this limit does not directly apply to continuous modulation (e.g. chain of burst stimulation applied continuously with a short period). As seen in Chapter 2, it is necessary to have a response time under 700 µs to provide a tactile feedback across the full frequency perception of the user (500 Hz).

4.4 OPTIMIZATION OF THE POWER CONSUMPTION THROUGH DUTY CYCLE REDUCTION

This section explores the possibility of taking advantage of the human tactile perception limits to reduce the power consumption of continuous friction modulation. This objective is achieved by reducing the duty cycle of such modulation while maintaining the same texture perception.

4.4.1 Introduction

Power consumption is a critical factor in the final integration of UL technology in mobile platforms. Similar haptic technology (vibrotactile), already included in all smartphones, is well known to draw heavily on the limited battery of the device. As for, the ultrasonic stimulator, it generally consumes power while applying a modulated stimulation to the finger pad of the user (simple temporal stimulation or texture reproduction). The friction modulation quickly alternates states of high and low friction while the user moves its finger across the active surface [93]. In most cases, this switching is simply implemented by applying a square modulation signal to the friction control device [94]. Perception of a specific texture is driven by the spatial frequency pattern of this texture. This pattern can then be recreated in the time domain by modulating the active phases in function of the exploration speed. This effect can be seen in Figure 4-6.

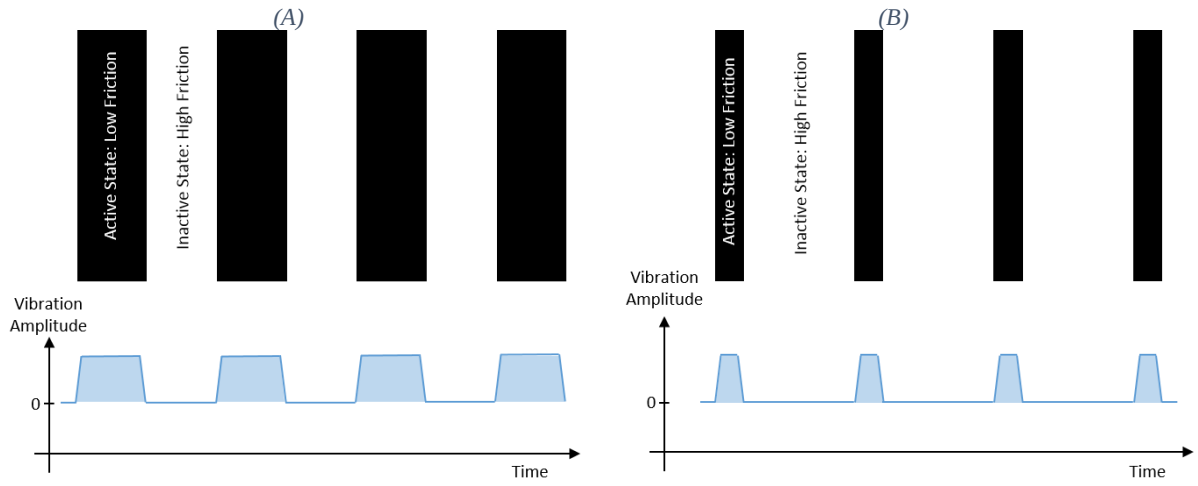

Figure 4-6: Graphical and temporal representation of a texture with the same fundamental frequency of modulation. Figure (A) presents a square duty cycle (50%), Figure (B) presents a smaller duty cycle of 20%, the modulation frequency remains the same but the active state and thus power consumption are significantly reduced.

We made the hypothesis that, since the perception of texture is mainly driven by its frequency pattern (as seen in Chapter 1), it could be possible to maintain the same perception between two temporal reproductions of textures if only the duty cycle is modified. This reduction could lead to a significant power consumption reduction in friction modulation devices. As seen in Figure 4-6 (B), a reduction of the duty cycle when applying a continuous friction modulation reduces proportionally the active state (shaded area where ultrasonic vibrations are applied) and thus the power consumption of the device.

To test this hypothesis, an experimental psychophysical protocol was put together to determine the maximum duty cycle reduction achievable, while keeping the same perception of the modulation by the participants. The potential duty cycle reduction was assessed for multiple frequencies within the human perception range. A wide range of modulation frequencies was tested to validate the proposed scheme across the frequency perception range of the human fingertip (described in Chapter 1).

4.4.2 Psychophysical protocols

Since the goal is to determine the minimal perceptive threshold between different signal durations, the protocol applied in this experiment is similar to the one presented previously in section 4.3. The main difference with the previous protocol is that the modulated signal is not presented only once or twice but in a steady stream at a specific frequency. For each set of modulation frequencies, the psychometric function and the JND of the duty cycle discrimination were determined. Similarly, to the previous experiment, a constant stimuli method was used. The participants explored the two stimuli up to 3 times and were then asked to report which stimulus offered the “strongest” stimulation. They had to choose one of the signals even if not sure of the answer.

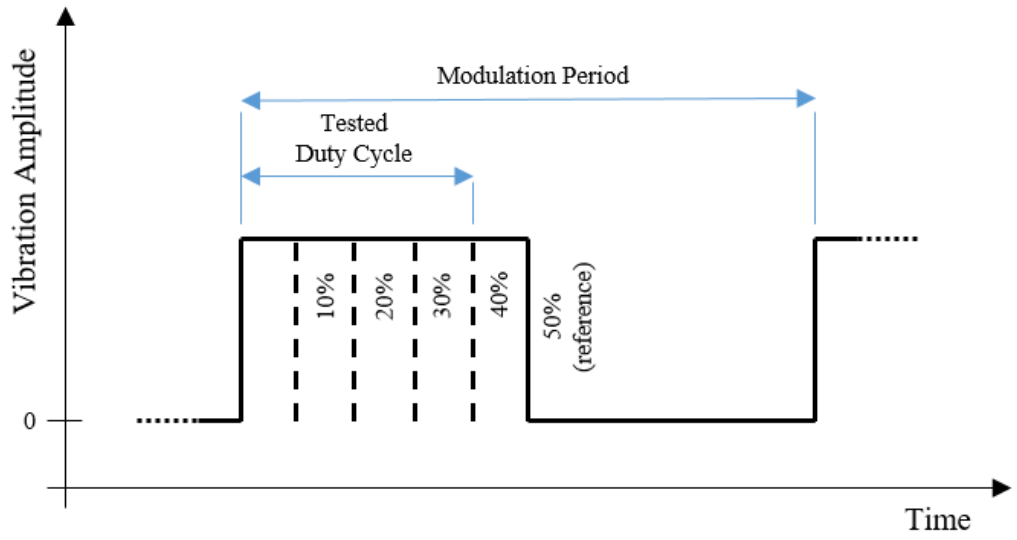

Figure 4-7: Reduction cases of the Duty Cycle

As in the first experiments, the test signals were presented in a pseudorandom order where one of the signals was always the reference and the other selected from a list of 4 duty cycles calibrated in advance. A first preliminary experiment (as described in subsection 4.2.1.2) demonstrated the need for a minimum duty cycle as low as possible for a proper fit of the psychometric curve. The selected list of possible duty cycles was 10 %, 20 %, 30 %, and 40 %, with the square 50 % duty cycle used as the reference stimulus (Figure 4-7). The experiment was once again stopped after each duty cycle was presented 10 times against the reference.

This same protocol was implemented 4 times for different modulation frequencies: 10 Hz, 20 Hz, 40 Hz and 80 Hz. For really low modulation frequencies, we noticed, in the preliminary

experiment, that participants can perceive a double stimulation (they report feeling the change from high to low and from low to high friction). To prevent this effect from affecting the results, we choose a minimum modulation frequency of 10 Hz. The highest modulation frequency is bounded at 80 Hz by the minimum rise time of the device, a higher frequency would prevent the resonating glass from reaching maximum amplitude in time at the lowest duty cycle (10 %). Each frequency measurement takes roughly the same time to complete as the rise time and signal duration experiments (approximately 20 min per frequency). Considering the length of this total experiment, to prevent fatigue, the 4 frequency measures were divided in 2 sessions separated by a one-hour break. Each of the twelve subjects was thus presented to a total of 160 signal comparison tests to extract the 4 duty cycle psychometric functions and JND values.

In each task, the psychophysical threshold was evaluated by fitting a logistic psychometric function based on the method of maximum likelihood to the psychophysical performance of the participants with the method detailed in 4.2.1.

4.4.3 Results of the duty cycle modulation

In this experiment, four modulation frequencies were explored in separate blocks. As was done in the time length and rise time experiment, the JND, which represented the minimum duty cycle that can be reliably discriminated from a reference duty cycle of 50%, was computed by estimating the interception point of a psychometric function fitted to the answers of the participants and a proportion of correct answers superior to 75 % as presented in section 4.2.1.1. The four fitted psychophysical functions calculated from this experiment can be seen in Figure 4-8.

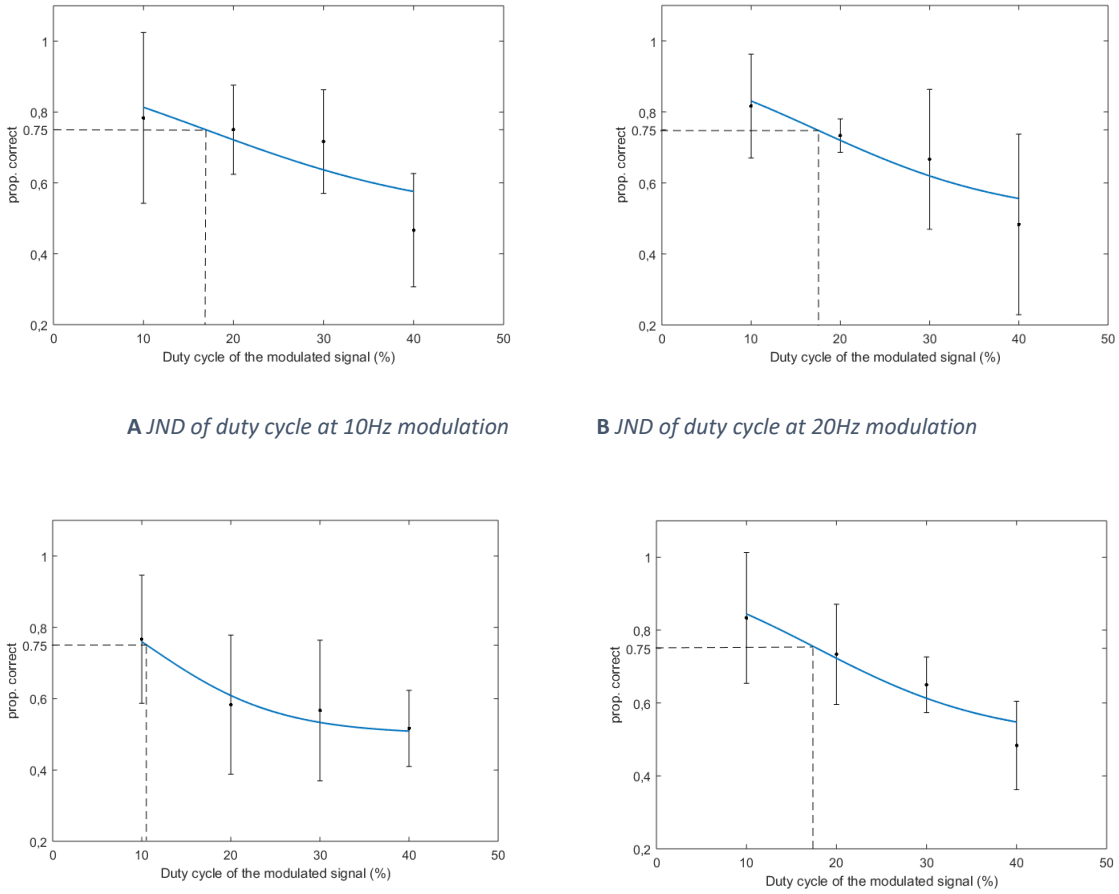

A *JND of duty cycle at 10Hz modulation*

B *JND of duty cycle at 20Hz modulation*

C *JND of duty cycle at 40Hz modulation*

D *JND of duty cycle at 80Hz modulation*

Figure 4-8: Psychometric functions associated with the discrimination rates of the shorter duty cycles (40%, 30%, 20% and 10%) from the reference standard (50%). Four conditions with different modulation frequencies have been tested: 10 Hz, 20 Hz, 40 Hz and 80 Hz.

The overall JND for the twelve subjects who participated in this experiment were calculated at a duty cycle of respectively 16.5, 17.5, 11 and 17.5 % for modulation frequency of 10, 20, 40 and 80 Hz. These analyses of the results tend to show that the frequency of modulation does not impact the perception of duty cycle reduction.

In order to understand clearly the meaning of theses psychometric fittings, a detailed explanation of the data presented in Figure 4-8 (D) is done in Figure 4-9. The reference of 50 % duty cycle is always larger than the test signals (40 % to 10 %), So we may expect that it should always be perceived as “strongest” by a perfectly sensitive participant. However, the real response observed is quite different since in most cases, the participant is not able to discern the difference between the different duty cycles and thus, respond randomly (wrong half of the time). From this figure, we can understand the following facts:

- The difference between the reference (50 %) and the test signal (10-40 %) is not perceivable for a low duty cycle difference (40 % duty cycle test signal). The correct response rate is close to 50%.

- In the case of a large duty cycle difference, the participant is almost always able to perceive it (10 and 20 % duty cycle). The correct response rate in this case is close to 100%.

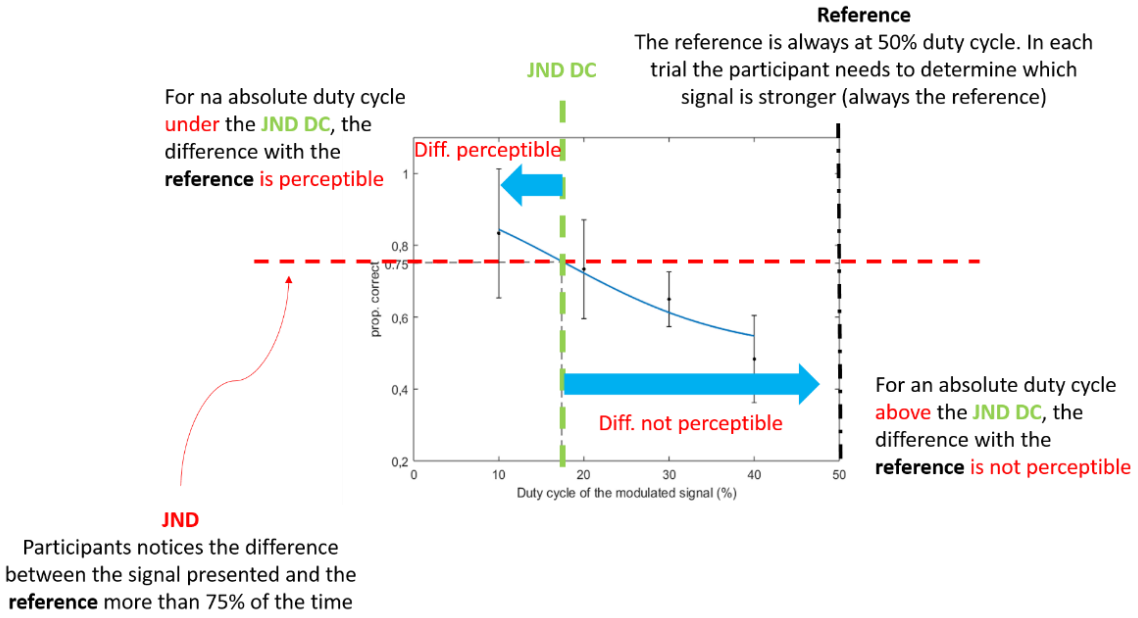

Figure 4-9: Interpretation of the 80 Hz psychometric functions associated with the discrimination rates of the shorter duty cycles (40%, 30%, 20% and 10%) from the reference standard (50%).

4.4.4 Impacts on the energy consumption

The results presented in subsection 4.4.3 show that reducing the duty cycle of a friction modulation signal is not always perceivable by the participant. Moreover, since a duty cycle of 50 % is commonly used to create regular gratings, we can normalize the reduction of the duty cycle compared to this value. These JND values then represent a reduction, relative to a standard duty cycle, of 50 % of respectively 67, 65, 78 and 65 % for modulation frequency of 10, 20, 40 and 80 Hz.

As seen in Figure 4-10 the possible duty cycle reduction without perception by a user is stable across the studied frequency spectrum. The modulation frequency does not seem to impact the duty cycle JND.

To assess the assumption of power reduction, the power consumption associated with each duty cycle has been measured with the help of a Tectronics oscilloscope and a current probe connected to the 5V DC supply of the piezoelectric driver, after a stabilization time of 2s.

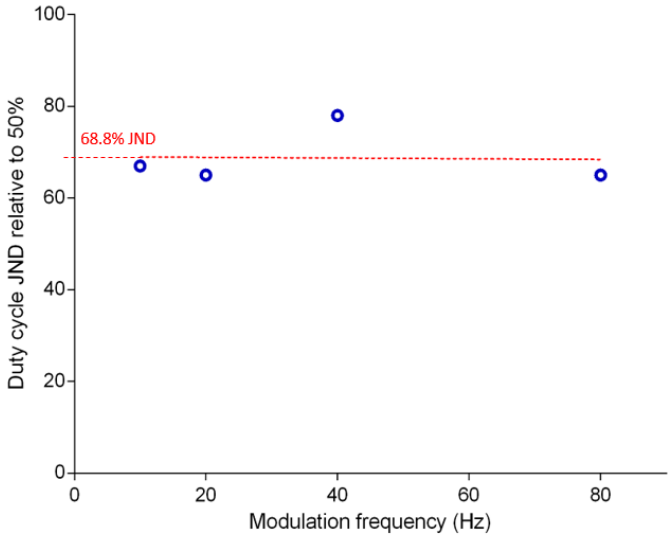

Figure 4-10: JND of the duty cycle in function of the modulation frequency. JND is relative to a standard duty cycle of 50%. Dotted line represents the mean JND across the spectrum.

The E-Vita device consumes approximately 0.4 W to power the BananaPro® computer and the LCD screen. The UL resonator itself presents a 7 W power consumption **in continuous operations (amplitude of 1.25 µm without any modulation)**. The measures in Figure 4-11 show a quasi-linear decrease of the UL device power consumption with the application of smaller duty cycles. Increasing the frequency of modulation induces a slightly higher power consumption of the E-Vita, due to lower efficiency of the internal boost convertor at these frequencies. This effect cannot be seen if the 12 V DC internal boost converter is replaced by an external laboratory DC power source to power the transformer based driver.

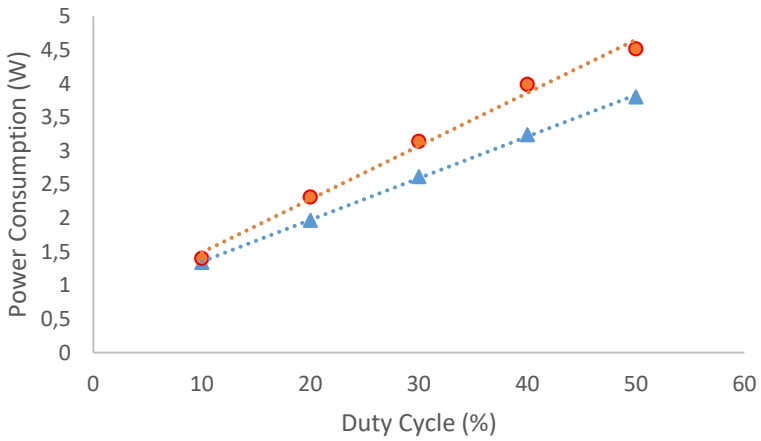

Figure 4-11: Power consumption of the E-Vita in function of the duty cycle of the friction modulation. Blue triangles are measured at 10 Hz and red points at 80 Hz

Since the linear decrease of the consumption is similar at different frequencies, we can propose that an average of 68.8 % power reduction is available from 10 to 80 Hz modulation frequency without any perceivable difference for the participants. The minimal usable duty cycle is thus of 16%.

4.4.5 Comparison with existing solutions and conclusion

In the previous paragraph, we have shown that it is possible to reduce the duty cycle of the continuous friction modulation while maintaining the same perception. It may be noted that this conclusion may be applied to all the friction modulation devices, in particular electrostatic stimulation systems, even if they do not have the same power consumption while in active state.

The current study uses a device based on Ultrasonic Lubrication as a proof of concept for the proposed temporal texture simulation strategy. We can nevertheless conclude that this new general control scheme, based on human perception, can significantly reduce power consumption of friction modulation devices. A power reduction of up to 68.8 % is confirmed for an ultrasonic device across the 10 to 80 Hz range of modulation studied. As can be seen in Table 4-11, in the case of the E-Vita at 80 Hz this significant power reduction means that the power consumption goes from 4.5 W in active state at 50% duty cycle, to only 1.85 W.

It is also possible to compare these values to the energy consumption of typical application cases used in the mobile phone industry. One method of comparison typically used by industrials is to calculate the average power consumption of a type of haptic actuator during a short pulsation or “Buzz”, defined as a 600 ms vibration. This method is reported by Texas Instrument® in [26] to compare power consumption of different vibrotactile technologies. Figure 4-12, reshown from chapter 1, illustrates three types of actuators typically used in mobile application to generate a perceptible vibration of the device’s screen: Eccentric Rotating Mass (ERM), Linear Resonant Actuator (LRA), and Piezo Actuator.

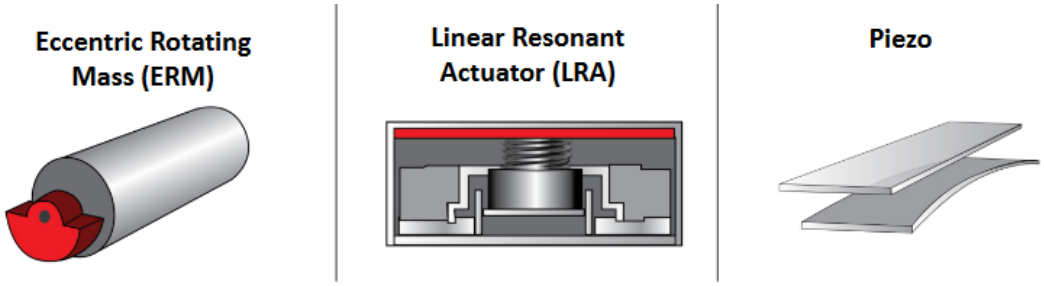

Figure 4-12: Three types of vibrotactile actuators used in mobile devices [26]

As presented in Chapter 1, these actuators operate on a different principle than UL stimulation; it is thus not possible to use the acceleration generated to normalize the level of haptic feedback as done in [26] . An energy requirement comparison with an UL stimulator is nevertheless interesting. We use the defined duration of 609 ms to calculate the energy necessary for a “buzz” of the UL stimulator at maximum tactile feedback (1.25 µm) and 80 Hz stimulation. This presents the largest power draw possible by the E-Vita, and is similar to a typical texture recreation event (one slide of the finger). The energy consumption during a haptic event is expressed in µAh as it can be seen in

Table 4-10.

Table 4-10: Comparison of the power consumption by different tactile stimulation technologies for a single 50 ms "click"

Technology	Vibrotactile ERM [26]	Vibrotactile LRA [26]	Vibrotactile Piezo [26]	UL 80 Hz 50 % D.C.	UL 80 Hz 16 % D.C.
VDD (V)	5	5	5	5	5
Mean Current (mA)	67.4	20	67.3	903	280
Power (W)	0.337	1.00	0.334	4.5	1.4
Time Window (ms)	609	752	609	609	609
Consumption (μAh)	11.41	3.38	11.4	152	47.7

These results allow only for a rough comparison since the tactile perception they generate involve totally different modalities and no psychophysical evaluation was done to compare the relative perception of their stimulation. Nevertheless, it is interesting to note that while the energy requirements of UL stimulation are quite high compared to vibrotactile solutions we can see that the power scheme proposed is necessary to reach the same order of magnitude of power consumption.

4.5 CROSS COMPENSATION OF UL MODULATION PARAMETERS

In this section, a potential limitation of the range of human perception is studied once more. Taking advantage of these limitations a control method is proposed to compensate an UL resonator low rise time.

4.5.1 Introduction

As seen in chapter 2, it is sometimes difficult to conciliate the different requirements necessary to obtain an optimized UL tactile feedback. This is especially true for the response time of the plate and its maximum amplitude of vibration. For example, in the “winglet” demonstrator presented in chapter 3, the winglets increased significantly the energy storage of the resonating plate and thus, increased the response time of the resonant system (to reach the maximal amplitude).

Due to these design constraints and tradeoffs, a Method to compensate for a slow rise time would be extremely useful for the optimal operation of the integrated UL device. The following section thus describes a psychophysical study aiming to prove the feasibility compensating a high time response by increasing the signal duration, in order to generate the same perception of both signals by the users.

4.5.2 Psychophysical protocol

To perform this experiment, the psychophysical protocol differs slightly from the ones used in sections 4.3 and 4.4. We propose the hypothesis that it is possible to compensate for a low Rise Time (RT) with a longer Signal Length (SL) in order to achieve the same perceived strength by the user. For that aim, the experiment was once again based on a forced choice task with a constant pool of stimuli (constant stimuli method). The participants had to compare the perceived strength of two stimuli, displayed in sequential order. A reference value of signal with a constant SL and RT was always randomly set as one of the two stimuli presented in the discrimination task. The other stimulus was a test value with a lower RT and different SL to compare against the baseline. The participants were free to explore the two stimuli up to 3 times and were then asked to report which stimulus offered the “strongest” stimulation (similarly to the experiment in section 4.3.2). They had to choose one of the signals even if not sure of the answer.

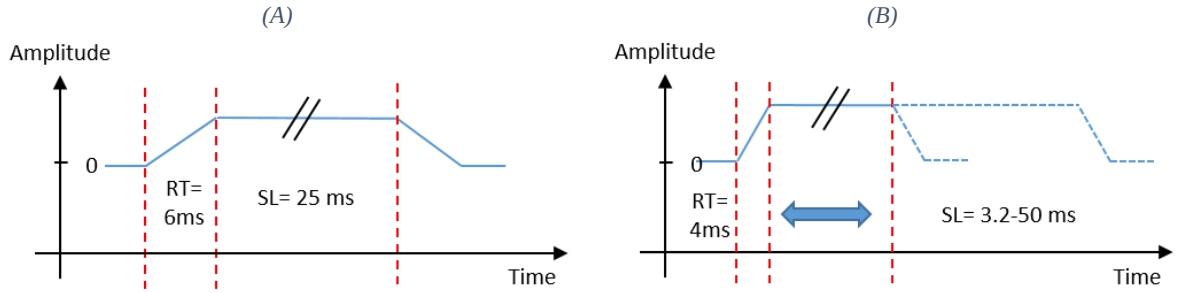

Figure 4-13: Timing representation of the two types of signals proposed to the participant in this experiment. Signal (A) is the reference signal, with RT=6 ms and SL=25 ms. In signal (B) both the rise time and the signal length are modified: RT=4 ms, SL=[3.2, 7.5, 15, 25, 50] ms

As shown in Figure 4-15, test signals were presented in a pseudorandom order where one of the signals was always the baseline and the other selected from a list of five signal length calibrated in advance. Since the experiment was in itself a preliminary study, the selected SL and RT value were determined arbitrarily from the lessons learned in section 4.3 in order to find the proper range of signal to use in the future full experiment. The possible SL were 3.2, 7.5, 15, 25 and 40 ms (with an RT of 4 ms) to be compared with a baseline of ST= 25 ms and RT=6 ms. The experiment was stopped after a signal of each length has been presented 10 times against the reference. Each of the participants was thus presented to a total of 50 signal comparisons.

This protocol was applied to a small pool of 4 participants in order to verify the preliminary hypothesis and to make sure that the words used to describe the perceptions of the participants made sense in the context of their actual perception. This last step is especially important to avoid misunderstanding by some participants, which usually leads to reversed or unusable psychophysical curves. Table 4-11 describes the participants that took part of the study.

Table 4-11: Pool of participant for the preliminary study of cross compensation

Participant	P1	P2	P3	P4
Age	28	26	29	29
Sex	M	M	M	M

4.5.3 Evaluation of the preliminary results

Due to the low number of participants tested in this preliminary study, it is useful to look directly at the raw results presented in Figure 4-14.

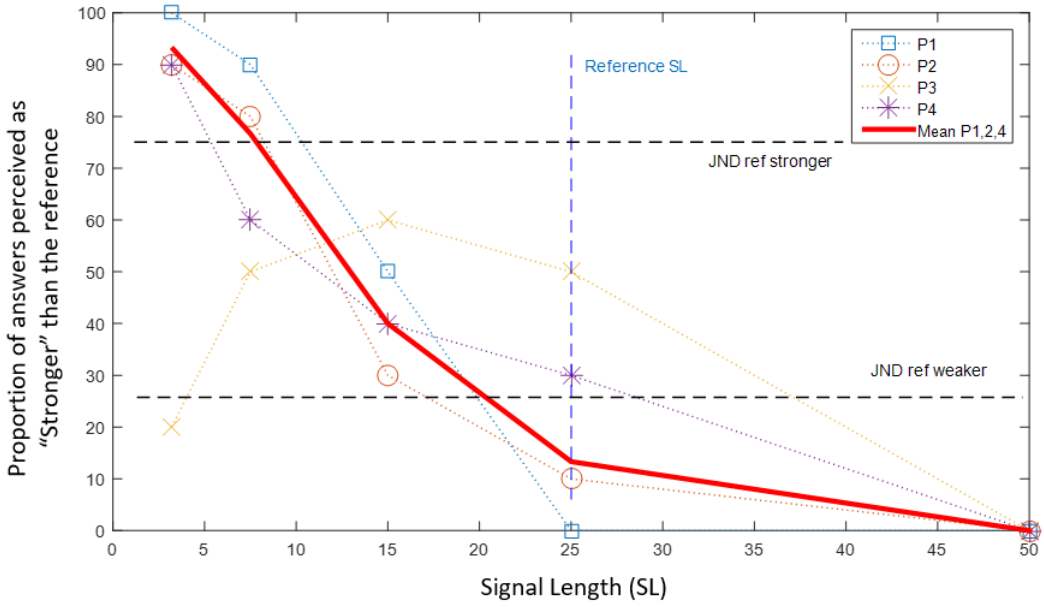

Figure 4-14: Results of the cross compensation study. The raw results of each participant are represented by the dashed lines. The mean of participant 1, 2 and 4 is represented by the red line.

We can see in Figure 4-14 that 3 out of 4 participants acted as anticipated; they present a close to 100 % "stronger reference" when the test signal duration tends toward 0 ms (they perceived the reference as stronger) and always perceive a 0 % "stronger reference" when SL of the test signal tends toward 40 ms (The test signal is perceived as stronger).

It is interesting to note a perceptual shift occurs when both reference and test signal have the same SL (SL=25 ms); the signal is clearly perceived as stronger in this case (below the JND at 25 %). This shift in strength perception can be explained by the difference in rise time between the two signals (4 and 6 ms). Finally, using the mean psychophysics curve calculated on P1, P2 and P4, we can see that this shift in perception can be balanced by decreasing the SL under the JND of 20 ms.

The definition of the perceived feedbacks was not clear to participant P3 who reported a significantly different perception than the others. The results presented in this preliminary experiment are currently limited to 4 participants and will thus need to be validated in a subsequent study with a larger number of participants. The misunderstanding of participant P3 highlights the fact that the protocol needs to be improved before expanding the study.

Nevertheless, the experiment proved a possible compensation of a deficiency in response time by increasing the signal duration without affecting too much the type of stimulation perceived by the participants. This discovery validates the proposed control scheme and warrant further studies to identify the limits of this phenomenon. The final objective of this experiment would be to measure the cross-compensation response on a full matrix of parameters, including RT and SL, but also the amplitude of vibration.

4.6 PERSPECTIVES AND CONCLUSION

4.6.1 Discussion on the fidelity of the psychophysical curves fitting

For the psychophysical evaluations performed in this chapter, the fitting of the psychometric functions was implemented using a logistic function with a maximal asymptotic value of 1 (or 100% distinguishability). This parametrization assumes that for highly over-threshold intensities of ultrasonic lubrication, the friction reduction is always perceived. However, as demonstrated by David Gueorguiev in his thesis [95], the psychophysical results on UL devices showed that even at high intensities, there is a consistent lapse rate around 5%. This lapse rate (participants are never able to recognize 100% of signals) might be caused by natural friction fluctuations like stick-slip or sudden excess of sweat. D. Gueorguiev proposes that Participants probably mistake these natural fluctuations for the signal that they are asked to detect and are hence biased by them. Thus, the results of the duty cycle analysis in section 4.4 were reevaluated. the psychometric fittings were re-implemented with all parameters identical except for the lapse rate at high intensities, which was allowed to take values between 0 and 5%, and the psychometric function was replotted for the tested frequencies of modulation: 10 Hz, 20 Hz, 40 Hz and 80 Hz.

The results from this more accurate fitting (Shown in Annex C) are significantly different than previously and the reductions at threshold are respectively 40.6%, 57.2%, 78.8% and 59.6% compared to the reference, displaying a U-shape rather than a straight line (See Figure 4-15). These results are also agreeing with our preliminary hypothesis that differences in duty cycle would be more perceivable at low frequencies since the difference in the duration of the ultrasonic signal would play a more prominent role than at high frequencies. It is unclear why the reduction at threshold would decrease for 80 Hz compared to 40 Hz, but the observed trend would need to be further validated for a larger pool of participants before performing a detailed analysis of the contact mechanics. However, differences probably stem out from the specificities of the mechanoreceptor's receptive fields and the respective contribution of the four psychophysical tactile channels.

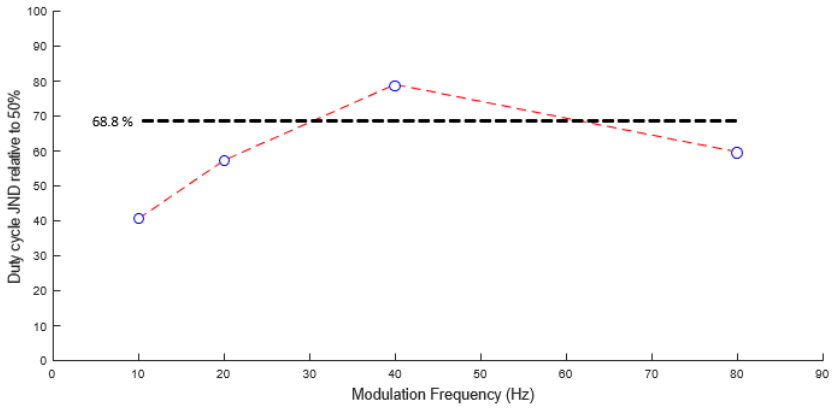

Figure 4-15: The reduction of the duty cycle at the psychophysical threshold is plotted against the modulation frequency and was found to follow a U-shape curve. The green line represents the simpler linear trend found in section 4.4

Since the discrepancies between the results presented here and in section 4.4 mostly concerns the low modulation frequency of 10 Hz, it might prove interesting to design an experiment in order to determine precisely the effect of duty cycle reduction at these low modulation frequencies. Similarly, the relatively large error bars present in the psychometric curve of the experiments in subsection 4.3, could also benefit from a better understanding of the limits of distinguishability.

4.6.2 Conclusions

Friction modulation is becoming a prevalent mode of control of UL device due to its clearer perception by the users compared to simple friction level. In this chapter, different friction modulation methods were analyzed to determine the limits of perceptions of human participants and propose potential control schemes to reduce the power consumption or simplify the design of the devices.

A general control scheme based on human perception to reduce power consumption in friction modulation devices was introduced. The results are validated using psychophysical measures on an ultrasonic lubrication device but are applicable to any friction modulation system. A power reduction of up to 68.8 % is confirmed for an ultrasonic device across the 10 to 80 Hz range of modulation studied.

Single pulse modulation was also studied as it presents a simple mean to convey local information about a single event or a small object. Psychophysical evaluation allowed us to determine a minimum variation of signal length and rise time that can be used and be meaningful to the user. Knowing these limits is important to avoid overdesigning the devices above what can be perceived by the human operators.

Finally, a control scheme was proposed to reduce the constraints imposed by the integration of UL displays. This method would permit the designer of UL display and tactile feedback algorithms to propose a standardized perception level across multiple devices independently of the exact physical parameters of the interface. This scheme was tested with a preliminary study but needs to be explored further to propose a simple standardization of the feedbacks presented to the users.

CONCLUSIONS AND PERSPECTIVES

This work aimed to provide a better understanding of the Ultrasonic Lubrication characteristics, and to propose an optimized design of HMI based on this concept. Previously proposed models of the UL effect were insufficient to describe precisely the evolution of friction and thus, made the design of UL devices adapted to mobile devices difficult.

In a first part, the human senses were described and a deeper look was given to the biological mechanoreceptors involved in the human tactile sense. The anatomical distribution and the electromechanical characteristics of the different mechanoreceptors used to perceive touch were described. Following this better understanding of the touch modalities, an introduction to the concept of tactile illusion was made, and a review of the different technologies adapted to the fingertip stimulation for mobile devices was conducted. Finally, the short history of the friction modulation mediated by Ultrasonic Lubrication (UL) effect was detailed, starting by the first discovery of the phenomenon made by F. Watanabe in 1995.

A series of tribology experiments was conducted to explore the fine influence of the amplitude of vibration on the dynamic friction coefficient. But also, the impacts linked more to the user, such as the velocity of exploration and the normal force applied. Finally, a specific experiment was conducted to measure which vibration frequencies are more adapted to UL. These experiments, combining artificial finger (probe) and *in vivo* experiments, was then used as the basis to validate a refined theory of UL effect. The lessons learned from this experimental and modeling approach lead to the proposition of a set of design rules, necessary for stronger and faster tactile stimulation.

Three HMI demonstrators applying these newly found design rules were then built. In parallel, a dedicated UL piezoelectric driver, capable of providing the necessary frequency and amplitude of vibration, was presented. Its design was also focused on the integration of all the control chain into a unique system with a low form factor. This approach is a first step toward the transition from laboratory environment to actual industrial implementation.

Finally, with the help of one of the advanced UL tactile HMI thus created, a series of psychophysical experiments were conducted to evaluate the limits of the human perception of UL effect. Control systems are then presented to take advantage of these limits. A general control scheme based on human perception to reduce power consumption in friction modulation devices was introduced. The results are validated using psychophysical measures on an ultrasonic lubrication device but are applicable to any friction modulation system such as those relying on electro-vibration and SAW. A power reduction of up to 68.8 % is confirmed for an ultrasonic device across the 10 to 80 Hz range of friction modulation studied. Single pulse modulation was also studied as it presents a simple mean to convey local information about a single event or a small object. The knowledge gain on user perception from these

experiments is useful to avoid overdesigning the devices above what can be perceived by the human operators.

As a perspective to the work presented, a study of the psychophysical effects created when visual and UL based tactile feedbacks are combined would prove enlightening. Friction modulation techniques present a large potential to expand the uses of touchscreen devices. Indeed, in most critical application today (e.g. robotic control, dangerous or vital systems, heavy machinery), touchscreen HMI are often considered too risky. These interfaces are not considered due to the high mistake rate caused by a lack of tactile feedback. A strong and reliable tactile feedback directly affecting the fingerpad of the users could solve this problem. A second benefit of these studies would be the evaluation of the mental load on the user; or also the way to share the information between the visual and tactile channels. For a given number of situations (mainly the drive operation), the visual load must be kept in a reasonable limit to assume the safety of the user. The tactile channel can be used to provide more information while keeping safety of interaction.

On a technological point of view, the integration issue of high frequency vibrating plate has still to be studied in view of the industrialization process: the question of the plate attachment within the mobile phone, the question of the robustness against crash-test, the question of aging and recyclability because of these new materials introduced.

Other scientific aspects may be also developed. To convince users and especially smart phone makers of the interest of tactile feedback, new applications must be proposed, as well as applications already well-known and which could be improved with the feedback. The keyboard interface for example is a very common way to communicate with the mobile devices, and because of the small size of the display, it is not always guaranteed to choose the accurate key with the finger above. The “button-click” function is a good mean to cope with this issue and is one of the major request for tactile feedback. However, the friction control principle for tactile feedback is not particularly well adapted for that aim. One possibility would be to add time reversal excitation on the device already equipped with UL principle actuators to obtain an activation of the surface in given points. This idea is already studied in L2EP Lab, however, for mobile applications, a great effort must be put on the energy consumption which must be mastered, as well as the cost of the device.

ANNEX A: BANDWIDTH ESTIMATION

Bandwidth is the highest sine wave frequency component that is significant in a signal. Because of the vagueness of the term "significant," unless detailed qualifiers are added, the concept of bandwidth is only approximate. We assume the signal is a 50% duty cycle clock signal that has a finite 10%-90% rise time. For this specific waveform, we can estimate the highest sine wave frequency needed to recreate the rise time.

Using a simple electrical analogy with RC= time constant:

$$V_{out} = V_{in}\left(1 - e^{-\mathrm{t}/\mathrm{RC}}\right) \quad (35)$$

For instance, assuming that Vin=1 V and the 10% voltage is obtained at time t_1.

Equation (35) becomes:

$$0.1 = 1 - e^{-\mathrm{t}_1/\mathrm{RC}} \quad (36)$$

And assuming 90% voltage is at time t_2

$$0.9 = 1 - e^{-\mathrm{t}_2/\mathrm{RC}} \quad (37)$$

We get the rise time $\mathrm{t}_r = \mathrm{t}_2 - \mathrm{t}_1$ and then t_r can be found using (36)and (37). Once solved we get t_r=2.197 RC. Also we know that cut off frequency f_c is defined as:

$$\mathrm{f}_c = \frac{1}{2\pi\mathrm{RC}} \quad (38)$$

so, from equation (38) we get:

$$\mathrm{f}_c = \mathrm{B}_w = 0.35/\mathrm{t}_r \quad (39)$$

ANNEX B: THIN FILM DEPOSITION FOR A TRANSPARENT 4 INCH DISPLAY

The deposition of the thin-film actuators was done at the CEA LETI in Grenoble. The devices were realized on a transparent reinforced glass substrate produce by EAGLE®. The plates were provided in wafer compatible with clean room technological process (200 mm and thickness of 700 µm). A first metallization step is first made on the back side of the plate to provide the necessary reflection for the subsequent steps of the process. The actuators were then deposited on the top face of the glass wafer.

1) 250nm of silicon oxide (SiO_2) are deposited directly on the glass substrate. This layer is used to passivate the glass.

2) 220nm of Molybdenum (Mo) are deposited and etched to form the bottom electrode of the actuator.

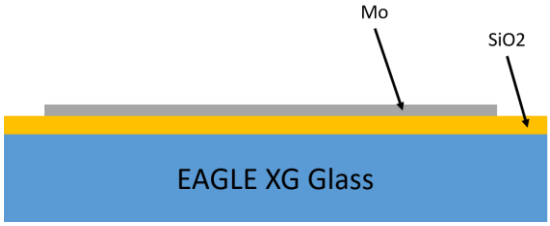

3) 2µm of piezoelectric Aluminum nitrate (AlN) are then deposited using a PVD process on the whole wafer

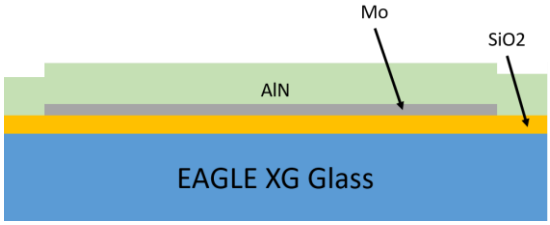

4) 220nm of Molybdenum (Mo) are again deposited in order to form the top electrode and form a mask the AlN etching process. The AlN is finally etched chemically.

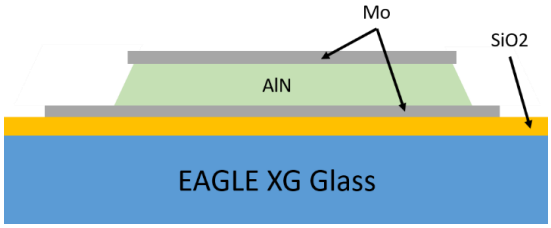

5) 300nm of silicon oxide (SiO_2) is deposited again to form a layer of passivation of the whole device.

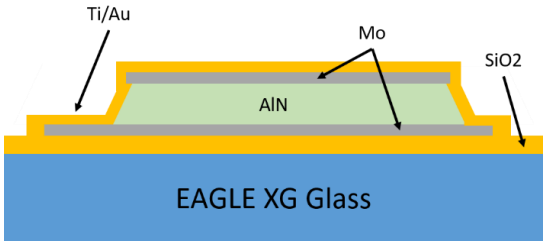

6) Top and bottom contacts are created by etching the (SiO_2) and proceeding to a deposition of 500nm of gold (Au) on top of 20nm of titanium.

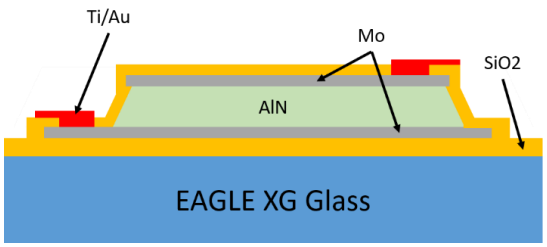

Figure A-1: Deposition of the AlN piezoelectric actuators

As a last step the reflective back side of the wafer was removed on some of the plates to provide a totally transparent central surface. The remaining devices possessing a metalized backside were used to characterize the resonant properties of the actuators and device. The finalized devices were observed using an electron microscope to check the thickness conformity of the deposited materials. A relative difference of 2.45% of the AlN thickness was observed (see Figure A-2).

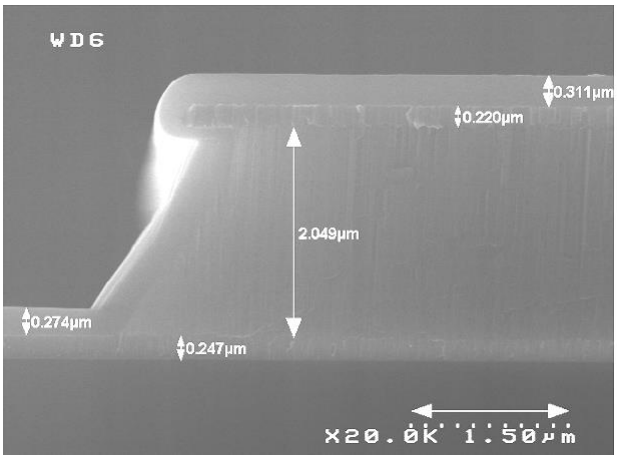

Figure A-2: AlN-on-glass SEM cross-section in order to measure the thickness of the different layers of the piezoelectric stack. [59] [60]

The AlN actuator technology was implement on a 200mm glass wafer which gave room to place multiple device on its surface. These devices include two full tactile devices and multiple small resonators and actuators added for characterization purposes (Figure A-3 a). All devices are finally cut to their final geometries as seen in Figure A-3 b.

(a) (b)

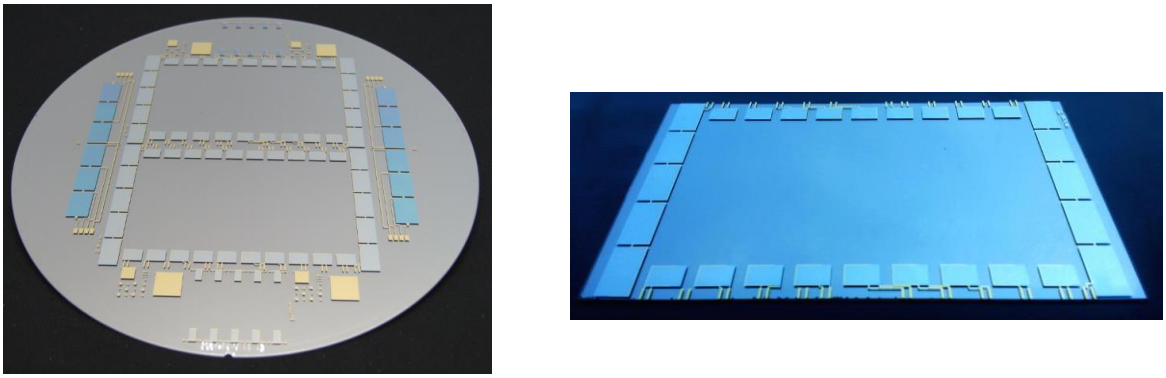

Figure A-3: (a) AlN-on-glass wafer with two AlN actuated 110 × 65 mm² haptic plates and with a reflective layer necessary for optical electromechanical characterizations. (b) UL haptic plate after separation from the wafer, the reported contacts are visible in gold on the side of the glass. [59]

ANNEX C: ALTERNATIVE PSYCHOPHYSICAL FITS

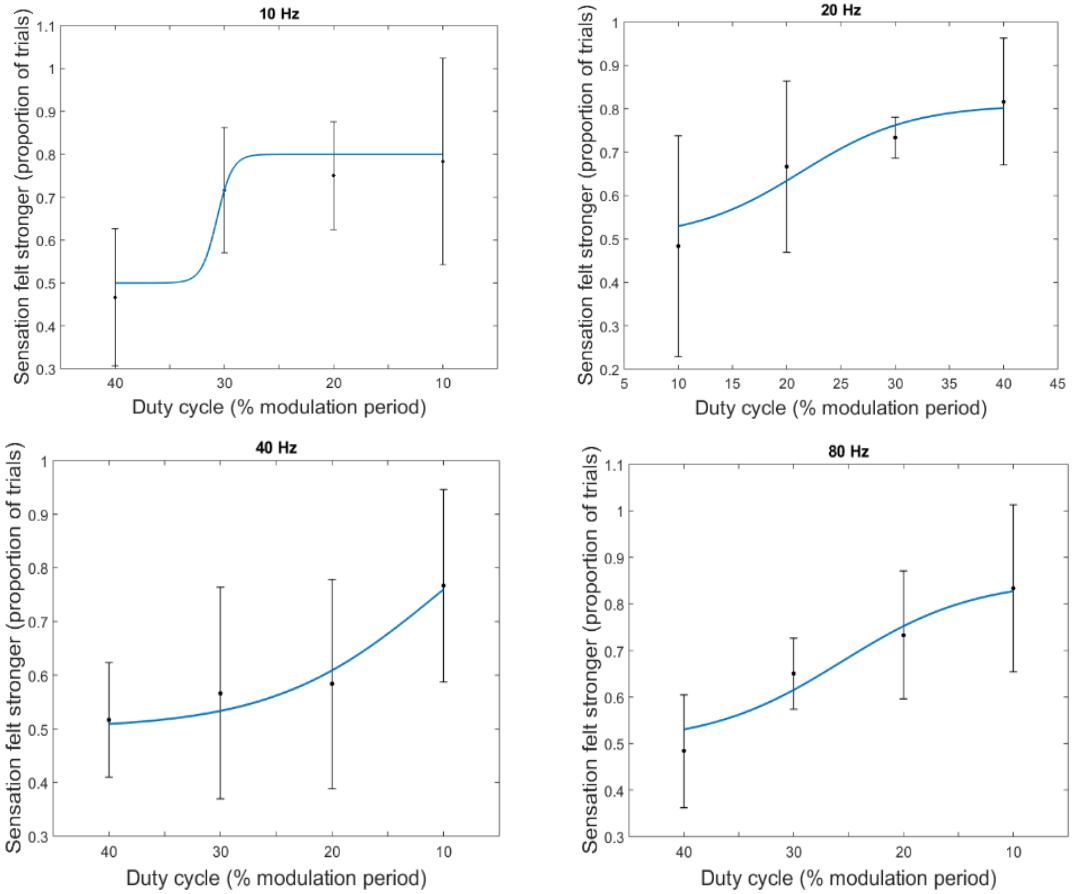

Figure A-1: Psychometric functions associated with the discrimination rates of the shorter duty cycles (40%, 30%, 20% and 10%) from the reference standard (50%). Four conditions with different modulation frequencies have been tested: 10 Hz, 20 Hz, 40 Hz and 80 Hz.

REFERENCES

[1] W. Buxton, R. Hill and P. Rowley, "Issues and techniques in touchsensitive tablet input," in *Proc. SIGGRAPH'85*, San Francisco, 1985.

[2] E. Vezzoli, PhD Thesis: Friction and Texture: A way to control and generate them, Lille: Laboratoire L2EP, Lille1, 2016.

[3] K. Johnson and J. Phillips, "Tactile spatial resolution. i. two-point discrimination, gap detection, grating resolution, and letter recognition.," *Journal of Neurophysiology,* p. 46(6):1177, 1981.

[4] M. Ziat, V. Hayward, C. Chapman, M. Ernst and C. Lenay, "Tactile suppression of displacement," *Experimental brain research,* vol. 206, no. 3, pp. 299-310, 2010.

[5] P. Delmas, J. Hao and L. Rodat-Despoix, "Molecular mechanisms of mechanotransduction in mammalian sensory neurons.," *Nature Reviews Neuroscience,* vol. 12, p. 139–153, 2011.

[6] D. Purves , G. Augustine and D. Fitzpatrick , Mechanoreceptors Specialized to Receive Tactile Information, MA: Sunderlands, 2001.

[7] "Microneurography," Wikipedia, [Online]. Available: https://en.wikipedia.org/wiki/Microneurography. [Accessed 13 Octobre 2016].

[8] K. Johnson, "The roles and functions of cutaneous mechanoreceptors," *Current Opinion in Neurobiology,* vol. 11, no. 4, p. 455–461, 2001.

[9] J. Wessberg, Introduction to microneurography, Gotheborg: University of Gotheborg, 2013.

[10] D. Blake, K. Johnson and S. Hsiao, "Monkey cutaneous sai and ra responses to raised and depressed scanned patterns: effects of width, height, orientation, and a raised surround," *Journal of neurophysiology,* vol. 78, no. 5, p. 2503, 1997.

[11] R. Johansson and A. Vallbo, "Tactile sensibility in the human hand: relative and absolute densities of four types of mechanoreceptive units in glabrous skin," *The Journal of physiology,* vol. 286, no. 1, p. 283, 1979.

[12] I. Birznieks, V. Macefield, G. Westling and R. Johansson, "Slowly adapting mechanoreceptors in the borders of the human fingernail encode fingertip forces," *The Journal of Neuroscience,* vol. 29, no. 29, p. 9370, 2009.

[13] M. Paré, R. Elde, J. Mazurkiewicz, A. Smith and F. Rice, "The meissner corpuscle revised: a multiafferented mechanoreceptor with nociceptor immunochemical properties," *The Journal of Neuroscience,* vol. 21, no. 18, p. 7236, 2001.

[14] M. Srinivasan, J. Whitehouse and R. LaMotte, "Tactile detection of slip: surface microgeometry and peripheral neural codes," *Journal of Neurophysiology,* vol. 63, no. 6, p. 1323, 1990.

[15] R. Johansson and G. Westling, "Roles of glabrous skin receptors and sensorimotor memory in automatic control of precision grip when lifting rougher or more slippery objects," *Experimental Brain Research,* vol. 56, no. 3, p. 550–564, 1984.

[16] J. Bell, S. Bolanowski and M. Holmes, "The structure and function of pacinian corpuscles: A review," *Progress in Neurobiology,* vol. 42, no. 1, p. 79 – 128, 1994.

[17] K. Johnson, T. Yoshioka and F. Vega-Bermudez, "Tactile functions of mechanoreceptive afferents innervating the hand," *Journal of Clinical Neurophysiology,* vol. 17, no. 6, p. 539, 2000.

[18] R. Johansson, U. Landström and R. Lundström, "Responses of mechanoreceptive afferent units in the glabrous skin of the human hand to sinusoidal skin displacements," *Brain Research,* vol. 244, no. 1, p. 17–25, 1982.

[19] A. Brisben, S. Hsiao and K. Johnson, "Detection of vibration transmitted through an object grasped in the hand," *Journal of Neurophysiology,* vol. 81, no. 4, p. 1548, 1999.

[20] T. Maeno, K. Otokawa and M. Konyo, "Tactile Display of Surface Texture by use of Amplitude Modulation of Ultrasonic Vibration," in *IEEE Ultrasonics Symposium*, Vancouver, 2006.

[21] V. Hayward and H. Dostmohamed, "Trajectory of contact region on the fingerpad gives the illusion of haptic shapes," *Experimental Brain Research,* vol. 164, pp. 387-394, 2005.

[22] R.-D.-L.-T. Gabriel and H. Vincent, "Force can overcome object geometry in the perception of shape through active touch," *Nature,* no. 412, pp. 445-448, 26 July 2001.

[23] Andrew H. Gosline, T. Emre and I. Brouwer, "What You Feel Isn’t Always What You Get," April 19, 2002.

[24] J. Pasquero, "PhD Thesis: Survey on communication though touch.," McGill University, 2006.

[25] C. Jacques, "Driven by Touch Screen Devices, Haptics Market to Grow 16-fold to $13.8 Billion in 2025," Lux research, [Online]. Available: http://www2.luxresearchinc.com/component/content/article/188.html. [Accessed 10 octobre 2016].

[26] Wang, Flora; Texas Instruments, "Haptic Energy Consumption," 2014.

[27] B. M. Schena, "Directional inertial tactile feedback using rotating masses". USA Patent US7182691 B1, 27 February 2007.

[28] M. Takasaki, Y. Fujii, H. Yousuke , T. Mizuno and T. Nara, "Proposal of tele-touch using active type saw tactile display," in *Intelligent Robots and Systems, 2006 IEEE/RSJ International Conference on*, Beijing, 2006/10/9.

[29] M. Takasaki, H. Kotani, T. Mizuno and T. Nara, "Transparent surface acoustic wave tactile display," in *Intelligent Robots and Systems, 2005.(IROS 2005). 2005 IEEE/RSJ International Conference on*, Sendai, 2005/8/2.

[30] E. Mallinckrodt, A. Hughes and W. Sleator , "Perception by the skin of electrically induced vibrations.," *Science,* vol. 118, no. 3062, pp. 277-278, 1953.

[31] D. J. Meyer, . M. A. Peshkin and E. J. Colgate, "Fingertip friction modulation due to electrostatic attraction," in *World Haptics Conference (WHC), 2013*, Daejeon, 2013/4/14.

[32] T. Nakamura and A. Yamamoto, "Multi-finger electrostatic passive haptic feedback on a visual display," in *World Haptics Conference (WHC)*, Daejeon, 2013.

[33] E. Vezzoli, M. Amberg, F. Giraud and B. Lemaire-Semail, "Electrovibration modeling analysis," in *In Proceedings of the Euro- haptic Conference*, Paris, 2014.

[34] F. Giraud, B. Lemaire-Semail and M. Amberg, "Merging two tactile stimulation principles: electrovibration and squeeze film effect," in *World Haptics Conference (WHC), 2013*, Daejeon, 2013/4/14.

[35] T. Watanabe and S. Fukui, "A method for controlling tactile sensation of surface roughness using ultrasonic vibration," in *Robotics and Automation, 1995. Proceedings., 1995 IEEE International Conference on*, Nagoya, 1995/5/21.

[36] O. Reynolds, "On the Theory of Lubrication and Its Application to Mr. Beauchamp Tower's Experiments, Including an Experimental Determination of the Viscosity of Olive Oil.," *Proceedings of the Royal Society of London,* vol. 40, pp. 191-203, 1886.

[37] S. Yoshimoto, H. Kobayashi and M. Miyatake, "Float characteristics of a squeeze-film air bearing for a linear motion guide using ultrasonic vibrations," *Tribology International,* vol. 40, no. 3, pp. 503-511, 2007.

[38] M. Biet, PhD Thesis: Conception et contrôle d'actionneurs électro-actifs dédiés à la stimulation tactile, Lille: Lille1 university, 2007/12.

[39] W. Gross, "Gas bearings: a survey," *Wear,* vol. 6, no. 6, pp. 423-443, 1963/12/31.

[40] M. Biet, F. Giraud and B. Lemaire-Semail, "Squeeze film effect for the design of an ultrasonic tactile plate," *Ultrasonics, Ferroelectrics and Frequency Control, IEEE Transactions on,* vol. 54, no. 12, pp. 2678-2688, 2007/12.

[41] L. Winfield, J. Glassmire, . J. E. Colgate and M. Peshkin, "T-PaD: Tactile pattern display through variable friction reduction," in *EuroHaptics Conference, 2007 and Symposium on Haptic Interfaces for Virtual Environment and Teleoperator Systems. World Haptics 2007. Second Joint*, Tsukuba, 2007/3/22.

[42] S. G. Manuel, R. L. Klatzky, M. A. Peshkin and E. J. Colgate, "Surface haptic feature attenuation due to contact on opposing surface," in *Haptics Symposium (HAPTICS), 2012 IEEE*, Vancouver, 2012/3/4.

[43] X. Dai, J. Gu, X. Cao, E. J. Colgate and H. Tan, "SlickFeel: sliding and clicking haptic feedback on a touchscreen," in *Adjunct proceedings of the 25th annual ACM symposium on User interface software and technology*, San Diego, 2012/10/7.

[44] J. Mullenbach, C. Shultz, M. A. Piper, M. Peshkin and J. E. Colgate, "TPad Fire: Surface Haptic Tablet," in *Proc of HAID*, Daejeon, 2013.

[45] P. Sergeant, F. Giraud and B. Lemaire-Semail, "Geometrical optimization of an ultrasonic tactile plate," *Sensors and Actuators A: Physical,* vol. 161, no. 1, pp. 91-100, 2010/6/30.

[46] F. Giraud, M. Amberg, B. Lemaire-Semail and G. Casiez, "Design of a transparent tactile stimulator," in *Haptics Symposium (HAPTICS)*, Vancouver, 2012/3/5.

[47] F. Giraud, M. Amberg and B. Lemaire-Semail, "Design and control of a haptic knob," *Sensors and Actuators A: Physical,* vol. 196, pp. 78-85, 2013/7/1.

[48] M. Amberg, F. Giraud, B. Semail, P. Olivo, G. Casiez and N. Roussel, "STIMTAC: a tactile input device with programmable friction," in *Proceedings of the 24th annual ACM symposium adjunct on User interface software and technology*, New York, 2011/10/16.

[49] F. Giraud, C. Giraud-Audine, M. Amberg and B. Lemaire-Semail, "Using an Ultrasonic Transducer to Produce Tactile Rendering on a Touchscreen," in *Applications of Ferroelectrics, International Workshop on Acoustic Transduction Materials and Devices & Workshop on Piezoresponse Force Microscopy (ISAF/IWATMD/PFM), 2014 Joint IEEE International Symposium on the*, 2014/5/7.

[50] W. B. Messaoud, B. LEMAIRE-SEMAIL, M.-A. Bueno, M. Amberg and F. Giraud, "Closed-Loop Control for Squeeze Film Effect in Tactile Stimulator," in *International Conference and exhibition on new actuators and drives (Actuator 2014)*, 2014/6/24.

[51] B. Baylan, U. Aridogan and C. Basdogan, Finite element modeling of a vibrating touch screen actuated by piezo patches for haptic feedback, Springer Berlin Heidelberg, 2012/1/1, pp. 47-57.

[52] Y. Liu, Procédé tactile à diffraction ultrasonore, PhD Thesis. Arts et Métiers ParisTech, 2010/12/15.

[53] K. J. Son, M. Kim and K. Kim, "Analytical modeling of disk-type piezoelectric variable friction tactile displays," in *Advanced Intelligent Mechatronics (AIM), 2013 IEEE/ASME International Conference on*, 2013/7/9.

[54] C. Winter, Friction feedback actuators using squeeze film effect, PhD thesis. École polytechnique fédérale de Lausanne, 2014.

[55] C. Winter, Y. Civet and Y. Perriard, "Optimal design of a squeeze film actuator for friction feedback," in *Electric Machines & Drives Conference (IEMDC), 2013 IEEE International*, 2013/5/12.

[56] E. C. Chubb, E. Colgate and A. Peshkin, "ShiverPad: A Device Capable of Controlling Shear Force on a Bare Finger," in *World Haptic*, Salt Lake City, 2009.

[57] E. C. Chubb, E. Colgate and M. A. Peshkin, "ShiverPad: A Device Capable of Controlling Shear Force on a Bare Finger," in *EuroHaptic*, Salt Lake City, 2009.

[58] D. J. Meyer, M. Wiertlewski, M. A. Peshkin and J. E. Colgate, "Dynamics of Ultrasonic and Electrostatic Friction Modulation for Rendering Texture on Haptic Surfaces," *IEEE Transaction on Haptics,* pp. 63-67, 2016.

[59] F. Bernard, PhD Thesis: Conception, fabrication et caractérisation d'une dalle haptique à base de microactionneurs piézoélectriques, Grenoble: Comunauté Universitaire, Grenoble Alpes, 2016.

[60] F. Casset, J. Danel, P. Renaux, C. Chappaz, F. Bernard, T. Sednaoui, S. Basrour, B. Desloges and S. Fanget, "4-inch transparent plates based on thin-film AlN actuators for haptic applications," *Journal of Mechatronics,* June 2016.

[61] F. Casset, J. Daniel, C. Chappaz, Y. Givet, M. Amberg, M. Gorisse, C. Dieppedale, G. Le Rhun, S. Basrour, P. Ancey and S. Fanget, "Low voltage actuated plate for haptic applications with PZT thin-film," in *Int. Conf on Solid-State Sensors, Actuators and Microsystems*, 2013.

[62] C. Nadal, C. Giraud-Audine, F. Giraud, M. Amberg and B. Lemaire-Semail, "Modelling of a beam excited by piezoelectric actuators in view of tactile applications," in *Valencia*, Spain, 2014.

[63] E. Samur, J. E. Colgate and M. A. Peshkin, "Psychophysical evaluation of a variable friction tactile interface," in *IS&T/SPIE Electronic Imaging*, 2009/2/5.

[64] W. Ben Messaoud, E. Vezzoli, M. Bueno and B. Lemaire-Semail, "Analyse des modulations de frottement par effet squeeze film et électrovibration: validité de la complémentarité," in *Journées Internationales Francophones de Tribologie-JIFT*, Mulhouse, 2014.

[65] W. Ben Messaoud, Thesis: Design and Control of a Tactile Stimulator for Real Texture Simulation: Application to Textile Fabrics, Lille: Lille 1 University, 06/2016.

[66] N. D. Marchuk, J. E. Colgate and M. A. Peshkin, "Friction measurements on a large area TPaD," in *Haptics Symposium, 2010 IEEE*, 2010/3/25.

[67] C. Chapman, "Active versus passive touch: factors influencing the transmission of somatosensory signals to primary somatosensory cortex," *Canadian journal of physiology and pharmacology,* vol. 72, no. 5, pp. 558-570, 1994.

[68] W. Ben Messaoud, M.-A. Bueno and B. Lemaire-Semail, "Relation between human perceived friction and finger friction characteristics," *Tribology international,* vol. 98, pp. 261-269, 2016.

[69] C. Winter and Y. Perriard, "Modeling of the air film pressure for a haptic touch actuator," in *Power Electronics and Applications (EPE 2011), Proceedings of the 2011-14th European Conference on*, 2011/8/30.

[70] T. Sednaoui, E. Vezzoli, B. Dzidek, B. Lemaire-Semail, C. Chappaz and M. Adams, "Experimental Evaluation of Friction Reduction in Ultrasonic Devices," in *World Haptic*, Chicago, 2015.

[71] H. Yoshizawa and J. Israelachvili, "Fundamental mechanisms of interfacial friction. 2. Stick-slip friction of spherical and chain molecules," *The Journal of Physical Chemistry,* vol. 97, no. 43, pp. 11300-11313, 1993/10.

[72] S. Rosen and H. Peter, Signals and Systems for Speech and Hearing, BRILL, 2011.

[73] V. Levesque, L. Oram, K. MacLean, K. Cockburn, N. Marchuk, D. Johnson and M. Peshkin, "Enhancing physicality in touch inter-action with programmable friction," in *SIGCHI Conference on Human Factors in Computing Systems*, Chicago, 2011.

[74] B. Camillieri and M. A. Buneo, "Doigt artificiel pour frottement sur surfaces pileuses," in *22nd Congrès Francais de Mécanique*, Lyon, France, 2015.

[75] T. Sednaoui, E. Vezzoli, B. M. Dzidek, F. Giraud, B. Leamire-Semail, C. Chappaz and M. Adams, "Friction Reduction through ultrasonic vibration part 2: eperimental data for real and artificial finger pads," *Submitt. IEEE - Transaction on Hpatics,* 2016.

[76] M. Biet, F. Giraud and B. Lemaire-Semail, "Implementation of tactile feedback by modifying the perceived friction," *The European Physical Journal Applied Physics,* vol. 43, no. 1, pp. 123 - 135, 2008.

[77] E. Vezzoli, Z. Vidrih, V. Giamundo, B. Lemaire-Semail, F. Giraud, T. Rodic, D. Peric and M. Adams, "Friction Reduction Through Ultrasonic Vibration Part 1: Modelling Intermittent Contact," *Submitt. IEEE Transaction on Haptic.*

[78] R. Fenton Friesen, M. Wiertlewski, M. A. Peshkin and J. E. Colgate, "Bioinspired artifical fintertips that exhibit friction reduction when subjected to transverse ultrasonic vibrations," in *IEEE - World Haptic*, Chicago, 2015.

[79] W. Ben Messaoud, E. Vezzoli, F. Giraud and B. Lemaire-Semail, "Pressure dependence of friction modulation in ultrasonic devices," in *World Haptic Conference*, Versaille, 2015.

[80] F. Giraud, M. Amberg, B. Lemaire-Semail and G. Casiez, "Design of a transparent tactile stimulator," *Haptics Symposium (HAPTICS),* pp. 485-489, 2012/3/5.

[81] N. D. Marchuk, J. E. Colgate and M. A. Peshkin, "Friction Measurements on a Large Area TPaD," in *IEEE Haptics Symposium*, Waltham, 2010.

[82] F. Giraud, M. Amberg and B. Lemaire-Semail, "Interface tactile transparente". France Patent 1153963, mai 2011.

[83] E. Vezzoli, T. Sednaoui, M. Amberg, F. Giraud and B. Lemaire-Semail, "Wide Bandwidth Ultrasonic Tactile: a Friction Coefficient Control Device," in *EuroHaptic*, London, 2016.

[84] M. Amberg, F. Giraud, B. Semail, P. Olivo, G. Casiez and N. Roussel, "STIMTAC: a tactile input device with programmable friction," in *Proceedings of the 24th annual ACM symposium adjunct on User interface software and technology*, 2011/10/16.

[85] W. Ben Messaoud, G. Frédéric, B. Lemaire-Semail, M. Amberg and M.-A. Bueno, "Amplitude control of an ultrasonic vibration for a tactile stimulator," *IEEE/ASME Transaction on Mechatronics,* vol. 21, no. 3, 2016.

[86] D. Mahns, N. Perkins, V. Sahai, L. Robinson and M. Rowe, "Vibrotactile frequency discrimination in human hairy skin.," *Journal of Neurophysiology,* vol. 95, p. 1442–1450, 2005.

[87] M. Biet, M. Casiez, F. Giraud and B. Lemaire-Semail, "Discrimination of virtual square grattings by dynamic touch on friction based tactile displays," in *Symposium on Haptic Interfaces for Visual Environment and Teleoperator Systems*, 2008.

[88] E. Vezzoli, W. Ben Messaoud, M. Amberg, F. Giraud, B. Lemaire-Semail and M.-A. Bueno, "Physical and perceptual independence of ultrasonic vibration and electrovibration for friction modulation," *Haptics, IEEE Transactions on,* vol. 8, no. 2, pp. 235 - 239 , 2015.

[89] G. Frédéric, M. Amberg and B. Lemaire-Semail, "Merging two tactile stimulation principles: electrovibration and squeeze film effect," in *World Haptic (WHC)*, Daejeon, 2013.

[90] G. Campion, A. H. Gosline and V. Hayward, "Roughness of Virtual Textures and Lateral Force Modulation," in *The Synthesis of Three Dimensional Haptic Textures: Geometry, Control, and Psychophysics*, London, Springer, 2011, pp. pp 129-136.

[91] K. A. Kaczmarek, K. Nammi, A. K. Agarwal, M. E. Tyler, S. J. Haase and D. Beebe, "Polarity Effect in Electrovibration for Tactile Display," *IEEE Transaction on Biomedical Engineering,* vol. 53, no. 10, pp. 2047-2054, 2006.

[92] F. a. Kingdom and N. Prins, "Psychophysics: A Pratical Introduction," 2009.

[93] D. J. Meyer, . M. A. Peshkin and E. J. Colgate, "Fingertip friction modulation due to electrostatic attraction," in *World Haptics Conference (WHC), 2013*, Daejeon, 2013/4/14.

[94] E. Vezzoli, T. Sednaoui, M. Amberg, F. Giraud and B. Lemaire-Semail, "Control Strategies for Texture Rendering with a Capacitive Based Visual-Haptic High Fidelity Friction Control Device," *Haptics: Perception, Devices, Control, and Applications,* vol. 9774, pp. 251-260, 2016.

[95] D. Gueorguiev, Tactile Perception of Natural and Simulated Textures: A Pshychophysical Approach, Brussels: Université Catholique de Louvain, 2016.

[96] M. Wiertlewski, Reproduction of Tactual Textures: Transducers, Mechanics and Signal Encoding, Springer, 2013/1/4.

[97] E. Vezzoli, T. Sednaoui, M. Amberg, F. Giraud and B. Lemaire-Semail, "Wide Bandwidth Ultrasonic Tactile: a Friction Coefficient Control Device," in *EuroHaptic*, London, 2016.

[98] E. Vezzoli, D. Brygida, T. Sednaoui, F. Giraud, M. Adams and B. Lemaire-Semail, "Role of fingerprint mechanics and non coulomb friction in ultrasonic devices," in *World Haptic*, Chicago, 2015.

[99] E. Vezzoli, M. Amberg, F. Giraud and B. Lemaire-Semail, "Electrovibration modeling analysis," in *9th International Conference, EuroHaptics 2014*, Versaille, 2014.